Cyprus
University of
Technology

Faculty of Engineering
and Technology

Doctoral Dissertation

PHANTOM FOR BLOOD BRAIN BARRIER OPENING USING FOCUSED ULTRASOUND AND APPLICATION IN ALZHEIMER'S DISEASE

Tereza Alekou

Limassol, July 2021

CYPRUS UNIVERSITY OF TECHNOLOGY

FACULTY OF ENGINEERING AND TECHNOLOGY

DEPARTMENT OF ELECTRICAL ENGINEERING, COMPUTER ENGINEERING AND INFORMATICS

Doctoral Dissertation

PHANTOM FOR BLOOD BRAIN BARRIER OPENING USING FOCUSED ULTRASOUND AND APPLICATION IN ALZHEIMER'S DISEASE

Tereza Alekou

Limassol, July 2021

Approval Form

Doctoral Dissertation

PHANTOM FOR BLOOD BRAIN BARRIER OPENING USING FOCUSED ULTRASOUND AND APPLICATION IN ALZHEIMER’S DISEASE

Presented by

Tereza Alekou

Supervisor: Faculty of Engineering and Technology, Dr Christakis Damianou, Professor

Signature ____

Member of the committee: Dr Takis Kasparis, Professor

Signature ____

Member of the committee: Dr Constantinos Pattichis, Professor

Signature ____

Cyprus University of Technology

Limassol, July 2021

Copyrights

I would like to express my gratitude to my advisor Dr Christakis Damianou for his continuous support during my Ph.D study. I am grateful for the immense knowledge, support and guidance I have gained from him. His instructions and patience during the entire duration of my research and especially in the execution of my experiments was valuable. I would like also to thank Dr Marinos Yiannakou for sharing his knowledge and experience with me and also, for his assistance during my research, making our collaboration pleasant and effective. Finally, I would like to thank my husband and parents for their endless support and patience for all the duration of my studies.

ABSTRACT

This doctoral dissertation is examining various challenges presented in the use of High Intensity Focused Ultrasound in brain applications. The study is separated into five different sub-studies in the area of agar phantoms and brain applications. The first study is concentrated on the design and creation of a suitable agar-based phantom to be used in HIFU application on the blood brain barrier opening. A model that currently is not available to researchers, whereas all experiments are performed on animal models. The second objective of this dissertation is the evaluation of the attenuation of agar-based phantoms with various concentrations. The next study includes the evaluation of the mechanical properties of agar-based phantoms such as the structure and the stiffness since these data will help in understanding the structure of the phantom according to its composition. The fourth study includes the evaluation of an alteration in the composition of an agar phantom with the use of a preservative and its effect on the life of the phantom in combination with the storing conditions. Finally, the last study examines an application for the reduction of amyloid β plaques in a rabbit model with the use of antibodies crossing the blood brain barrier.

Keywords: ultrasound, phantom, blood brain barrier, agar

TABLE OF CONTENTS

LIST OF TABLES

LIST OF FIGURES

LIST OF ABBREVIATIONS

HIFU:	High Intensity Focused Ultrasound
BBB:	Blood Brain Barrier
MRI:	Magnetic Resonance Imaging
FDA:	US Food and Drug Administration
MRgFUS:	Magnetic resonance-guided focused ultrasound
TMM:	Tissue mimicking material

1 Introduction

1.1 Introduction to High Intensity Focused Ultrasound (HIFU)

HIFU technology was first investigated in 1942. Lynn et al [1] designed a transducer and examined whether ultrasonic waves can be focused on a surface. The energy concentrated on the focal spot was found approximately 150 times higher than other surfaces closer to the transducer. From experiments performed on animals, it was realized that tissue changes can be both temporary and permanent according to the parameters used.

In the following years further research was done on the MRI-guided ultrasound technology for surgery purposes [2][3]. Experiments in both gel phantoms and muscle were performed while monitoring the temperature and thermal effects of ultrasound. Experiments performed on dog muscle in 1993 demonstrated that tissue necrosis created from sonication could be visible by the MRI [3]. It was demonstrated that MRI showed the exact dimensions of the lesion and that sonication could be performed in the magnet.

Furthermore, Hynynen et al in 1994 proceeded in investigating the effect of injecting a contrast agent by performing experiments in thigh muscles of rabbits [4]. The contrast agent was injected before the sonication. From the results, it was concluded that a contrast agent can give evidence for the volume of the necrosed tissue, since during experiments the contrast agent increased the signal intensity only at the muscles and not on the necrosed tissue.

The first approved application of HIFU by the US Food and Drug Administration (FDA) in October 2004 was for the treatment of uterine fibroids. Since the first feasibility report in 2003 [5], Magnetic resonance-guided focused ultrasound (MRgFUS) has been used to treat symptomatic uterine fibroids. The ultrasound was located outside the abdomen, thus performing noninvasive thermal ablation of the targeted area. Nine women with symptomatic leiomyomas participated in the first clinical trial [5]. It was proven that HIFU can be effectively used for thermocoagulation and necrosis and that MRI was suitable for imaging the entire procedure and monitoring the temperature elevation. A study by Ikink et al [6] optimized the MRgFUS system by adding a cooled interface (direct skin cooling device) between the ultrasound and the patient providing constant cooling on the skin. This resulted in having less undesired heating in the area and fewer time intervals between the sonications for the area under cooling which results in reduced treatment duration.

HIFU has been tested through numerous studies for its use in the treatment of cancer using ablation. With the involvement of thermal effects, the temperature can reach levels of more than 60 ^{o}C and destruct tumor cells. A big success for HIFU is the fact that tumors were ablated even in difficult locations as described in a study by Orsi et al [7]. In this study patients with tumors in main blood vessels, heart, stomach, bowel, and gallbladder were identified and treated with HIFU effectively. The characterization of the tumors as 'difficult' was done according to their distance from a critical organ at risk. All of the 38 tumors in 31 different patients were less than 1 cm away from a critical organ and were ablated with HIFU. Organs that gave promising research results were the pancreas, prostate, liver, kidney and breast [8][9].

For the treatment of prostate cancer, many trials have been performed during the last decade [9]. Basic research began in the 1980s, while early clinical trials during the 1990s found a correlation between HIFU and the coagulated prostate volume [10]. Experiments performed on patients with proven prostate cancer using a phased-array focused ultrasound proved that the use of MRgFUS ablation can be used with no side effects and short-term complications. The procedure followed was approximately 84 min with 7 to 11 sonications per patient. Figure 1 demonstrates the equipment used [11]. A study conducted for the quality of life of patients treated with HIFU showed very promising results. Side effects were limited and some infections reported were mostly treated with antibiotics [12].

As previously mentioned, HIFU can be used also for the treatment of breast cancer as an alternative option. Used mainly for small breast tumors, HIFU offers preservation and function of the breast with zero bleeding, scaring and radiation and no need for surgical exposure [8]. Many clinical studies on HIFU treatment were performed [13]–[16]. Hynynen et al reported that 9 patients were treated with HIFU with almost no adverse effects [17]. In another clinical trial, HIFU was performed on 48 women before mastectomy evaluating potential side effects. The results were very encouraging since mild pain and skin burn that was observed soon disappeared. Both breast cancer cells and normal tissues undergone necrosis around the targeted tissue, but according to immunohistochemical staining no malignant behaviors (metastasis, invasion) were observed.

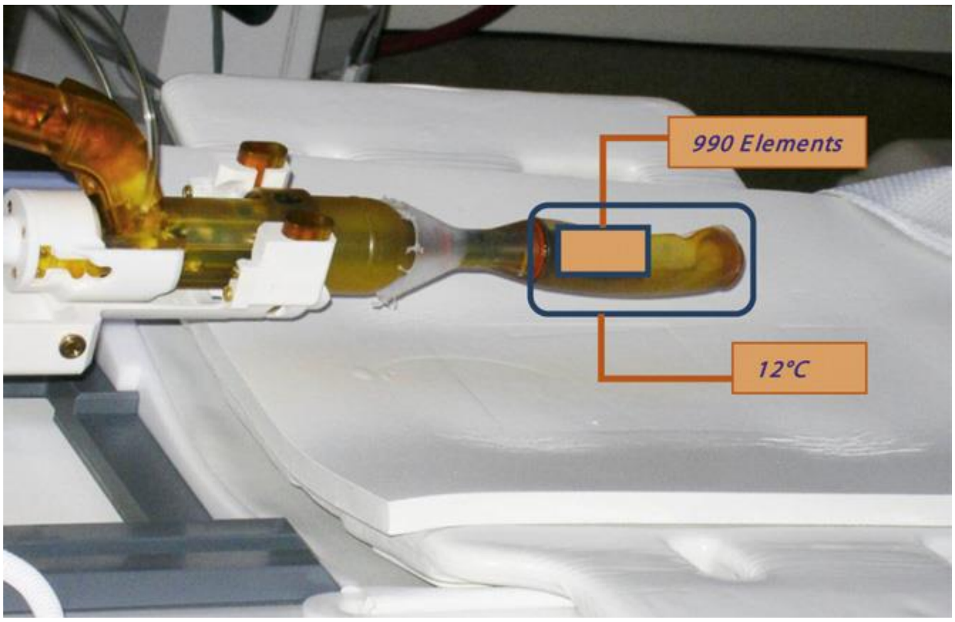

Figure 1 : The insertion arm, featuring the 990-element phased-array focused ultrasound for MRgFUS system for prostate ablation [11].

Another potential area for HIFU is ablation for liver cancer. Due to the respiratory movement of the liver, the existence of the ribs and the tumors size, this application faces many challenges [8],[18]. Until now the most commonly method followed was the one of resection and transplantation. With studies on animal models [19] and after the first successful HIFU liver ablation in 1993, new approaches have been investigated concentrating on patients with unresectable hepatocellular carcinoma. A study done on 39 patients with 42 tumors in total [20] proved that HIFU can be used for creating lesions with no major blood vessel injury. With the largest tumor being 22 cm long, it was a great achievement since half of the tumors were completely treated while the rest were ablated by more than 50 %. These facts provided promising evidence that a non-invasive treatment application like HIFU can be used also in liver cancer.

A sector in which HIFU remains as an investigative procedure, but with many improvements is on kidney tumor ablation [9]. This type of cancer is currently diagnosed at early stages where most of the tumor is of small size. The most commonly used treatment method is surgery. However, there is a new shift to nephron sparing procedures. One of those procedures is HIFU. Ritchie et al reported that 17 patients with mean tumor size of 2.5 cm underwent extracorporeal HIFU. Fifteen of them were treated according to protocol with no major complications [21]. Like other areas HIFU is suitable for kidney tumor ablation providing the patients a nephron sparing procedure with less recovery times and less radiation or chemotherapy.

Lastly, one of the most difficult to treat cancers is pancreatic cancer. With this cancer more than 80 % of the patients diagnosed are inappropriate for surgical treatment. An area where prognosis is very poor and the only treatments are chemotherapy, radiotherapy or combination of both [8]. The aim for these patients is pain relief and improvement of the quality of life. Studies has shown that HIFU can have a direct effect on pain palliation [22]–[24].

1.2 Research topics on HIFU for Brain Diseases

1.2.1 Blood Brain Barrier

The Blood Brain Barrier (BBB) is a specialized structure that blocks the delivery of molecules in the brain parenchyma [25]. It is consisted of capillary endothelium and under normal conditions it prevents molecules bigger than 400 – 500 Da to penetrate the brain parenchyma [26][27]. A big part of brain research is dedicated in finding ways to temporary disrupt the BBB and be able to apply medicinal treatments for several diseases.

McDannold et al in 2008 investigated the effects of burst length, pulse repetition frequency (PRF) and ultrasound contrast agent dose on the resulting BBB disruption [28]. Twenty-six rabbits were sonicated in a total of 100 brain locations with different parameters. Bursts of 0.1, 1 and 10 ms were tested and PRFs of 0.5, 1, 2, 5 Hz along with peak negative pressure amplitudes of 0.1 to 1.5 MPa. The ultrasound contrast agent doses were also tested with doses of 50, 100 and 250 μl/Kg. It was concluded that for the range of parameters used the magnitude of BBB disruption did not depend on the PRF or the dosage of the ultrasound agent. On the other hand, burst length had significant effect. For all the parameters used though, no histological alterations were observed [28].

A different study was made by Choi et al in which sonications on mice skulls were applied, but with no skull removal prior to sonication [29]. Ex vivo and in vivo experiments were done. For the ex vivo experiments, 5 mice were sacrificed and their skulls were removed and for the in vivo experiments 4 mice were anesthetized and sonicated. For imaging of the procedure, a diagnostic ultrasound was used in parallel with HIFU as shown in Figure 2. Indeed, opening of the BBB was achieved through the intact skull and skin with a single-element transducer. The amount of attenuation was small although in some areas some difficulties were observed due to different skull thickness. These results were a great achievement proving that with the use of a single-element transducer it is feasible to disrupt the BBB.

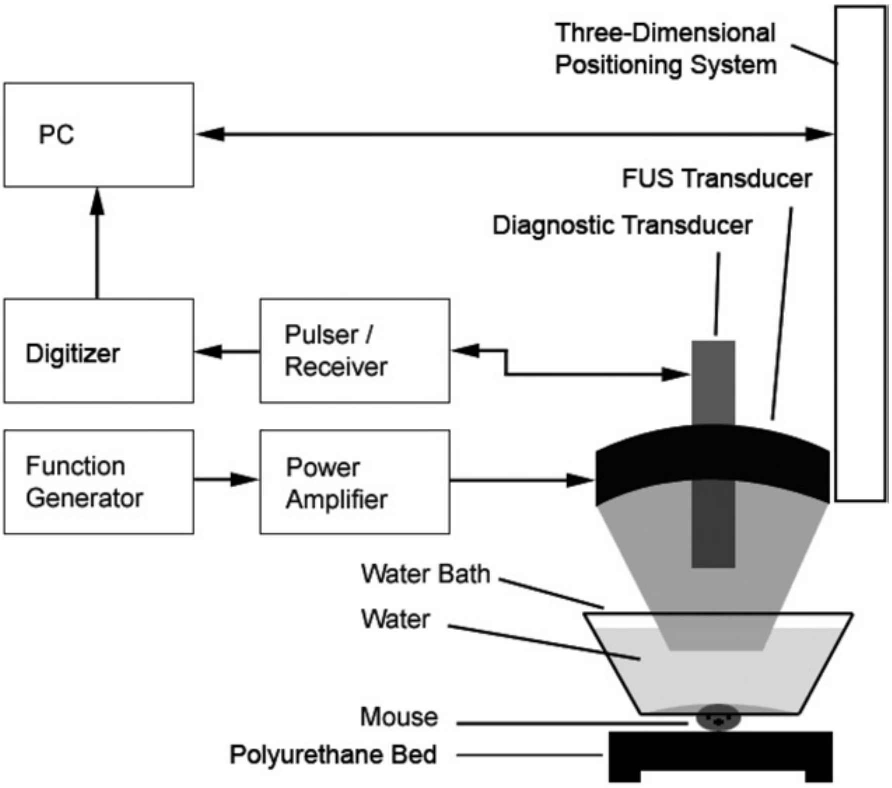

Figure 2 : Experimental set-up using both a diagnostic transducer and a HIFU transducer [36].

Choi et al [30] proceeded in examining which pharmacological compounds could pass through the BBB according to the molecular weight of the drug[30]. The BBB was disrupted in mice through the intact skull and dextran of three different molecular weights was administered. The findings were analysed using fluorescence microscopy to investigate which dextrans can be distributed in the targeted region. Dextrans of 3 KDa and 70 KDa weight passed through the BBB and into the brain whereas 2000 KDa dextran couldn’t. Therefore, by using this method non-invasively, pharmacological agents of at least 70 KDa can be delivered at the targeted area of the brain. With this study, it is now known that the limit of molecular weight that can travel through the BBB is somewhere between 70 and 2000 KDa [30].

Several studies were performed by Marquet and his team first on human and primate skulls [31]-[32] and then on actual non-human primates [33]. At first, they tested a single-element transducer at frequencies between 300 to 1000 KHz on primate and human skulls. They concluded that the frequency of 500 KHz resulted to optimum ultrasound propagation in the case of human skulls and the frequency of 800 KHz on primates [31]. With a frequency of 500 KHz they explored the capability of targeting different structures. They observed that the lateral displacement was found to be small compared to the resolution of the transducer for the human skull and the thermal build-up in the skull was minimal [32]. BBB disruption was tested on an actual animal model [33]. They chose to use non-human primates and specifically 2 male macaques in 3 sessions. For this experiment, 2 different types of microbubbles were used. The first one was manufactured in-house and the second was the widely used Definity®. To keep the animal steady, a frame was placed around its head in order to precisely target with ultrasound. With the help of MRI, BBB disruption was confirmed at four locations. With different pressures being investigated, it was observed that maximum BBB opening was accomplished at 0.6 MPa. Therefore, this feasibility study successfully demonstrated BBB opening in non-human primates for the first time [33].

Additional studies tested two different types of microbubbles (in-house or Optison® vs Definity®) [34]–[36]. One of them was made by Wang et al [36] where a total of 18 mice were tested with either Definity® or in-house microbubbles. Different pressures were tested and BBB disruption was monitored by MRI. It was concluded that the type of microbubbles can have a significant effect on BBB opening at lower pressures, but less on higher pressures. This was observed with no significant difference between Definity® and in-house microbubbles at higher pressures (0.45 and 0.6 MPa), but at a lower pressure (0.3 MPa), the in-house microbubbles showed higher permeability and opening volume. This fact was attributed to the cavitation that ruled the phenomenon [36].

For BBB disruption except from single element transducers, many researchers have used phased array transducers of multiple elements [37]–[40]. McDannold et al tested this technology on rhesus macaques in 2013 [37]. For their experiment, they used ExAblate 4000 (InSightec, Israel) was used which is a hemispherical phased array transducer with 1024 elements. Overall, 185 locations in 7 monkeys with specific targeted areas such as the thalamus and the hippocampus were sonicated. BBB disruption was successful and confirmed with MRI. It was demonstrated that using such system for patient treatments, BBB can be opened repeatedly with no significant tissue damage. The animals were tested for their behaviour showing that their functions were normal and there were no deficits [37]. Liu et al [40] on the other hand designed a 256-channel phased array system and tested it on swine. They followed 3 patterns using different acoustic parameters each time and evaluated BBB opening by measuring the deposition of Evans blue dye. These preliminary animal experiments demonstrated the ability to disrupt the BBB through an intact skull with both single and scanned targeted regions. A system was developed that penetrated through the human skull in the future.

Finally, several studies were conducted using glioma-bearing rat models [41]–[47]. It is known that malignant glioma remains one of the most deadliest forms of cancer in humans [41]. HIFU with the effects of cavitation, radiation and microstreaming can improve the permeability of drugs by disrupting the BBB. Yang et al [41] investigated the relative permeability after HIFU application on 4 glioma-bearing rats (4 were used as control with no treatment). Figure 3 shows the timelines used in this experiment. The ultrasound contrast agent was first administered through the vein and then pulsed HIFU was applied.

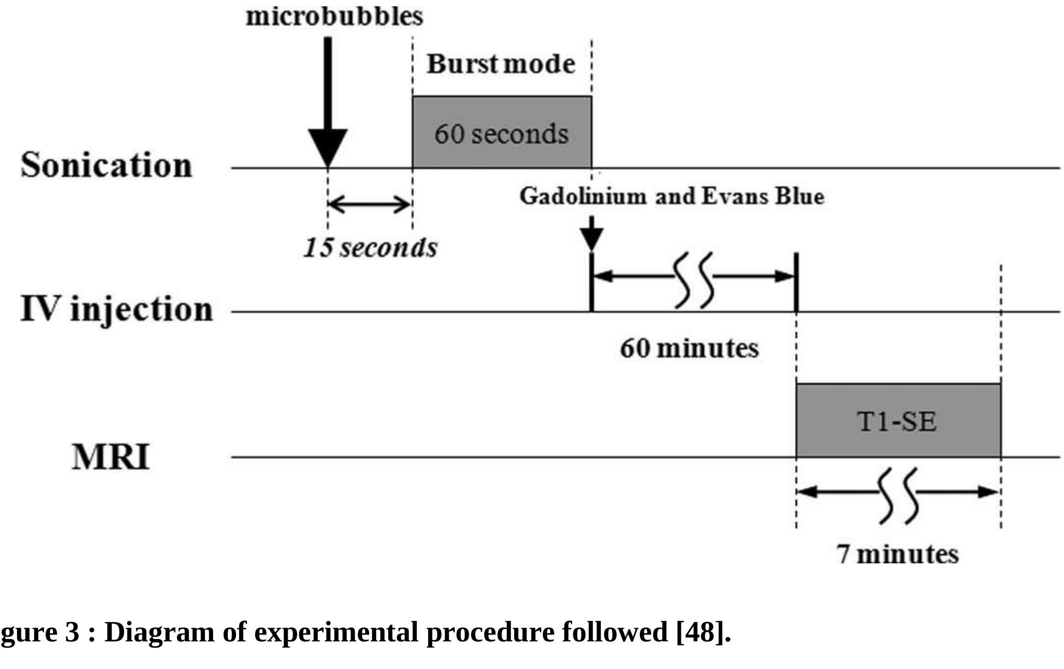

Figure 3 : Diagram of experimental procedure followed [48].

Immediately after sonication each rat was injected with MRI contrast agent and Evans blue dye to quantify the extravasation. The MRI scan was performed after 60 minutes of administration. The initial hypothesis was confirmed: pulsed HIFU application increased the tumor permeability and induced blood tumor disruption compared to intact brains. This could be applied for targeted chemotherapy and allow pharmaceuticals to cure brain diseases.

Yang et al [42] performed more experiments later using a different experimental timeline. The difference with the first study was that Evans blue was injected at the beginning and several minutes before sonication. The second step was to inject the UCA and afterwards the sonication followed. Thirty minutes after sonication the rats were perfused and tested for Evans blue extravasation. This study proved that HIFU not only can increase the permeability of the blood tumor barrier, but also it can increase the tumor to brain drug ratio in the focal region that was caused by HIFU [42].

Many studies have been conducted throughout the years for BBB disruption. Each one of them used different animal models, ultrasound contrast agents or ultrasound parameters. Table 1 lists these parameters and their main results.

Based on the studies mentioned on the Table 1, it is observed that the most common animal model used was the New Zealand white rabbits. Many studies preferred using rats (Wistar, Sprague-Dawley and Fischer). Three different types of ultrasound contrast agents were widely used (Optison®, Sonovue® and Definity®) with a small majority preferring Optison® as a contrast agent. Some studies also used 2 of the available ultrasound contrast agents in order to compare their effectiveness. The UCA doses ranged from 10 μl/kg to 0.4 ml/kg. The MRI contrast agent used in most of the studies was Magnevist® with the most common dose to be equal to 0.125mmol/kg for New Zealand white rabbits. Among the different ultrasound parameters examined, the most common ones were pulses of 10 ms with pulse repetitions of 1 Hz and duration of 20 s. Peak negative pressures varied from 0.071 MPa to 3.1 MPa. Therefore, it is obvious that BBB disruption can be achieved with numerous combinations of parameters and on different animal models

Table 1: Parameters and Results of BBB studies

Group	**Year**	**Animal model**	**Dose ultrasound contrast agent**	**Dose MRI contrast agent**	**Peak negative pressure or intensity**	**Pulse (ms)**	**Pulse repetition (Hz)**	**Time (s)**	**Main results**
Hynynen et al [48]	2001	18 male New Zealand white rabbits	0.05 mL/kg Optison®	0.125 mmol/kg Magnevist®	0.2-11.5W, 16–690 W/cm2	10 or 100	1	20	Opening of the blood-brain barrier was confirmed with detection of MR imaging contrast agent at the targeted locations. The lowest power levels used produced blood-brain barrier opening without damage to the surrounding neurons.
Schlachetzki et al [49]	2002	7 male volunteers	10 mL of Levovist® or 3 mL of Optison®	0.3 mmol/kg Magnevist®	<2.69 MPa	-	3500	-	Ultrasonic contrast microbubble destruction by HIFU even at low power levels can influence BBB permeability for Gd-based MR contrast agents without any damage to endothelial cells, neighbouring astrocytes, or neurons.
Sheikov et al [50]	2004	10 adult male New Zealand white rabbits	0.05 ml/kg Optison®	0.05mL/kg Magnevist®	1- 3MPa	100	1	20	Induced changes in endothelial cell fine morphology that resulted in the BBB opening. Mechanisms of macromolecules passage to BBB were identified.
Hynynen et al [51]	2005	22 New Zealand white rabbits	0.05 ml/kg Optison®	0.125 mmol/kg Magnevist®	-3.1 Mpa	10	1	20	BBB disruption is possible at a frequency of 0.69 MHz with minimal damage to the exposed brain parenchyma cells.
McDannold et al [52]	2005	24 New Zealand white rabbits	0.05 mL/kg Optison®	0.125 mol/Kg magnevist®	0.7-1 MPa	100	1	20	Ultrasound-induced BBB disruption is possible without inducing substantial vascular damage that would result in ischemic or apoptotic death to neurons.

Table 1: Parameters and Results of BBB studies (continuation)

Group	Year	Animal model	Dose ultrasound contrast agent	Dose MRI contrast agent	Peak negative pressure or intensity	Pulse (ms)	Pulse repetition (Hz)	Time (s)	Main results
Yang et al [53]	2007	16 male Wistar rats	0-90 µL/kg Sonovue®	-	0.9 MPa, 1.2 MPa	10	1	30	If a proper quantity of UCA is used before performing HIFU the BBB disruption can be increased and localized especially in higher HIFU pressures (1.2 MPa).
McDannold et al [54]	2007	15 New Zealand white rabbits	10 µl/kg Definity® and 50 µl/kg Optison®	0.125 mmol/kg Magnevist®	0.2-1.5 MPa	10	1	20	BBB disruption is possible using Definity® for the dosage of contrast agent and the acoustic parameters tested in this study. Optison® produced a larger effect for the same acoustic pressure amplitude.
Choi et al [29]	2007	9 brown CB57-b16 type mice	0.4 mL/kg Optison®	0.5 mL Omniscan	2.0, 2.5 and 2.7 MPa	20	10	30	Accurate and precise opening of the BBB through the intact skull and skin in mice with a single-element FUS transducer.
McDannold et al [28]	2008	26 New Zealand white rabbits	50, 100, 250 µl/kg Optison®	0.125 mmol/kg Magnevist®	0.1-1.5Mpa	0.1, 1, 10	0.5, 1, 2, 5	20	BBB disruption is not affected by PRF or ultrasound contrast agent dose. Both the BBB disruption magnitude and its threshold depend on the burst length.
Sheikov et al [55]	2008	25 Wistar rats	0.05-0.07 ml/Kg Optison®	0.03 mmol/kg Magnevist®	1.1MPa	10	1	-	Tests at several time periods after sonication showed that leakage of agents was accomplished. At 6 and 24 h after sonication function was fully restored and no leakage was observed.
McDannold et al [26]	2008	11 Male New Zealand white rabbits	50µl/Kg Optison®	0.125 mmol/kg Magnevist®	0.3 to 2.3 MPa	10	1	20	BBB disruption threshold expressed in terms of the peak negative pressure amplitude increased as a function of the frequency.

Table 1: Parameters and Results of BBB studies (continuation)

Group	**Year**	**Animal model**	**Dose ultrasound contrast agent**	**Dose MRI contrast agent**	**Peak negative pressure or intensity**	**Pulse (ms)**	**Pulse repetition (Hz)**	**Time (s)**	**Main results**
Choi et al [30]	2010	13 wild-type male C57BL/6 mice	25 mL Sonovue®	-	570 kPa (peak-rarefactional pressure)	20	10	30	Pharmacological molecules of 3 and 70 KDa can pass through the BBB when sonicated with HIFU while molecules of 2000 KDa can't.
Chopra et al [56]	2010	12 New Zealand white rabbits, 25 male Wistar rats	10 µL/kg Definity®	0.1 mmol/kg Omniscan®	0.2-0.8Mpa	10	1	30-1200	Exposures less than 180 s in duration are linked with a low probability of irreversible damage to brain tissue. Lower power sonications for longer time gives higher permeability to the brain.
Marquet et al [33]	2011	2 male rhesus macaques	500µl In-house microbubbles and Definity®	0.2 mL/kg Omniscan®	0.3, 0.45 and 0.6MPa	10	2	120	Transcranial HIFU is shown for the first time to induce BBB disruption in non-human primates in 2 animals with different pressures and microbubbles type.
Cho et al [57]	2011	20 male Wistar rats	0.02mmL/kg Definity®	-	0.071 to 0.25 MPa	10	1	120	Different types of leakage can be attained by controlling peak negative pressure amplitude of sonication.
O'Reilly et al [58]	2011	28 Wistar rats	0.02 ml/kg Definity®	0.2 mL/kg Omniscan®	0.54Mpa	0.003-10	0.2-2	1-300	Use of short burst lengths has the potential to decrease treatment times. PRF of 2 Hz may increase enhancement over a 1-Hz PRF when used with infusion microbubbles delivery.
Yang [41]	2011	8 male Fischer rats	450 µL/kg SonoVue®	1 mmol/kg Omniscan®	0.5 Mpa	50	1	60	Pulsed HIFU enhances the relative permeability of the BTB in glioma bearing rats.

Table 1: Parameters and Results of BBB studies (continuation)

Group	**Year**	**Animal model**	**Dose ultrasound contrast agent**	**Dose MRI contrast agent**	**Peak negative pressure or intensity**	**Pulse (ms)**	**Pulse repetition (Hz)**	**Time (s)**	**Main results**
Choi [59]	2011	99 C57Bl6 male mice	0.01, 0.05, 0.25 µL/g Definity®	-	0.46MPa	0.03-30	0.1- 25	660	Reducing the total number of emitted acoustic cycles was found to facilitate a more spatially uniform distribution of delivered dextran.
Yang [42]	2012	27 male Fischer rats	300 µL/kg SonoVue®	1 mmol/kg Omniscan®	5.72W	50	1	60	Pulsed HIFU significantly elevated the tumor:brain drug ratio in the focal region.
Wei et al [60]	2013	29 swine	0.3 mL/kg/min SonoVue®	0.1 mmol/kg Magnevist®	0.26- 0.56 MPa	10	1	30	Successful use of a neuronavigation system to guide FUS-induced BBB opening high advantages compared to MR-guided approach.
Chu et al [43]	2013	34 male Sprague-Dawley rats	2.4μL/kg SonoVue®	0.3 mL/kg Magnevist®	0.47MPa	10	1	90	BBB opening dynamics characterization in normal and tumor tissues using Gd-DTPA and Evans Blue determined from tissues after sacrifice.
Liu et al [40]	2014	10 swine	0.3 mL/kg/min SonoVue®	-	0.52- 0.78 MPa	10	0.1-1	30	Prototype design of a 256-channel for transcranial BBB opening in the brains of large animals. Capability of dual-frequency exposure to potentially enhance the BBB-opening effect.
Wang et al [61]	2014	18 C57BL/6 mice	1 µl/g in-house or Definity®	0.3 mL Omniscan®	0.3, 0.45, 0.6 Mpa	20	10	60	Microbubbles have significant effects on FUS induced BBB opening at lower pressures, less important at higher

1.2.2 Drug Delivery

Several methods have been developed to overcome the BBB and deliver drugs into the brain. The most common is the surgical approach in which needles or pumps are used and drugs are delivered with direct injections to the brain [25]. Although clinical trials showed encouraging results, the damage of healthy tissue and the risks due to surgery and anaesthesia lead researchers to explore other ways to deliver drugs into the brain [62]. A different method tested was applying the injection into the cerebrospinal fluid and not directly into the brain. But this could not predict the drug doses at the area of interest. Other novel methods turned their interest in improving the drug itself and increase its uptake by the brain and bypass the BBB. However, the concentrations of the agents that reached the brain were lower than the therapeutic ones [62-63].

With these facts, BBB disruption with HIFU gave its way for a new innovating approach for targeted drug delivery. A variety of tracers and therapeutic agents were delivered in the brain of rodent models. Gadolinium-based contrast agents (500 – 900 Da) used during MRI imaging were successfully delivered to the brain with HIFU [64]. Trypan blue and Evan’s blue (70 KDa) were also commonly used to visualize the BBB disruption, proving the BBB opening [43]. Other tracers that were examined were horseradish peroxidase [50][55], Dextran molecules [57][65], Lanthanum chloride and superparamagnetic iron oxide [66-67].

One of the sectors that research on HIFU enhanced drug delivery was focused on is for the treatment of glioblastoma. Nearly 20’000 patients are diagnosed every year with malignant brain cancer, with more than 50 % to be glioblastoma multiforme [68]. Yang et al [46],[69–71] showed that pulsed HIFU along with human atherosclerotic plaque - specific peptide-1 (AP-1) which was combined with doxorubicin containing liposomes (Lipo-Dox) could act insynergy for treating brain glioblastoma. The experiments were performed on a brain tumor mouse model which was sonicated with HIFU after administering AP-1 Lipo-Dox or just Lipo-Dox intravenously. Indeed, these animals showed increased accumulation of the drug in tumor cells in conjunction with control animals that were not sonicated. Also, these experiments demonstrated that with the combination of these two methods the tumor growth ratio was decreased compared to chemotherapy itself. The results are shown of Figure 4.

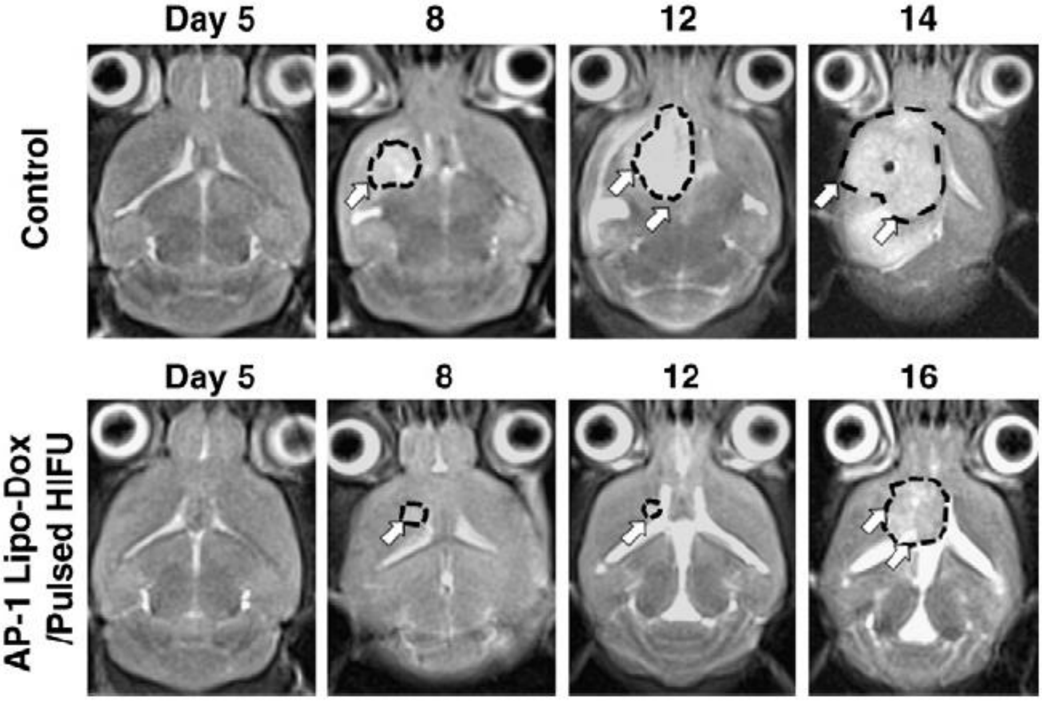

Figure 4 : Decrease in tumor size in treated mice [71]

Aryal et al [72] also tested Doxorubicin (DOX) with HIFU for the treatment of glioblastoma in three weekly sessions on rat glioma tumors. It was concluded that the median survival time was significantly increased compared to animals that received DOX treatment only.

Similar experiments were also performed by Treat et al [73] using FUS with microbubbles in gliosarcoma baring rats which resulted in increased survival time after a single treatment of HIFU with DOX compared to DOX treatment only. It was also suggested that this method of treatment significantly increased the antineoplastic efficacy of liposomal DOX in the brain. Temozolomide (TMZ) was also tested for glioma treatment by Liu et al [74]. Mice with U87 human glioma cells were sonicated and administered with TMZ with doses ranging from 2.5 to 25 mg/Kg. The results demonstrated an increase in TMZ uptake, but also in TMZ degradation time in the tumor core. An improved tumor progression (up to 15 %) and survival rate (up to 30 %) depending on the TMZ doses was reported. A preclinical study using TMZ was also performed by Wei et al in 2013 [75]. Fischer rats were implanted with glioma cells and TMZ was quantitated in cerebrospinal fluid after sonication. Their results showed a reduction in tumor progression and an increase in median survival. All the above studies demonstrate that the delivery of TMZ or DOX was enhanced with HIFU which gives great potential for future improvements in brain tumor treatment.

Experiments were also performed on metastatic breast cancer cells into the brain [76–78]. The first study in 2006 by Kinoshita et al [76] was focused on delivering Herceptin (trastuzumab) in the CNS of mice through the BBB. According to the extent of the BBB disruption through MRI they indirectly calculated the amount of Herceptin delivered. They demonstrated that Herceptin could possibly pass the BBB and offer a promising technique for future development. Wu et al [78] on the other hand examined DOX along with HIFU hyperthermia on a mice model. Indeed, short-time HIFU hyperthermia had enhanced the delivery of DOX into the brain tumors after a single treatment. The concentration of DOX was significantly greater in treated tumors with HIFU compared to control groups.

DOX was also tested on virus-induced anaplastic squamous cell carcinoma (Vx2 tumors) on superficial thigh muscles of rabbits [79]. Fifteen rabbits were randomly assigned in 3 treatment groups: the first was treated with DOX, the second with low temperature sensitive liposomes (LTSLs) and the third with HIFU (mild hyperthermia) and LTSLs. DOX concentration was determined with high-pressure liquid chromatography analysis of the tumor. The results showed an increased concentration of DOX on the third group in both the periphery and core of the tumor. The other two groups showed lower DOX concentrations with its main distribution only on the tumor’s periphery. With only 25 % of the tumor volume being heated, showed potential for clinical applications for drug delivery on solid tumors.

HIFU has a wide range of applications for enhanced drug delivery. Different studies have been made, each one of them using a different type of cancer or disease and different types of drugs. Such example is a study made by Park et al [80] regarding the use of HIFU with the chemotherapeutic drug Cetuximab in a colon cancer mice model. Cetuximab, HIFU therapy or both were administered three times per week on nude mice which had been injected with tumor cells 8 days before. With monitoring of the tumor growth for up to 34 days, it was observed that the combination therapy group showed the most suppressed tumor growth compared to all other groups.

A different type of method for enhanced drug delivery includes the use of nanoparticles with HIFU. These therapeutic nanoparticles are 1 mm – 100 nm in diameter and are delivered when HIFU transiently increases BBB permeability. The most commonly used nanoparticle is Au (AuNPs) which is non-toxic and bio-inert [81]. In studies where the BBB remained intact and AuNPs of 10 – 250 nm were used, only particles of 10 nm could be detected in the brain in very low concentrations [82]. The first demonstration of focal enhanced delivery of AuNPs was made by Etame et al [81]. Particles of 50 nm coated with thiolated PEG were delivered into the right hemisphere of 7 Wistar rats prior sonication and were observed with the help of MRI. Histological examination showed AuNPs in the perivascular spaces and 150 μm from the site of disruption. This proves that a significant amount of AuNPs were delivered into the brain with MRgFUS with no major adverse effects. Other studies have been conducted with AuNPs and HIFU, with all of them giving promising results for future development [83–86]. Magnetic nanoparticles (MNPs) were also used in experiments performed by Liu et al [87].

Nanoparticles were also used along HIFU in other regions. Two feasibility studies were made using drug loaded nanoparticles [88][89]. The first one included the chemotherapeutic drug Docetaxel loaded in Pluronic nanoparticles (NPs) [88]. The NPs were extravasated into the interior cells in tumor tissue using HIFU without any severe tissue damage. This increased concentration of NPs in the tissue was observed at exposure of 20 W/cm^2 since on higher exposures the tumor tissue was destructed due to the effect of thermal ablation, decreasing the concentration of the NPs. The second study made by Zhang et al [89] tested methotrexate (MTX)-loaded poly(lactic-co-glycolic acid) (PLGA) nanobubbles (NBs) which were further connected with anti-HLA-G antibodies (mAb$_{\text{HLA-G}}$) on nude mice. They concluded that the NBs can be used as a targeted drug carrier, an ultrasound contrast agent, but also in synergy with HIFU ablation for the treatment of choriocarcinoma.

Finally, HIFU can be used also in activating a drug to release its active ingredient in localized regions. These type of drugs can be temperature sensitive liposomes or bubbles [90]. The main procedure for this type of drug delivery is the injection of the temperature sensitive formulation intravenously and HIFU to be applied externally on the target area. The elevated temperature due to HIFU will trigger drug release in the specific region. In this way, only the area of interest will receive the needed therapy. Some applications include delivery to the heart [91], the skeletal muscle [92] and cancer treatment [93].

1.3 Conclusions

HIFU technology has been in the foreground for years as an alternative non-invasive method for the treatment of various conditions. Its benefits were discovered many years ago and since then a great number of studies have been performed with numerous different types of applications. These include among others BBB disruption, targeted drug delivery and tumor ablation. It was not long until FDA approved the first HIFU application in the successful treatment of uterine fibroids [5]. Research continued with experiments on tumor ablation with thermal effects giving promising results. Trials were done for treating prostate [9]-[12], breast [13]-[17], liver [18]-[20] and pancreatic cancer [22]-[24] but also for the ablation of kidney tumors [21].

It was then decided to examine the potential of using HIFU in one of the biggest challenges in the treatment of brain diseases with BBB opening. The BBB is a structure of capillary endothelium which prevents the large molecules from entering the brain parenchyma. This has as a result most of the known pharmaceuticals used until now to be blocked by the BBB preventing them from treating brain diseases. Due to this specialized structure only four diseases that occur in the brain can be treated (depression, chronic pain, epilepsy and affective disorders). All of the rest including Alzheimer's disease, Parkinson's disease, brain tumors and autism have no effective therapy. With these facts in hand, researchers turned their interest in contriving ways to disrupt the BBB and access the brain. HIFU which is noninvasive is a promising method. It was observed that with the use of HIFU in combination with microbubbles, BBB could be temporarily disrupted non-invasively, with no acute tissue damage. The microbubbles are injected intravenously, contract due to the ultrasonic waves and interact with the endothelial cells disrupting the BBB. Numerous studies were done on different animal models including rabbits [29-30], [34-35], [57-58], rats [31-33], [58-61] swine [47], [62], human primates [38-39] but also on human patients [55]. All of them used different combinations of ultrasound parameters (such as pulse repletion frequency, pulse duration and total time), different ultrasound contrast agents (Optison®, Definity®, SonoVue® or in-house UCA) and different MRI contrast agents (Magnevist®, Omniscan®) but reached to the same main conclusion: the BBB was effectively disrupted with no tissue damage and the increase of this disruption was correlated with the above-mentioned parameters.

Since the BBB disruption was achieved with HIFU, research advanced in examining drug delivery with the help of HIFU for specific diseases. Studies performed on glioblastoma bearing mouse models showed that drugs like Doxorubicin and Temozolomide were delivered into the brain giving positive results in tumor growth and survival rates. Other different drug delivered were Herceptin (which was delivered in mice with metastatic breast cancer into the brain), Doxorubicin (which was administered in tumors on superficial thigh muscles and squamous cell carcinoma cells) and Cetuximab (used in colon cancer mice models). With the use of HIFU various nanoparticles were also managed to pass through the BBB [81-87]. This includes among others gold nanoparticles, doxetaxel loaded pluronic nanoparticles and methotrexate loaded nanobubbles.

HIFU constitutes a very useful tool for non-invasive treatment of different diseases. Apart from cancer treatments, novel research proved that HIFU plays a dynamic role in the treatment of brain diseases with achieving BBB disruption. A barrier that for decades was considered the main issue in treating brain diseases, has been bypassed with the help of HIFU. Extensive research has already been made in this area, but more knowledge is yet to be discovered and create treatments for diseases that today are considered non-treatable. Therefore, there is a need for a BBB phantom that can be used to test different HIFU protocols.

2 Focused ultrasound phantom model for Blood Brain Barrier Disruption

2.1 Introduction

As mentioned before, the BBB is a specialized structure that blocks the delivery of molecules in the brain parenchyma [25]. It is consisted of capillary endothelium and under normal conditions it prevents molecules bigger than 400 – 500 Da to penetrate the brain parenchyma [26][27]. From the well-known diseases only depression, chronic pain, epilepsy and affective disorders respond to lipid-soluble small-molecule drugs that can pass through the BBB [27]. Neurodegenerative diseases such as Alzheimer’s disease (AD) and Huntington’s disease have no therapy. Multiple sclerosis, brain tumors, stroke, Human Immunodeficiency Viruses (HIV) infections, brain and spinal cord trauma, autism in children, ataxis and fragile X syndrome have no effective therapy either. Even Parkinson’s disease that is treated with L-dopa drugs, do not offer any cure to stop neurodegeneration caused by the disease [27]. A big part of brain research is dedicated in finding ways to temporary disrupt the BBB and be able to apply medicinal treatments for all the diseases mentioned above. [47], [51], [55], [62], [94]–[96].

Some of the techniques of BBB disruption tested in the past were based on the use of hyperosmolar solutions such as mannitol to loosen the tight junctions of the barrier or even intracranial operations with the use of a needle. The latest advancements include the use of High Intensity Focused Ultrasound (HIFU) with microbubbles to disrupt temporarily and non-invasively the BBB [25]. The mechanism behind this disruption is not well understood yet. The microbubbles are injected intravenously and contract with the use of ultrasonic waves at the same frequency. In this way, the microbubbles interact with the endothelial cells and eventually disrupt the BBB [97]. Figure 5 shows schematically the principle of BBB opening.

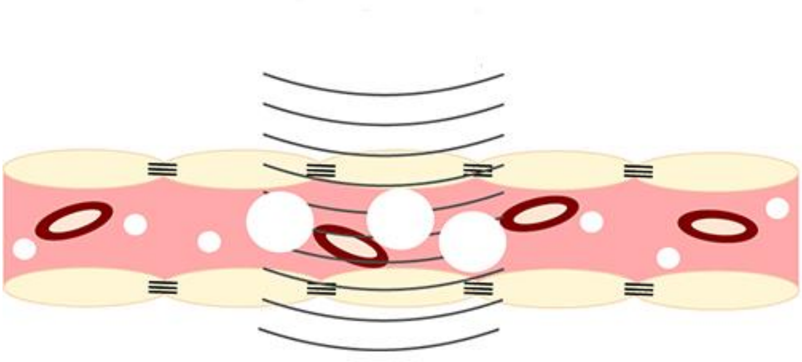

Figure 5 : Concept of the BBB disruption [28].

Experimental studies for BBB disruption started in 2001 by Hynynen et a [48] by sonicating the brain of 18 rabbits. The rabbits were sonicated in four to six locations with 0.2 to 11.5 W power. At first, a piece of skull was removed, and the skin was replaced to cover that area. On the day of the experiment, the animals were placed on their backs and the targeted area was fixed in position by a holder. Figure 6 shows the experimental arrangement followed. MRI was used for imaging and monitoring of the temperature and tissue changes while a contrast agent with microbubbles was injected via the ear vein before each sonication.

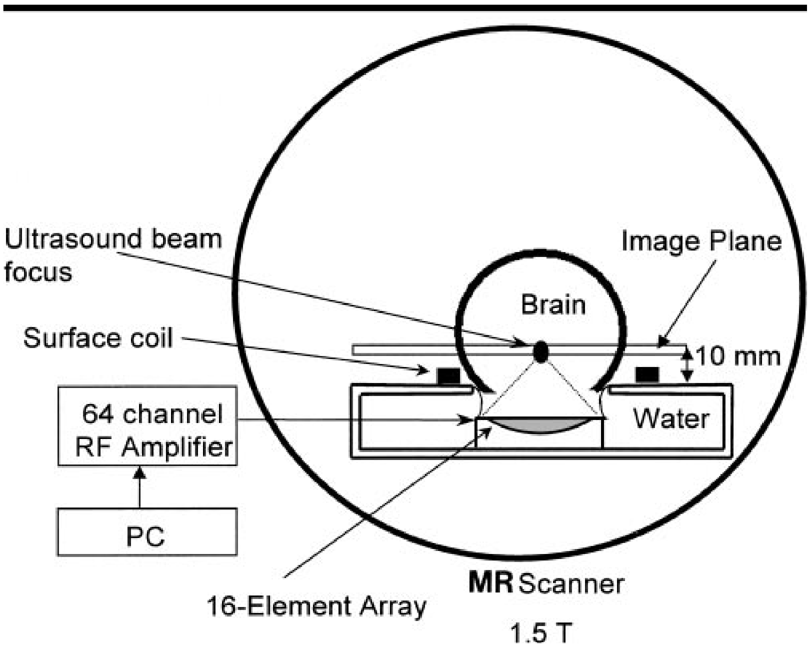

Figure 6 : Diagram of experimental arrangement for BBB opening [29].

The results showed that the BBB was indeed disrupted with no visible tissue damage. The contrast agent was leaked into the brain which means it was able to pass through the BBB. Tests performed in several time periods after the experiment showed that the BBB eventually returned to its initial state, while the histological examination showed some tissue damage depending on the pressure amplitude used. In conclusion, this study gives evidence that BBB can be opened with the use of HIFU and allow drugs like chemotherapeutic agents pass into the brain [48].

In the following years, many important studies were performed in animal models (rabbits, mice, rats, swine and human primates) using different parameters of HIFU proving that the BBB can be disrupted for a short period with minimal side effects [47], [51], [55], [62], [94]–[96]. One of these studies was the one performed by Sheikov et al in which the cellular mechanisms that take part during BBB disruption were investigated [50]. Until then these mechanisms were mostly unknown. Experiments done on rabbits were studied for their endothelial cell fine morphology changes induced by ultrasound. For this to be done they followed an immunocytochemical procedure (for endogenous immunoglobulinG) along with electron microscopy. Their results showed that there are different mechanisms that macromolecules use to pass through the BBB after sonication: transcytosis, endothelial cell cytoplasmic openings, opening of a part of tight junctions and free passage through injured endothelium. Also, it was demonstrated that immunoglobulinG was delivered at the targeted brain areas by passing through the BBB. With these findings, this study was the first that actually described the routes of the macromolecules passage giving evidence for new developments in gene or drug delivery to the brain.

Research continued with experiments on Wistar rats by Yang et al in 2006 [53]. The correlation between the ultrasound contrast agent (UCA) dose with the amount of Evans blue extravasation was investigated. Sixteen male rats were anesthetized, windows of skull were removed and sonicated by a 1 MHz transducer in two locations (one in each hemisphere). It was demonstrated that UCA can enhance BBB disruption. A higher UCA dose causes a higher cavitation degree while it concentrates the ultrasound energy on the focal region. Therefore, if a proper quantity of UCA is used before performing HIFU the BBB disruption can be increased and localized especially in higher HIFU pressures (1.2 MPa). Figure 7 shows the distributions of Evans Blue in the focal region at different

UCA doses and ultrasound pressures [53]. It is obvious that both the size and degree of staining were increased according to the UCA dose and in higher ultrasound pressures.

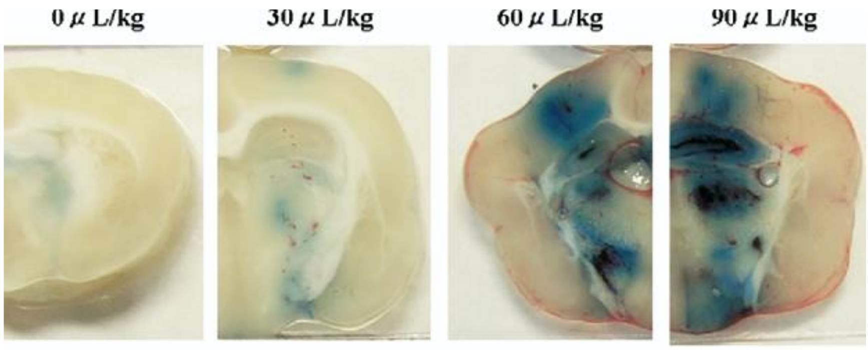

(a) 0.9 MPa sonication

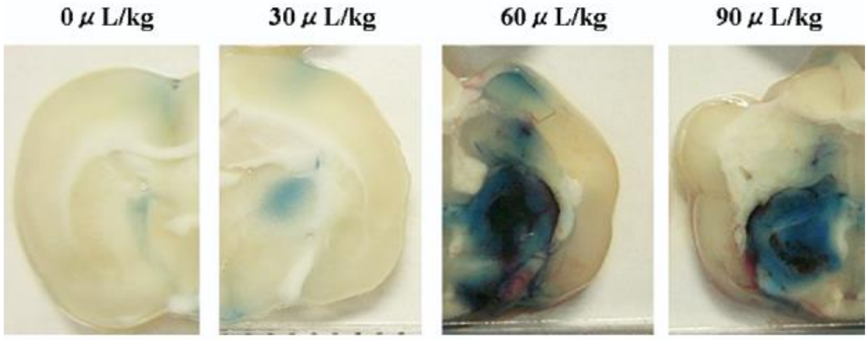

(b) 1.2 MPa sonication

Figure 7 : Distributions of Evans Blue extravasation in the brain for UCA at four doses and ultrasound pressures of 0.9 MPa and 1.2 MPa [31].

A similar study in 2007 was made by Sheikov et al [55] on 25 rats with 1.5 MHz ultrasound bursts at two locations of the brain and a contrast agent to induce BBB disruption. The evaluation of results included also the examination of the distributions of TJ-specific transmembrane proteins (occludin, claudin-1, claudin-5 and submembranous ZO-1). These proteins are critical components of the tight junctions that prevent diffusion [98]. Tests performed at several time periods after sonication showed that leakage of agents was accomplished after application. At the same time periods, disintegration of the TJ proteins was also observed which proves the BBB disruption. At 6 and 24 h after sonication the function of the TJs was fully restored and no leakage was observed anymore. This means that the BBB disruption was achieved and then restored in its initial state with no side effects [55].

The difference in use of the ultrasound contrast agent was also investigated in 2007 [54]. McDannold et al performed experiments on rabbits using both Optison® and Definity® contrast agents on different rabbits to examine the feasilbility of using Definity® for BBB disruption. The same dosages of agents were used on 15 animals (9 with Definity® and 6 with Optison®) which were sonicated with twenty 10 ms pulses at a repetition frequency of 1 Hz. The two contrast agents had a similar probability of BBB disruption correlated with the pressure amplitude. However, for the conditions and parameters used in this specific experiment (at 0.5 MPa) Optison® produced larger effects with more areas of extravasations [54].

Marty et al investigated the leakage of magnetic resonance (MR) contrast agents according to their hydrodynamic diameter, but also estimated the duration of the BBB opening, something that was not defined until then [99]. Forty-seven rats were anesthetized and injected with different MR contrast agents with values of hydrodynamic diameters ranging from less than 1 nm to 65 nm. It was observed that nanoparticles with diameter of up to 65 nm could be delivered without any edema or hemorrhages while the BBB recovered fully within 24 hours. Small molecules (around 1 nm) could pass the BBB for more than 10 hours from sonication, where larger particles (around 25 nm) could only pass for a few minutes. This showcases that if large molecules are to be injected it should be done right after or during sonication.

Experiments for delivering exogenous and endogenous antibodies to the brain through the BBB using HIFU were made as a possible treatment for AD. One of these was conducted by Jordao et al on transgenic TgCRND8 mice [100]. The mice received a tail vein administration of ultrasound microbubbles to disrupt the BBB and the Magnetic Resonance Imaging (MRI) contrast agent Gadolinium, followed by an intravenous injection of an anti-Aβ antibody BAM-10. After the application of HIFU, it was observed that the mice that were sonicated and treated with BAM-10 showed a significant reduction of the plaques compared to other groups demonstrating that HIFU could disrupt the BBB and aid in delivering exogenous antibodies to the brain.

Another application that HIFU research was focused on is for the treatment of brain tumors. Nearly 20’000 patients are diagnosed every year with malignant brain cancers, where more than 50 % of them are considered to be as glioblastoma multiforme [68]. Yang et al [46][69]–[71] showed that pulsed HIFU along with human atherosclerotic plaque -specific peptide-1 (AP-1) which is combined with doxorubicin containing liposomes (Lipo-Dox) can act together for brain glioblastoma. The experiments were performed on a brain tumor mouse model which was sonicated with HIFU after administering AP-1 Lipo-Dox or just Lipo-Dox intravenously. Indeed, these animals showed increased accumulation of the drug in tumor cells in conjunction with control animals that were not sonicated. Also, these experiments demonstrated that with the combination of these two methods the tumor growth ratio was decreased even more compared to chemotherapy itself.

Apart from animal models, HIFU research is widely based in the use of gel phantoms for performing experiments. Phantoms consist a valuable tool for gaining knowledge and for further development of HIFU applications. Unfortunately though, there is no well-known phantom to be used to represent BBB disruption until now. There are different materials used to create a phantom which mimics tissue and its acoustic properties. Phantoms can be made from various materials: gelatin [101]–[103], agar [104]–[106], polyurethane [107], polyacrylamide [21]- [22], N-isopropylacrylamide [110] and polyvinyl alcohol cryogel [111]. Gelatin based gels are low cost and used mainly for mimicking soft tissue while different additive materials are used. If no preservatives are added, they are vulnerable to microbial contamination. Also, they have a low melting point of 35 ^{o}C [101]–[103]. Agar phantoms are cheap and easy to produce, durable in high temperatures, nontoxic, disposable and with a melting point of 65 ^{o}C [112]. On the downside they lack of long term stability [112]. Polyacrylamide phantoms are also widely used in combination with bovine serum albumin [113]. They are transparent and can be used several times. Their production though includes handling of acrylamide which is a known neurotoxin and a carcinogen.

This study aims to develop a phantom which mimics the BBB and can be used to evaluate HIFU protocols. This phantom improves the way experiments on the BBB are performed, because animal models can be avoided. This significantly reduces the cost and time needed for the experiment to be done providing a new innovative option for researchers. Also, it is a useful tool for training purposes and gives new opportunities for research in this area to develop with a faster pace and more precise protocols. Tubes demonstrate the function of the BBB vessels which do not allow any drugs to leak into the phantom and get disrupted when acoustic waves of HIFU are applied.

The aim of this study was to demonstrate a model that would have a constant liquid circulation that would allow liquid leakage only after HIFU were applied. There was no attempt to use materials that would have the same structure as BBB but establish a model that produced liquid leakage during the application of HIFU protocols.

2.2 Materials and Methods

An experimental setup that was used in all experiments was developed, which included a proper holder for the ultrasound transducer and the tube representing the artery. The design was done using the software Autodesk Inventor Professional 2019 (Autodesk, United States) and then printed in acrylonitrile butadiene styrene (ABS) plastic material by a 3D printer (FDM400, Stratasys, 7665 Commerce Way, Eden Praire, Minesota, 55344, USA). The design drawings of the experimental setup can be shown in Figure 8. Figures 8A and 8B demonstrate the complete drawing of the setup, Figure 8C shows a side view of the setup and Figure 8D shows the top view. The set up comprised a holder for the ultrasound transducer at the bottom and a holder for the tube which is used to mimic liquid circulation. Then this is immersed in a degassed water bearing container, which provides the coupling needed for the transducer to interact with the tube or phantom. The water in all cases is degassed using a two-stage vacuum pump (VP2RS-3, VC2523AG, Vacuum Chambers, Poland). The tube holder’s height is always adjusted so that the transducer’s focal spot is exactly at the point the sonication is needed.

The concept of this model is to use a proper tube that would be placed steadily in the tube holder, having a liquid circulation through it. During the experiments different types of tubes were developed and tested. Tubes of different dimensions bearing holes in numeral sizes and shapes were used attempting to seal these holes by testing various materials. Some of the materials unsuccessfully used were gypsum, glue, instant glue, tape, 3D printer support, plasticizer etc [114].

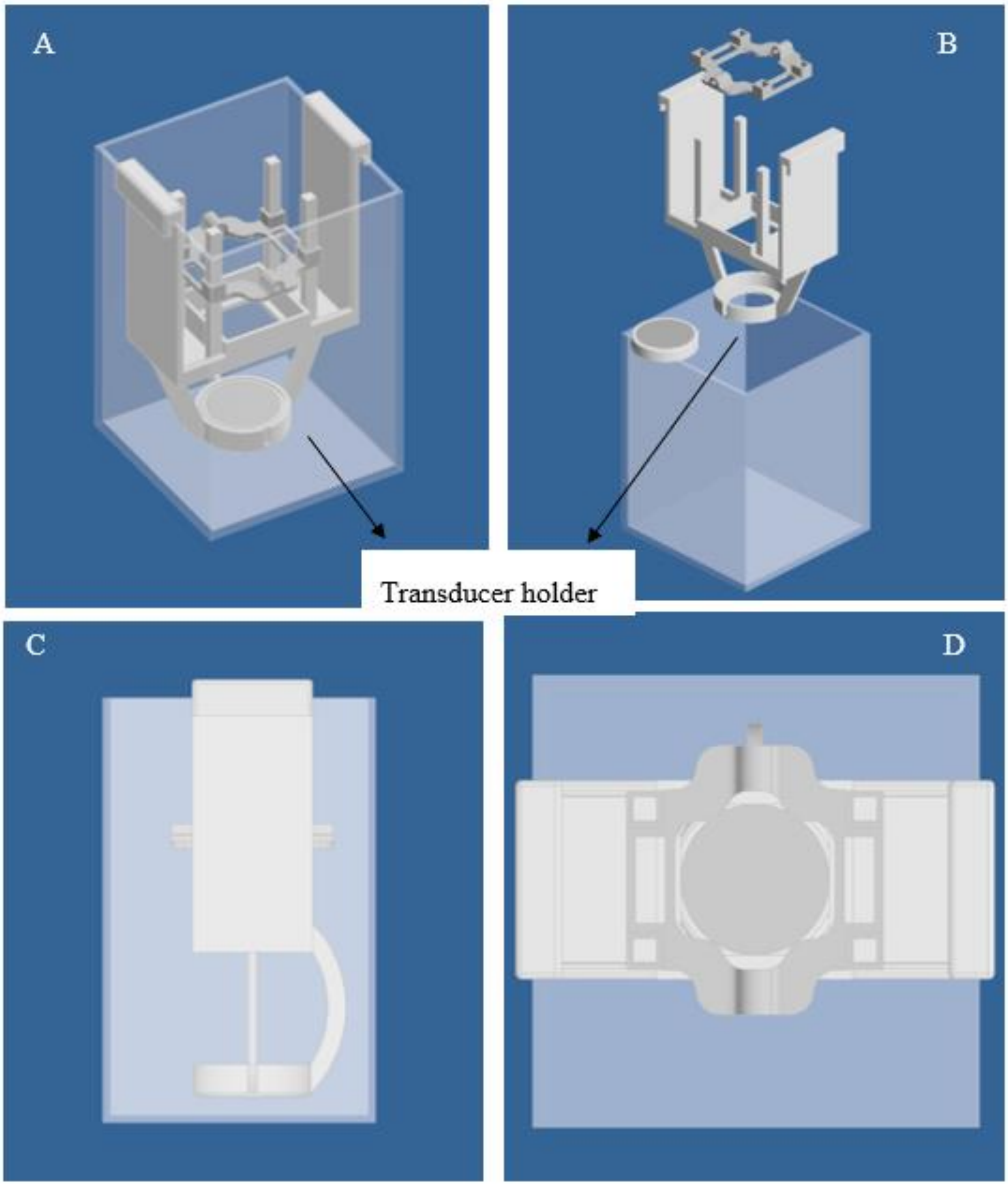

Figure 8 : (A) and (B) complete view of the experimental setup, (C) side view of set up and (D) top view of set up

The first successful experiment performed using a tube designed with Autodesk Inventor Professional 2019 (Autodesk, United States) and 3D printed with polylactic acid (PLA) plastic using the 3D printer (Ultimaker 3, Ultrimaker, Gendermalsen, Netherlands). The tube has a diameter of 4.4 mm, length of 40 mm and wall thickness of 1 mm with multiple openings of 0.4 mm thickness around its perimeter. The tube has three similar openings at an angle of 120°. Figure 9A and 9B show the design drawing of this tube, Figure 9C shows the actual printed tube and Figure 9D shows the internal view of the tube with all three openings. The liquid to be circulated used in this experiment was natural pomegranate juice (100 % natural juice, HCS AE, Greece) which is easily visualized during leakage. This liquid is circulated using a peristaltic pump (7518-60, Masterflex L/S, Germany). The tube lesions are hermitically sealed with a homogenous thin layer of a mixture of paraffin and vegetable oil wax.

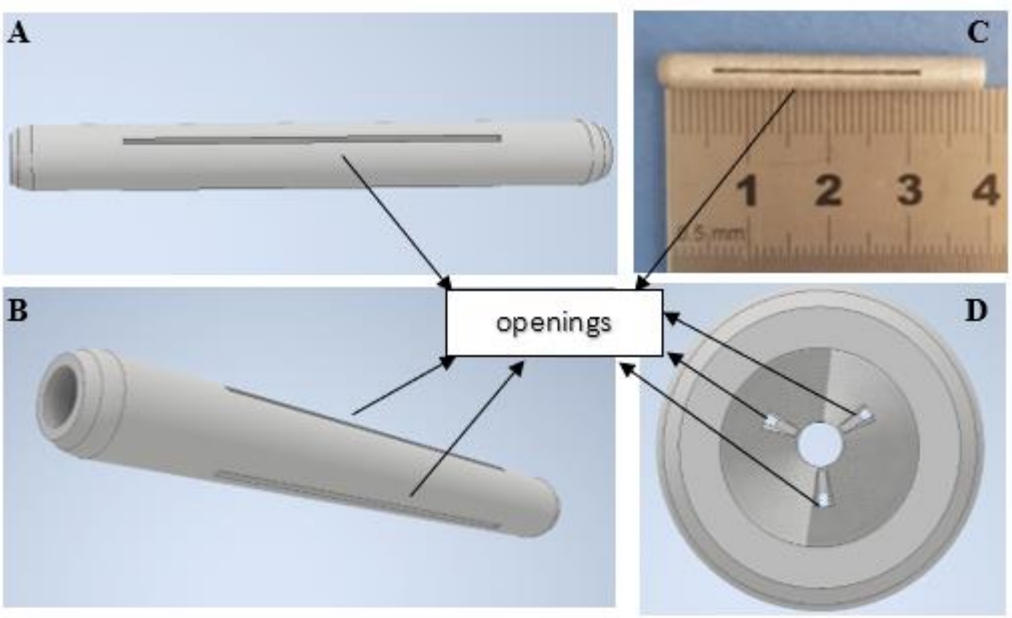

Figure 9 : (A) and [B] View of the tube design, (C) actual printed tube showcasing the dimensions and [D] inner view of the tube showing the three openings.

The HIFU system used in all experiments is consisted of a spherical in-house transducer operating at 0.5 MHz with a diameter of 50 mm and geometric focus of 100 mm. The transducer was driven by an RF generator (RFG 750, JJA instruments, Duvall, WA 98019, USA). The sonication was adjusted using an in-house software previously developed in C# (Visual Studio 2010 Express, Microsoft Corporation, USA) [115]. The electrical power of 150 Watt was applied with a duty factor (DF) of 10 % and pulses of 10 ms for a duration of 60 seconds. The -3 dB radial width was 3.2 mm and the -3 dB axial length was 26 mm. The purpose of the sonication was to provide short and strong pulsed waves to disrupt the sealing barrier by mechanical means. During the sonication, temperature of the tube was measured with a 100 μ thermocouple (Omega engineering).

In some of the experiments, prior to the application of the HIFU exposure an ultrasound contrast agent (SonoVue; Bracco SpA, Milan, Italy) was injected in the tube at a dose of 0.02 mL per 300 mL of liquid but results regarding this were inconclusive.

The sonication protocol described above was applied on the sealed tube and investigated visually whether a disruption of the wax layer could be achieved releasing the liquid in the container. After eight seconds of sonication, a leakage was visually observed demonstrating that the ultrasound pulses disrupted the layer releasing the liquid from the tube's lesions. Figure 10A shows the experimental setup before and Figure 10B shows the set up after sonication. After the disruption was achieved, liquid was released. Figure 11 shows the disrupted layer from the tube after the sonication was done and the tube removed from the set up. During the sonication the maximum temperature never exceeded 1.5 ^{o}C indicating mechanical effects.

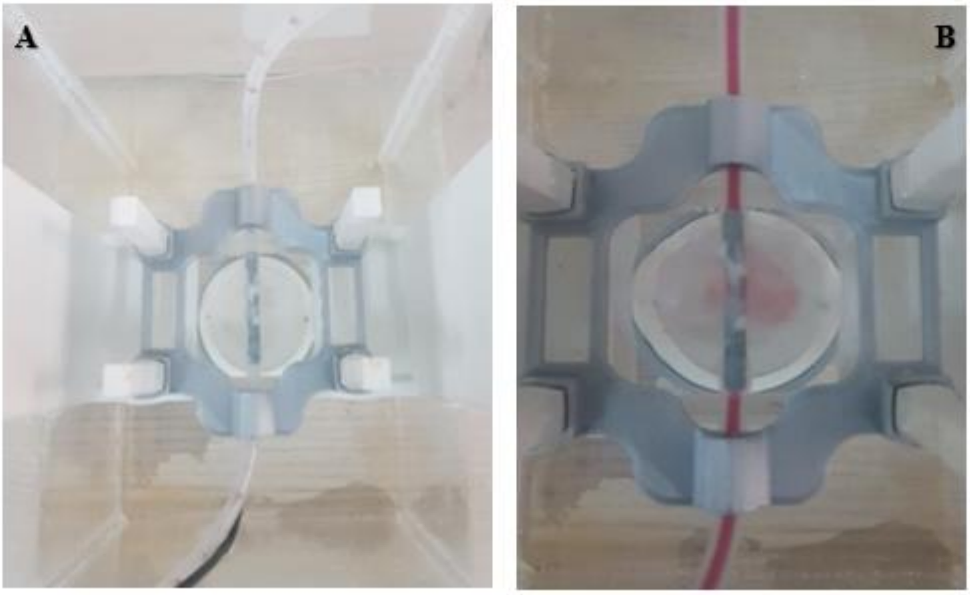

Figure 10 : A) Experimental set up before any sonication (B) Experimental setup during sonication and after liquid leakage with 150 W, DF 10 %, PRP 10 ms, pulse duration 60 sec, frequency 0.5 MHz, diameter 50 mm and geometric focus 100 mm.

Figure 11 : The disrupted layer of wax on the tube caused by the ultrasound sonication.

The experiment was repeated using the same exact parameters and protocols, to evaluate the repeatability of the model. It was observed that leakage was achieved also in that experiment, showcasing that the set up and protocol used produces constant results. Figure 12 shows the leakage during this experiment.

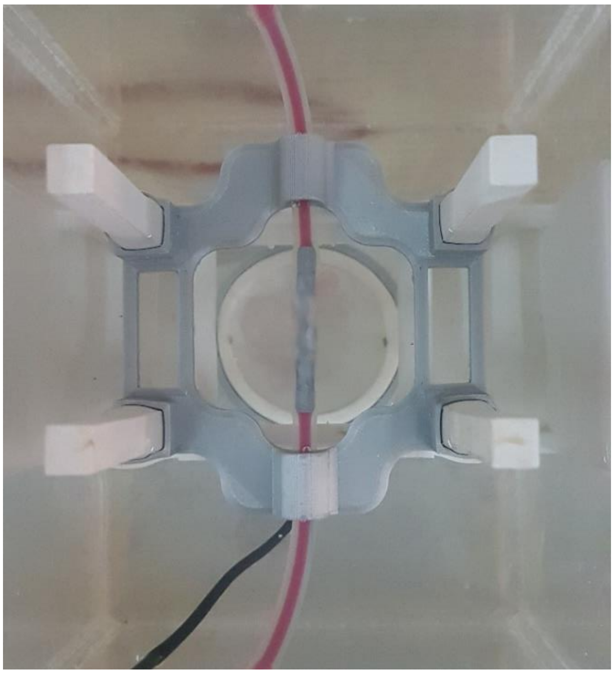

Figure 12 : Leakage during HIFU application using parameters 150 Watt, DF 10 %, PRP 10 ms, pulse duration 60 sec, frequency 0.5 MHz, diameter of 50 mm and geometric focus of 100 mm.

In order to define more parameters with this model, an experiment was performed varying the electrical power used. In this case, using the same tube and wax sealing, four experiments were done, ranging the electrical power from 50 W to 200 W and keeping the rest of the parameters the same. This was done to investigate at which exact power level a leakage was achieved, but also to find a correlation of the leakage amount with increasing power. The actual values used were 50 W, 100 W, 150 W and 200 W. Liquid leakage and therefore disruption of the wax layer was only observed using electrical power of 150 W and 200 W. It was also observed that with higher power, a greater leakage was achieved. Figure 13 shows the leakage of these two experiments. Figure 13A shows the leakage using 150 W power while Figure 13B the leakage with 200 W power.

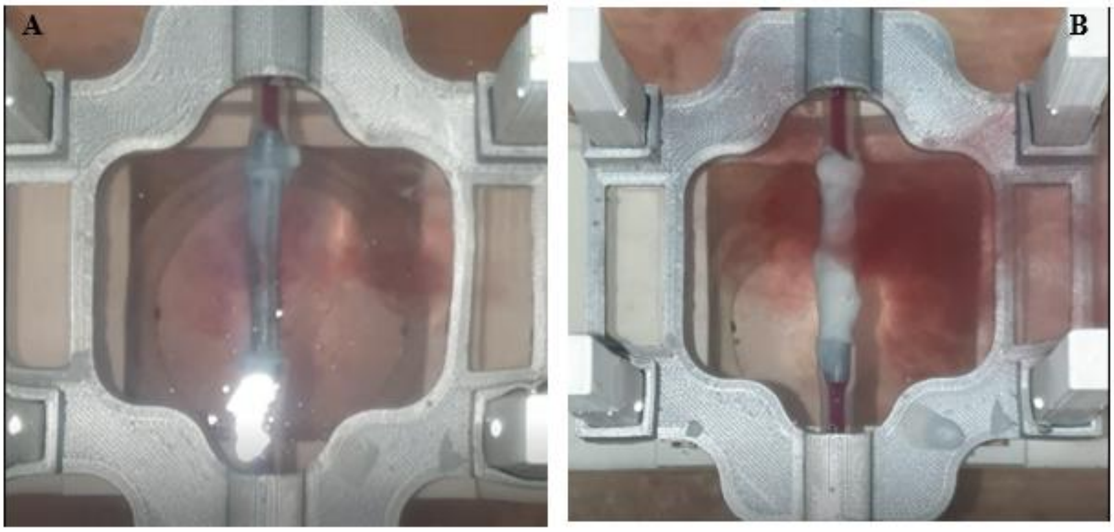

Figure 13 : (A) Liquid leakage using 150 W power (B) Liquid leakage using 200 W power and HIFU parameters, DF 10 %, PRP 10 ms, pulse duration 60 sec.

In addition, the setup was also slightly changed for this experiment implementing a volumetric cylinder in between the liquid circulation as shown in Figure 14, so the loss in liquid caused by the leakage would be measured. This could help in quantifying the liquid leakage apart from the visual observations. Since the liquid circulation is in a closed system, any loss is attributed to the liquid leakage caused by the layer disruption. In this case, the difference in the liquid volume (initial liquid volume – end liquid volume) was determined. During the first two experiments using 50 W and 100 W power, there was no difference in the liquid volume since there was no disruption of the wax layer. In the case of the third experiment using 150 W power, the calculated liquid leakage was found equal to 2 ml while in the case of 200 W power the leakage was 13 ml. This confirms that the higher power causes a larger leakage and effect compared to 150 W. This observation can be made visually also from Figure 13 where the leakage is significantly greater causing a bigger disruption of the layer. In this way, more liquid is released.

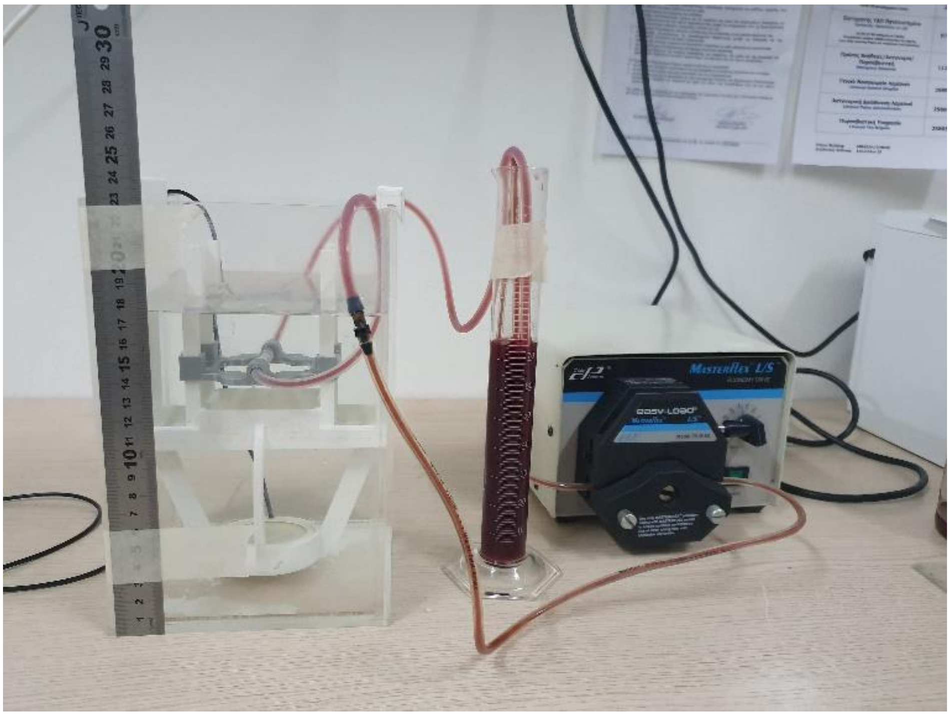

Figure 14 : Experimental setup including a volumetric cylinder to quantify the leakage.

In a continuation of the previous experiments, an attempt to standardize the thickness of the wax layer was made. Although in the experiments a correlation between the layer thickness and the leakage is not observed, since the layer never exceeded a thickness of 3 mm at any point, it is important to have a uniform layer throughout the tube eliminating any chance that this could have an effect. Therefore, a mold was designed using the software Autodesk Inventor Professional 2019 (Autodesk, United States) and then printed in chlorinated polyethylene elastomer (CPE) plastic material by a 3D printer (Ultimaker 3, Ultimaker, Utrecht, Netherlands). The set is comprised from a base that withholds the mold in a stable position and two identical compartments that create the mold when connected to each other. This design was made in order to be able to remove the connector easily from the mold without damaging the wax layer. The design drawings of the experimental setup can be shown in Figure 15. Figures 15A and 15B demonstrate the complete drawing of the setup, Figure 15C and 15D show the compartment from different angles.

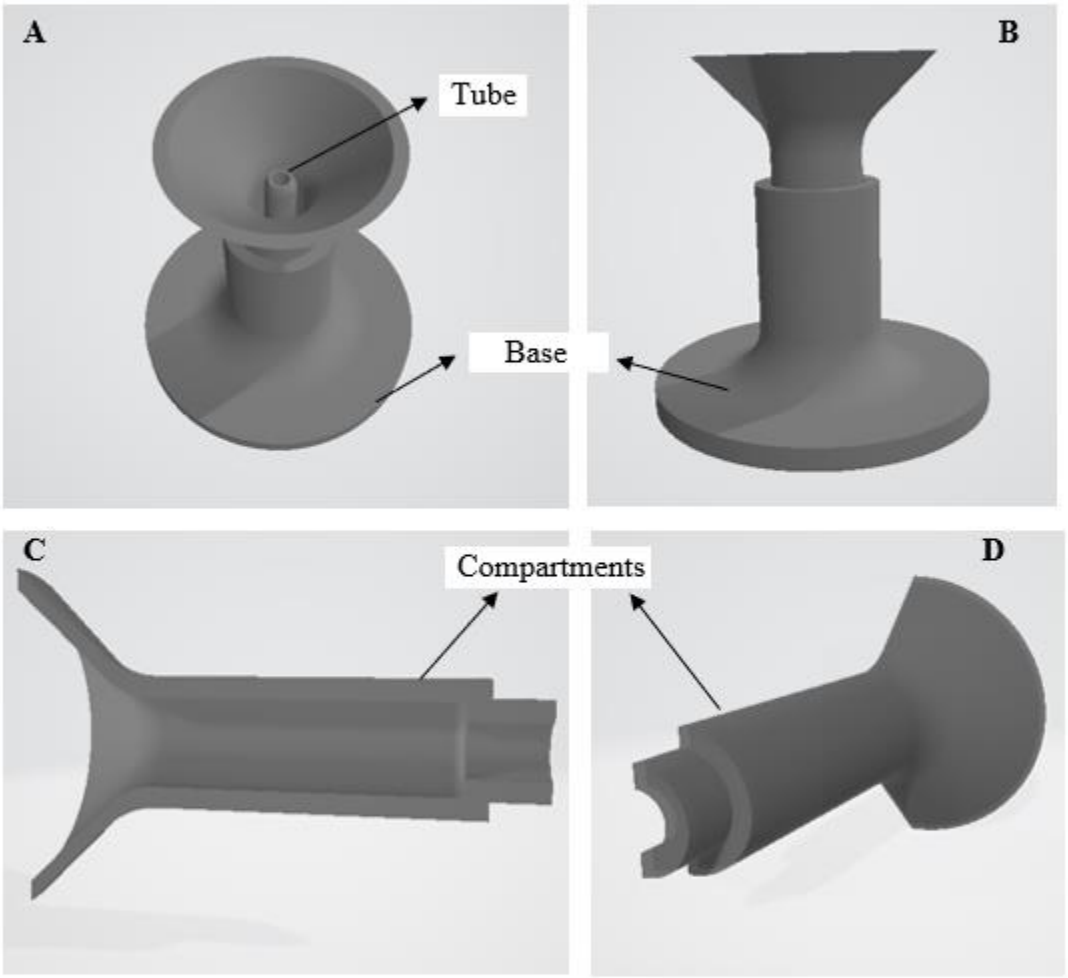

Figure 15 : Complete drawing of the setup (A), (B), Compartments from different angles (C), (D).

The mold was tested for its use, placing the tube connector in it, pouring liquid wax and waiting to solidify for a few minutes. The connector was then easily removed from the mold with a homogenous wax layer of 2 mm formed on its surface. Figure 16 shows the wax layer on the connector. The connector was tested with a HIFU sonication. Two differences are implemented on this experiment comparing with the previous trials. The RF generator is replaced by a combination of a signal generator Agilent (20MHz Function / Arbitrary Waveform Generator, LXI, California, USA) and an amplifier AG 1012 (AG Series Amplifier, T&C Power Conversion Inc., New York, USA). The output used was exactly the same as previously (150 W), while voltage of 520 mV produced the same power. Another change implemented, is the replacement of the pomegranate juice with a cherry red food colorant (Flair Color, Essex, UK) which again provides the desired red

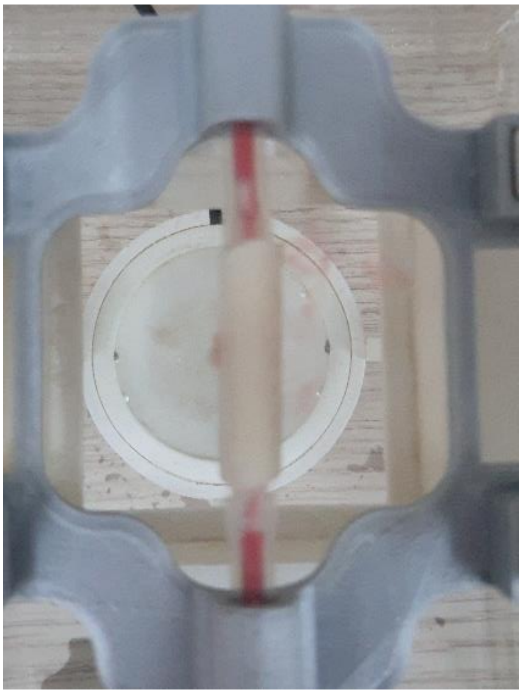

Figure 16 : Liquid leakage using 150 W power, DF 10 %, PRP 10 ms, pulse duration 60 sec, frequency 0.5 MHz, diameter of 50 mm and geometric focus of 100 mm.

colour but has more stability in time. After the protocol was applied, liquid leakage was observed as shown in Figure 16.

A different approach was investigated by replacing completely the tube connector and the wax layer by another material. The concept was to test if by removing these elements and by using only the silicone tube wiring could have the same effect and a more simple structure. Holes of 2 mm diameter were punctured on the silicone tube. This size allowed no liquid leakage before HIFU application, providing possibility of a leakage after HIFU application. Therefore, this setup was tested using again the same equipment and parameters (520 mV, 150 W, DF 10%, PRP 10 ms and pulse duration 60 s). After sonication, liquid leakage was observed from the tube, but in a small amount compared to previous experiments. Figure 17A and 17B show this leakage.

An important part of the creation of the phantom model for BBB disruption was also to test this setup in an agar phantom and see what evidence can be extracted from this combination.

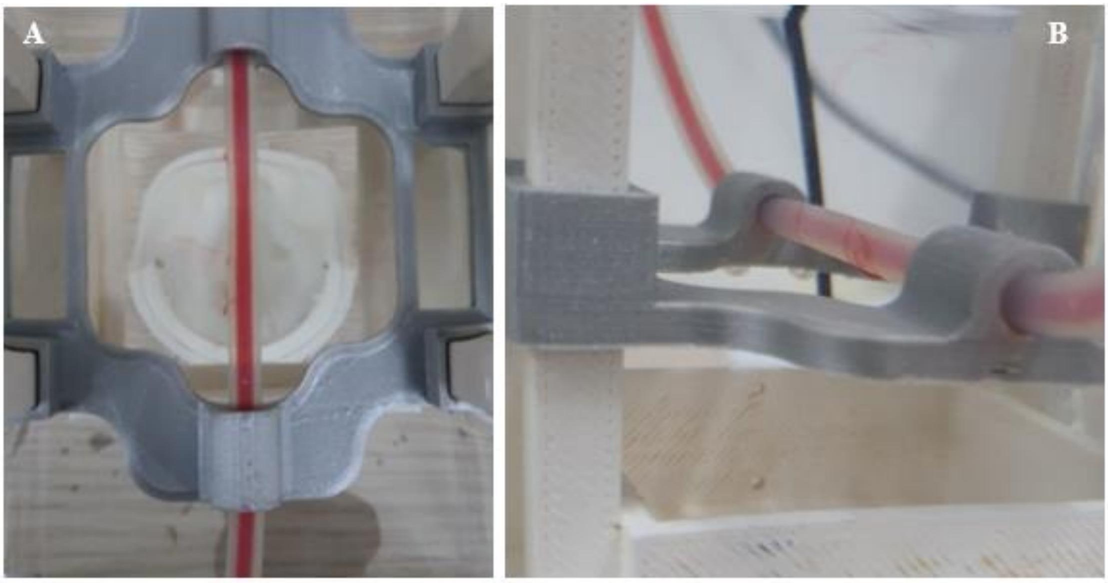

Figure 17 : (A) and (B) Liquid leakage from the silicone tube using 150 W power, DF 10 %, PRP 10 ms, pulse duration 60 sec, frequency 0.5 MHz, diameter of 50 mm and geometric focus of 100 mm.

Two experiments were performed in this direction, using a tissue mimicking phantom created in-house using 6 % w/v Agar, 4 % w/v Silicon Dioxide and 30 % evaporated milk. These concentrations were selected from previous studies resulting in a phantom mimicking brain tissue [112]. The preparation includes dissolving agar and silicon dioxide in water and heating it to 90 ^{o}C. After it reaches the desired temperature the mixture is let to cool down and when it drops to 50 ^{o}C, the evaporated milk pre-warmed also at 50 ^{o}C is added. The mixture is then poured in a container and let to solidify. For the purpose of these experiments, the previously used tube was sealed with wax prior the phantom preparation and then placed in the phantom as described below. The HIFU protocol used for sonication was slightly modified now: the power was increased to be able to overcome the attenuation of the agar phantom. According to the correlation between the signal generator voltage of the Agilent generator (20MHz Function / Arbitrary Waveform Generator, LXI, California, USA) and the electrical power from the amplifier AG 1012 (AG Series Amplifier, T&C Power Conversion Inc., New York, USA) as shown in Figure 18, for the maximum achievable electrical power of 500 W the equivalent voltage to use was 1320 mV. This comes to an equivalent value of 156 W acoustical power. The rest of the HIFU parameters remained the same (0.5 MHz, 10 % DF, 10 ms PRP and pulse time 60 s).

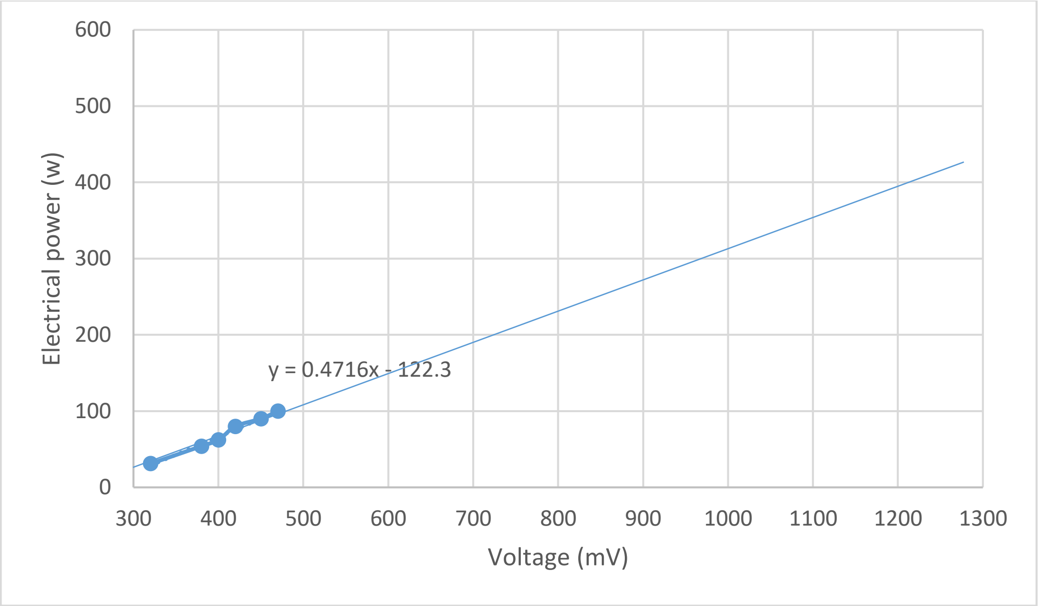

Figure 18 : Correlation between voltage and electrical power.

The first experiment was done using the same 3D printed PLA tube connector with 0.4 mm holes in 120^{o} angle between them. The tube was placed in the tube holder and was sealed with a wax layer as shown in Figure 19.

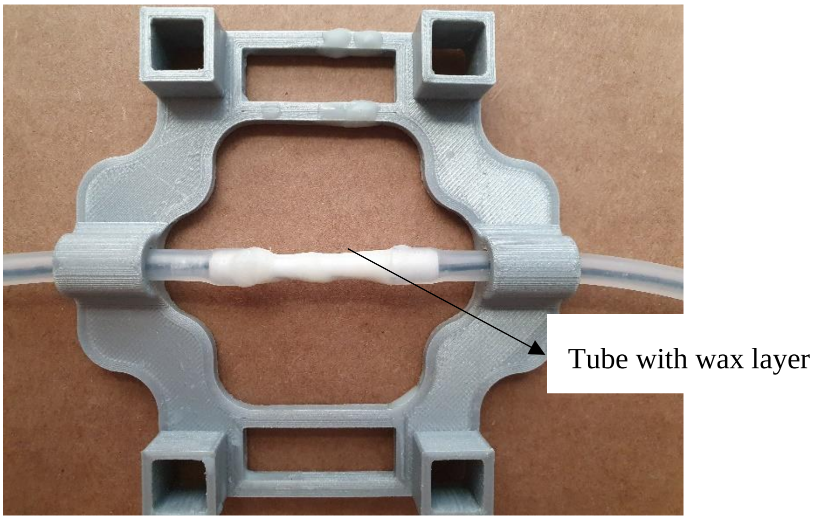

Figure 19 : Tube connector sealed with wax and placed in position on tube holder.

Then, the agar phantom was prepared as previously described but before pouring it in the desired container, the tube holder was placed in steady position in the container. In this way the tube holder would be included in the phantom creating in this way a layer of 2 cm of phantom around the sealed tube. The phantom solidified and then sonicated. Figures 20A and 20B show the phantom with the tube holder.

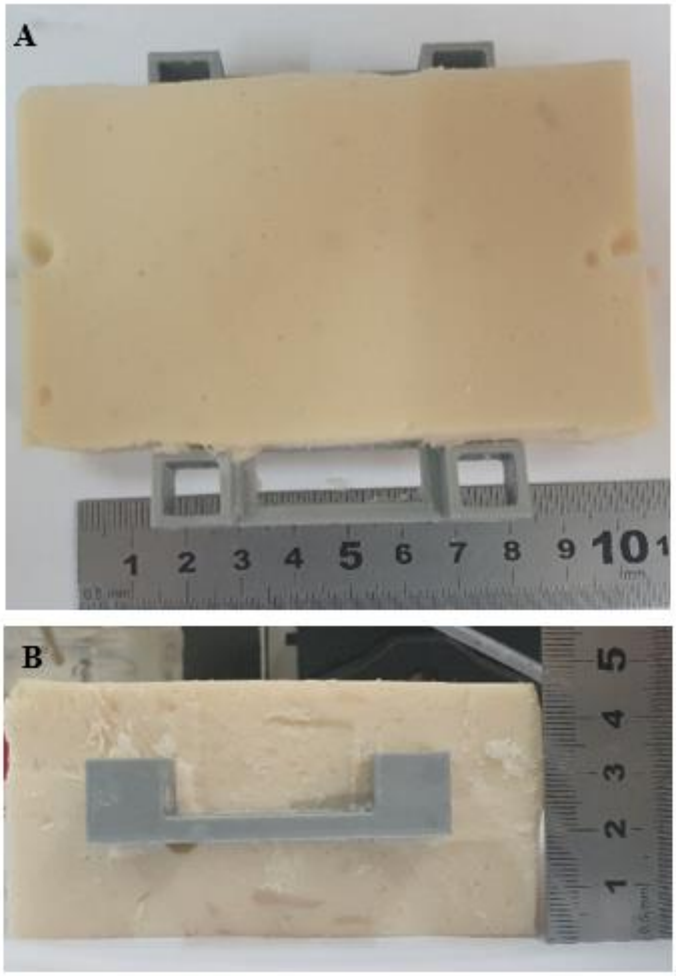

Figure 20 : A) Agar phantom containing sealed tube and holder top view and B) side view.

Before sonication the phantom was again tested for any possible leakage due to a wax disruption that might occurred during the preparation of the phantom. The phantom was then placed in position and was sonicated using the parameters mentioned before. No obvious leakage was observed when applying the sonication. The phantom was removed, cut open and the wax layer was examined carefully for any signs of disruption. No visible signs were observed. After the removal of the agar phantom, the tube was placed back in position and tested for leakage with HIFU application and the same protocol as previously used. The layer was disrupted causing some small leakage.

In order to investigate also the fact the maybe the agar phantom holds tightly the wax layer without allowing it to be disrupted, a second experiment was performed with one difference. A hole of 9.5 mm was punctured on the phantom from edge to edge so that the sealed tube would pass through it leaving a gap of 3 mm between the tube and the

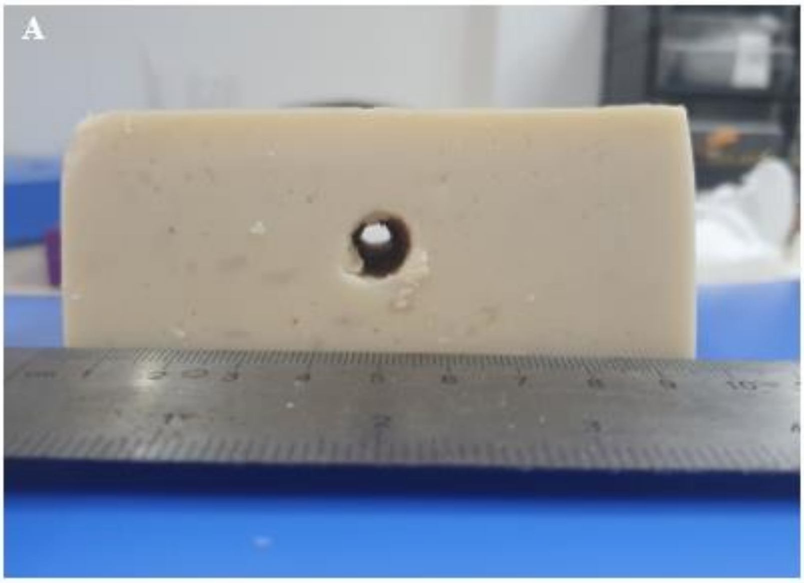

Figure 21: Agar phantom with hole to include a sealed tube.

agar phantom. In this case, the phantom would not block any possible disruption of the wax and the tube holder was no longer needed. Figure 21 shows the phantom with this modification.

Figure 22 shows the experimental setup of the phantom and tube before sonication. The tube holder was placed on top to provide more stability. The same sonication protocol was applied with no visible signs of leakage. After the end of the sonication, the phantom was removed, cut open and checked for any leakage or disruption of the wax layer. No visible signs of disruption were observed for this experiment.

2.1 Conclusions

This study was inspired by the fact that all of the experiments performed for BBB disruption are usually done on animal models thus there is a need for a model of BBB opening so that HIFU protocols can be easily tested. This makes experiments in this area expensive and time consuming. Therefore, trials have been made in order to create a suitable phantom model that would represent the BBB function and disruption during HIFU applications, showcasing the leakage that actually occurs during this disruption. An initial model was achieved, showcasing a liquid flow in a closed system under normal conditions and a liquid leakage after HIFU application, just like what actually happens during BBB disruption applications of HIFU. This can be used as a base for advancing

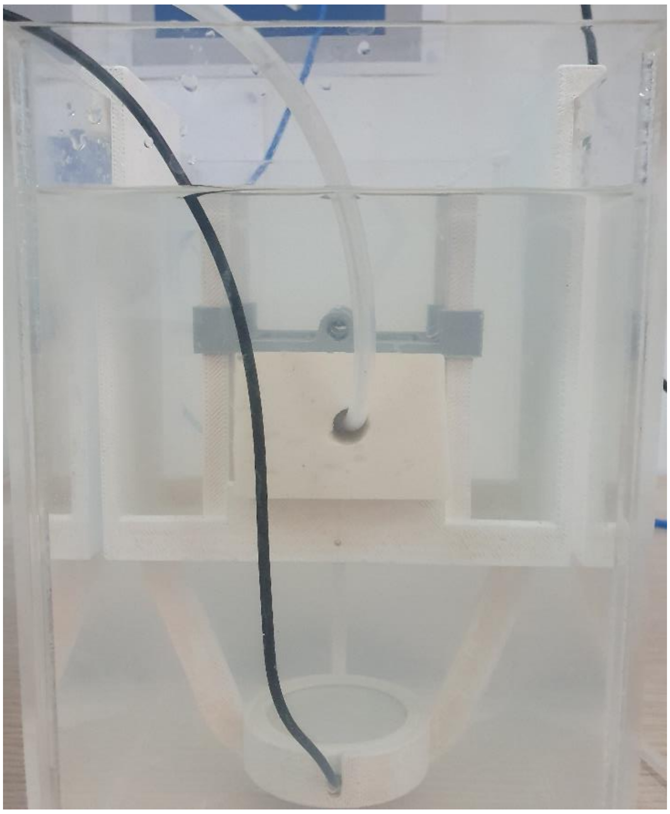

Figure 22 : Experimental setup before sonication.

and developing an accurate and innovative phantom model that will replace animal models in experiments. In this way researchers will be able to perform more accurate and cost-effective experiments using a phantom, testing several different protocols and parameters and gaining valuable knowledge for BBB disruption.

The proposed model is simplistic regarding its physical structure. Liquid leakage can be established with HIFU protocols. The intention with this study is to inspire researchers to develop more advanced models that mimic BBB opening. The attenuation of the agar phantom did not allow liquid leakage with the current equipment. This model though can be used as a basis for others to advance further and create a more complex model.

3 Ultrasonic attenuation of agar, silicon dioxide, and evaporated milk gel phantoms

3.1 Introduction

The attenuation coefficient is recognized as being a foundational acoustic property of tissue since it essentially governs the wave-tissue interaction. This main ultrasonic feature of tissues is attracting considerable the interest of many researchers over the last decades. The research interest arises from the need to achieve an accurate measurement of the attenuation coefficient which has been questioned as the results of several studies deviate using various techniques. The correct quantification of human tissues and TMMs attenuation coefficient is of great importance since it represents a key factor in the establishment of optimal HIFU treatment strategies [116].

An immersion technique to estimate the attenuation coefficient is the pulse-transmission method. This method was introduced by Nolle et al [117] in order to estimate the attenuation coefficient in high polymers. Following the same path in the 1960s and 1970s, McSkimin [118] suggested a method to measure the attenuation coefficient which was similar to the pulse-transmission technique. The different approach is that the pulsed signal is transmitted through the sample and received by a receiving transducer placed on the opposite side from the transmitting transducer. Two signals are recorded and analyzed, one without the sample and the other with the sample. A technique that compares the signals as received with different sample thicknesses was presented by Umchid et al [119]. In another technique [120], the attenuation coefficient was estimated using a transmitter and a receiver transducer with the main advantage that density estimation was not necessary.

The above techniques have been widely used to estimate the attenuation coefficient of numerous materials and tissues. Emphasis has been given in changing the attenuation coefficient concerning the percentages of different liquid or solid materials for the manufacture of TMMs with desired values close to those of humans. The main target of TMMs is the replacement of human tissues and their use for testing diagnostic ultrasound and HIFU applications. Although the attenuation measurement methods may have imperfections and inaccuracies, nevertheless, the estimation of the attenuation coefficient of human/animal tissues and TMMs with the same technique would give comparable results.

In recent years there has been considerable interest in TMMs in the field of focused ultrasound. In the literature, there is a surprisingly high number of developed TMMs for which their attenuation coefficient was estimated and identified with values close to many tissues. The attenuation coefficient of polyvinyl chloride-plastisol (PVCP) gels doped with powder (PVC or graphite) was investigated using the through-transmission technique [121]. The acoustic attenuation values of this material were found to be similar to fat tissue. Polyacrylamide gels combined with bovine serum albumin (BSA) were also prepared and tested [122]. Different amounts of intralipid were added to modify the ultrasonic absorption properties. The increase of intralipid concentration caused an increase in the attenuation coefficient from 0.26 dB/cm-MHz without intralipid to 0.78 dB/cm-MHz with 60 % volume to volume (v/v) intralipid concentration.

The pulse-echo method was used in another study to estimate the attenuation of agarose phantoms doped with alumina powder granulation (Al_2O_3) in 3 different manufacturing techniques (manual, mechanical, or magnetic stirring) [123]. The acoustic attenuation of phantoms differed with the various stirring techniques. The developed phantoms with mechanical stirring presented a higher attenuation coefficient than the other 2 manufacturing techniques. Polyvinyl-alcohol cryogel (PVA-c) phantoms with a different number of freeze-thaw cycles have been produced and their attenuation was investigated [124]. The attenuation coefficients were in the range of 0.085–0.124 dB/cm-MHz with the lowest value resulting from a single freeze-thaw cycle and the highest one from three cycles.

The suggested attenuation coefficient slopes for use in phantom materials vary from 0.3-0.7 dB/cm-MHz [125]. Whole milk, evaporated milk, liquid, and solid agar-based TMMs were previously developed and tested [126]. Bovine milk has been reported to exhibit a proportionality between the attenuation coefficient and a frequency over a wide range of 1-40 MHz. The attenuation of homogenized whole milk was also measured, and a slope of 0.35 dB/cm-MHz was found [126]. Thereby, whole milk can be only considered as a valuable liquid material to replicate low soft-tissue attenuation coefficient. Evaporated milk contribution to attenuation was studied and an attenuation coefficient slope of about 0.8 dB/cm-MHz was calculated [126]. The dissolution of evaporated milk with water enables the selection of any lower slope attenuation coefficient in the range of 0.3-0.7 dB/cm-MHz. Estimating the attenuation of agar-based gels at frequencies greater than 20 MHz makes them possible for potential use in high-frequency applications [127]. The attenuation of an agar-based phantom that mimics brain and muscle tissue was also reported in a study by Menikou et al [112]. The brain tissue-mimicking gel resulted in an attenuation value of 0.59 dB/cm-MHz and the muscle TMM in a value of 0.99 dB/cm-MHz.

The slopes of the ultrasonic attenuation coefficient versus frequency for agar-based gels doped with glycerol have been shown to lay in the range of 0.35–0.46 dB/cm-MHz at 22 ◦C, which serves as a good approximation for the attenuation of many soft tissues [128]. For weight percent concentrations of up to 10 % of glycerol, the increase in attenuation coefficient slope was less than 0.02 dB/cm-MHz. Typical hydrogel values have been reported to be in-line with the attenuation values of non-doped agar-based gels and polyacrylamide (PAA) materials with values lower than 1 dB/cm [109], [129]. Polydimethylsiloxane (PDMS) samples demonstrated significantly higher attenuation values compared with samples of agarose and PAA materials [128]. Although attenuation values increase with material concentration, there were no statistically significant variations between the different quantities of non-doped materials. For high nanoparticle concentrations, statistically important variations were observed approximately between doped and non-doped samples [130].This demonstrates that the addition of barium titanate ($BaTiO_3$) nanoparticles increases the attenuation coefficient of agarose, PAA, and PDMS gel phantoms.

Gelatin-based phantoms comprised of dry gelatin, n-propanol, and preservatives were produced and their attenuation was adjusted between the range of 0.2-1.5 dB/cm-MHz by varying the concentration of graphite [131]. It has been stated that the attenuation increases as the amount of gelatin powder increases [102]. In another study [132], the attenuation of poly(vinyl alcohol) cryogel was found to be low in the range of 0.075 to 0.28 dB/cm-MHz. However, the addition of enamel paint increases the values close to the values of human tissues. Standard BSA polyacrylamide hydrogel was also found to have a low attenuation coefficient using the pulse-echo method [108]. Despite this, the addition of scattering glass beads and the rise of the concentration of acrylamide to 30 % increased the attenuation coefficient of polyacrylamide gels close to the value of diagnostic ultrasound systems. Commercial phantoms that are used in HIFU applications are available with an attenuation coefficient of 0.6 dB/cm-MHz [133]. Furthermore, the attenuation of polyacrylamide gels (with 9 % BSA) was approximately 8 times lower than that of soft tissues [113].

Agar has already been used as a fundamental material of TMMs due to its ability for having a high melting point (> 90 °C) [24]. This particular property makes agar ideal material for HIFU applications and ablative procedures without losing its integrity. The agar was selected to provide intermediate stiffness and elasticity to the phantom. Agar-based phantoms can resist to HIFU forces without cracking when HIFU applications are evaluated. Additionally, silicon dioxide powder was added to control scattering independently whereas evaporated milk served as a low scatter material that enhanced absorption [134].

This study reports the observed changes in the attenuation coefficient of agar-based phantoms with different agar, silicon dioxide, and evaporated milk concentrations. The attenuation coefficient of each sample was estimated using the through-transmission techniques for varying agar, silicon dioxide, and evaporated milk concentration.

3.2 Materials and Methods

Measurements of the attenuation coefficient were performed in tissue-mimicking agar-based materials and excised rabbit tissues. No patient data were included in this study. Therefore, no informed consent from patients or approval from an ethics committee was required.

3.2.1 Samples preparation

Agar-based gels with different concentrations of agar (Merck KGaA, EMD Millipore Corporation, Darmstadt, Germany), silicon dioxide powder (Sigma-Aldrich, St. Louis, Missouri, United States), and evaporated milk (Nounou, Friesland Campina, Marousi, Greece) were formed.

The following nine samples were prepared: three samples with different w/v agar concentrations for each sample (2 %, 4 %, 6 %); three samples with different concentrations (w/v) of silicon dioxide (2 %, 4 %, 6 %) for agar concentration of 6 %

w/v; and three samples with different v/v concentrations of evaporated milk (10 %, 20 %, 30 %) for 6 % w/v agar and 4 % w/v silicon dioxide.

The manufacturing process until the addition of agar was the same for all the samples. The procedure was slightly differentiated after the addition of agar and depended on the number of materials used. Initially, ultrapure degassed/deionized water was slowly heated and continuously stirred using a magnetic stirrer (SBS, A160, Steinberg Systems, Germany) for a period of 10 minutes until its temperature reached 50 ^{o}C. During the procedure, the temperature increase was monitored using an electronic thermometer (Omega Thermometer, HH806AU, Omega Engineering, Norwalk, Connecticut, USA).

For every batch, the agar content was added slowly in degassed/deionized water to mitigate aggregation. It is worth mentioning that since agar was in granular form with a particle size of approximately 1400 μm, it was first ground into powder before mixing with water to promote homogeneous jellification in the absence of impurities. In case no other material was added, the mixture was let to heat until it reached 90 ^{o}C and then to cool down to 50 ^{o}C. High temperatures allowed agar's bonds to break and bind to the rest of the mixture (in case other materials were added). During the cooling period, the mixture was continuously stirred with the magnetic stirrer. The mixture started to solidify when the temperature dropped at around 50 ^{o}C. The amount of water that evaporated during boiling was replaced. The evaporation of the water was estimated by following the same procedure without the insertion of the solid materials. The evaporated water was calculated by subtracting the remaining volume of water from the initial volume. Care was taken by stirring the solution gently to avoid the creation of air bubbles that are known to reflect ultrasound waves. When other materials were added to the mixture, the silicon dioxide was first added 2-3 minutes after the agar insertion. The mixture including both the agar and silicon dioxide was heated until it reached 90 ^{o}C. Afterward, the mixture was left to natural cool down to 50 ^{o}C. Following this, the evaporated milk (v/v) was heated to 50 ^{o}C and added to the rest of the mixture. For a final step, the whole mixture was stirred well to allow full dissolvement of all ingredients.

The preparation procedure for each phantom was simple and did not last more than 20 minutes. The mixture was poured into a Polylactic Acid (PLA)-designed mold and was let to jellify overnight at room temperature. The dimensions of each mold were 40 mm in height, 26 mm in width, and 32 mm in length with 3 mm thickness. Two open circular holes of 22 mm diameter were left on both sides of the mold container to allow ultrasound waves to propagate through the sample. The designed molds could be easily attached and fitted to the experimental setup, making them ideal for accurate attenuation coefficient measurements.

Attenuation measurements for the nine samples were taken within 24 hours post-fabrication to avoid decomposition by microbial growth. Thus, preservatives were not added but their use can be beneficial for prolonging shelf life needed when characterizing properties and their change over time. Figure 23A illustrates a computer-aided design (CAD) drawing of the PLA mold and Figure 23B shows the samples with different agar, silicon dioxide, and evaporated milk concentrations.

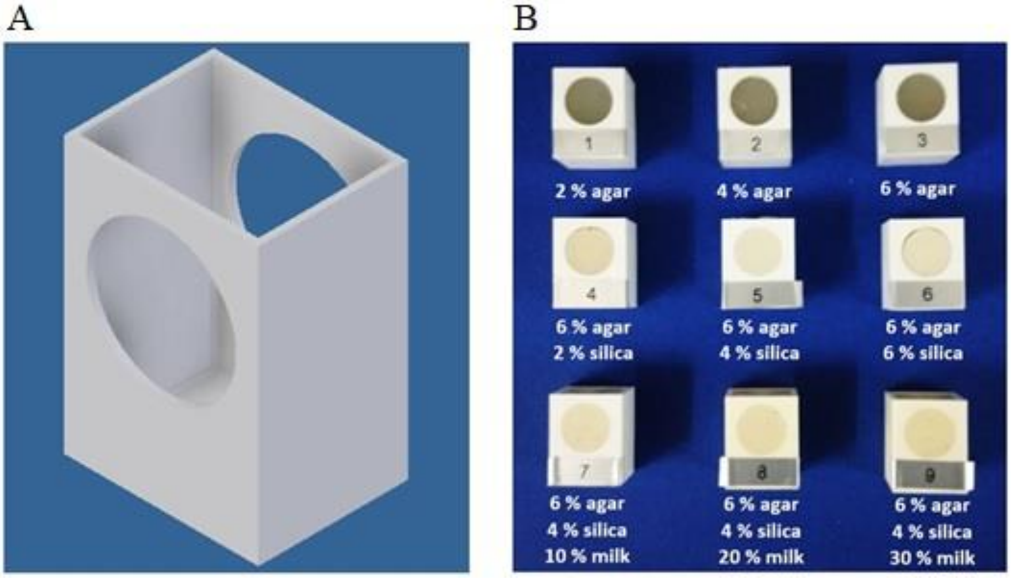

Figure 23 : A) Drawing of the PLA mold. B) Front view of the developed samples with different amounts of agar, silicon dioxide, and evaporated milk.

3.2.2 Experimental setup to measure the attenuation coefficient of agar-based gels

Attenuation measurements were conducted using the through-transmission technique, previously reported by Madsen et al [135]. Attenuation coefficient is an important acoustic property of tissues and gel phantoms especially designed for HIFU applications since it governs the efficiency of acoustic energy transformation into heat. Therefore, adequate matching with the respective replicated soft tissue coefficient is a matter of great importance.

Two well-known methods are broadly used to estimate the attenuation coefficient; pulse-echo and through-transmission method. Both techniques require the submersion of the sample in a tank filled with degassed/deionized water and all measurements are performed with immersion planar ultrasonic transducers. The through-transmission technique that was used herein, involved two planar transducers; one for transmitting the continuous ultrasound signal and one for receiving.

For the experimental setup, a special acrylonitrile butadiene styrene (ABS) plastic holder was designed (Inventor Professional 2018, Autodesk, California, USA) and printed using a 3D printer (F270, Stratasys Ltd., Minessota, USA) as shown in Figure 24. The ABS holder retained the planar transducers and the sample at fixed positions and provided stability for more accurate measurements. The holder included two cylindrical cavities for tightly fitting the transducers with their active elements facing each other. A 30 mm diameter planar immersion transducer (CeramTec, Plochingen, Germany) operating at 1.1 MHz, transmitted an amplified sinusoidal acoustic wave signal that propagating through 26 mm of the sample. The same type of transducer located 65 mm from the transmitter was used to record the attenuated resulting signal, which was displayed on a digital oscilloscope (TDS 2012, Tektronix, Inc., Karl Braun Drive, United States). Each sample was positioned in the near field of the emitting transducer where the intensity of the sound wave is relatively constant with distance traveled. Figure 24 shows the experimental setup for the attenuation coefficient measurements.

3.2.3 Analytical method to calculate the attenuation coefficient of agar-based gels

The attenuation in dB was calculated from the difference between the peak-to-peak voltage of the recorded signal from each sample compared to a reference signal traveling for the same distance in degassed/deionized water under the same experimental conditions. The attenuation coefficient was calculated in units of dB/cm-MHz by dividing the measured attenuation in dB with the product of the transmitting frequency (1.1 MHz)

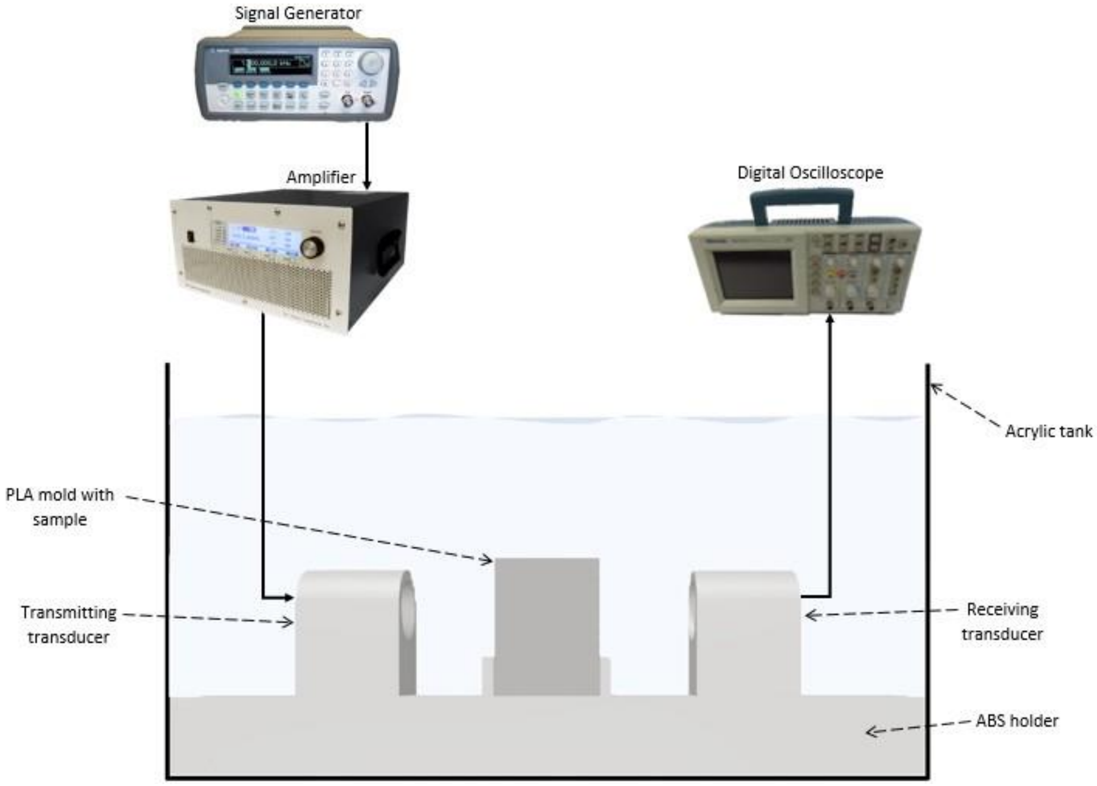

Figure 24 : Experimental setup for the measurement of the ultrasonic attenuation coefficient of agar-based gels with different amounts of agar, silicon dioxide, and evaporated milk.

and sample thickness. The calculated result included the attenuation induced by the propagation of the acoustic wave in water. One advantage of this technique is that there was no need to calculate the reflection or transmission coefficients at each interface [136]. The attenuation coefficient in units of dB/cm-MHz was calculated using equation 1 [137],

$$\boldsymbol{\alpha} = \frac{\mathbf{20}}{\boldsymbol{ln}\ (\mathbf{10})} * \left[\frac{\boldsymbol{ln}\ (\frac{\boldsymbol{A_s}}{\boldsymbol{A_r}})}{\boldsymbol{\Delta_x} * \boldsymbol{f}} + \boldsymbol{a_w} \right] \tag{1}$$

where $\mathbf{A_s}$ corresponds to the reference peak-to-peak voltage without the sample, $\mathbf{A_r}$ to the peak-to-peak voltage at the receiver side with the addition of each sample between the two planar transducers, $\boldsymbol{\alpha}_\mathbf{w}$ is the attenuation of water in Np/cm-MHz, $\boldsymbol{\Delta}_\chi$ is the sample's thickness in cm and **f** is the transmitting frequency in MHz.

This procedure was repeated 10 times, for each one of the phantom recipes under test. Ten (10) different samples of each recipe were manufactured and attenuation calculation was performed for each one, thus evaluating the stability of the measurement system and estimating the uncertainty in measurements.

3.2.4 Ultrasound imaging

A diagnostic ultrasound imaging system (UMT-150, Shenzhen Mindray Bio-Medical Electronics Co., Ltd., Shenzhen, P.R. China) was used to scan the sample with 6 % w/v agar and 4 % w/v silicon dioxide in order to check the echogenicity and the structural homogeneity of the sample.

3.2.5 Frequency dependence of attenuation

The frequency dependence of attenuation of the phantom recipe with 6 % w/v agar and 4 % w/v silicon dioxide was investigated in the frequency range of 1 to 2 MHz. For each ultrasonic frequency, the attenuation coefficient was calculated according to the previously described method, using equation 1.

3.2.6 Insertion loss

A slightly different method was then used, in order to estimate the insertion loss in the phantoms. The attenuation coefficient of the agar-based gels was estimated according to the variable-thickness method, using the same experimental set up described in the previous subsections (two identical transducers of 1.1 MHz central frequency fitted inside an acrylic tank at specific locations). Although, a different procedure was followed in the case of the variable-thickness technique, in which the signals through samples of different thicknesses are compared. For that purpose, specifically designed thinner molds (with a total volume of 10.0 cm^3) were printed using PLA material. In this case, the acoustic waves propagated through a 13 mm sample, as shown in Figure 25.

First, the thinner sample ($x_1 = 13\,mm$) was placed and the peak to peak voltage was measured on the oscilloscope. The procedure was repeated by replacing the specimen with the thicker one ($x_2 = 26\,mm$). The attenuation coefficient of each recipe was estimated by including the measured voltage in the presence of the thinner ($\boldsymbol{A_{x_1}}$) and thicker ($\boldsymbol{A_{x_2}}$) samples, together with the thickness of the samples and the ultrasonic frequency $\boldsymbol{f}$, in the following equation [13]:

$$\boldsymbol{a = \frac{1}{f} * \frac{20}{x_2 - x_1} * \ log\left(\frac{A_{x_2}}{A_{x_1}}\right)} \qquad (2)$$

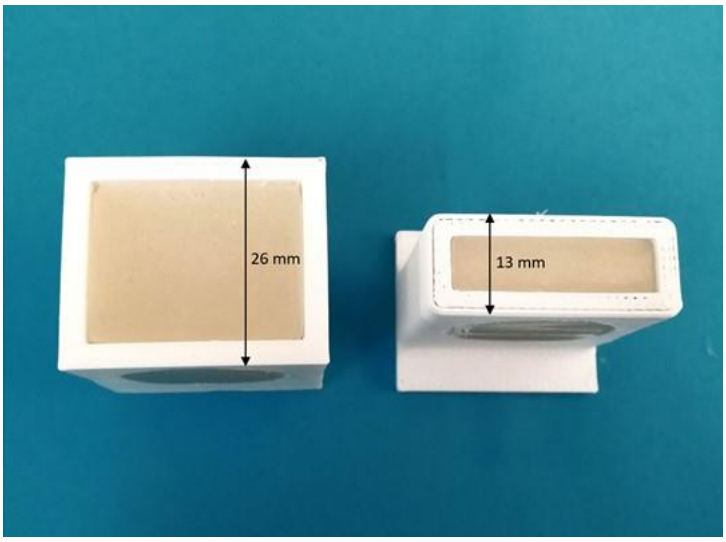

Figure 25 : Top view of the thinner and thicker mold used in the variable-thickness technique.

3.2.7 Ultrasonic attenuation in rabbit tissue

Ultrasonic attenuation in freshly excised rabbit tissues, including liver, kidney, and muscle was estimated according to the through-transmission method of the two identical planar transducers of 1.1 MHz central frequency, previously described for the attenuation measurement of the agar-based gels. Firstly, the soft tissues were carefully cut at a thickness of approximately 4 mm, placed in a vacuum chamber, and degassed such that microbubbles accidentally trapped in tissue were eliminated. The attenuation coefficient of each tissue was calculated using equation 1.

3.3 Results

Samples of different amounts of agar, silicon dioxide, and evaporated milk were prepared following a simple preparation procedure. The attenuation coefficient of each sample was calculated using the through-transmission immersion technique. In total 10 calculations of the attenuation coefficient were made for each recipe, in 10 different phantoms designed with the same concentration of agar, silicon dioxide, and evaporated milk, from which a mean value and a corresponding standard deviation were obtained. The estimated values can be seen in Table 2. Figure 26 shows the estimated attenuation coefficient with respect to the measurement number, for a recipe with 6 % and 4 % w/v agar and silicon dioxide respectively. The estimated values are normally distributed around a mean value of 1.10 ± 0.09 dB/cm-MHz.

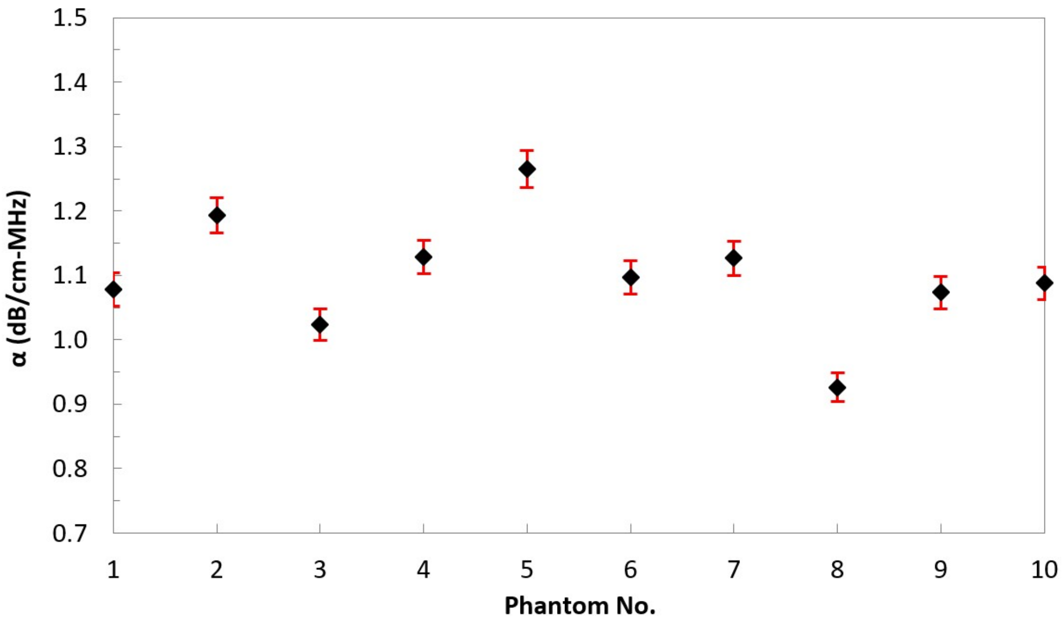

Figure 26 : Attenuation coefficient vs measurement number of the phantom with the optimum recipe (6 % agar, 4 % silicon dioxide). Uncertainty bars represent standard deviations.

The optimum recipe was defined as the recipe that was found (6 % w/v agar and 4 % w/v silicon dioxide) to possess an attenuation coefficient close to that of human muscle [138].

Initially, experiments were performed to estimate the attenuation coefficient by varying the agar concentration. Figure 27 shows the attenuation coefficient as a function of agar concentration (n=10) without any amount of silicon dioxide and evaporated milk. This was to done to assess the attenuation purely induced by agar in the absence of other materials that enhance scattering or absorption.

The next step was quantify the attenuation coefficient of agar-based gels by varying the amount of silicon dioxide and evaluate its effect on attenuation. Figure 28 shows the attenuation coefficient dependence of silicon dioxide concentration (n=10) using 6 % agar and 0 % evaporated milk. At low doses of silicon dioxide (< 4 %), the attenuation coefficient increased with an increase in silicon dioxide percentage. Although the increase of silicon dioxide concentration above 4 % increased scattering, however that scattering increment further lowered the ultrasonic absorption at a significant level as previously found [25] and the overall attenuation coefficient decreased.

According to the linear regression analysis ($R^2 = 0.995$), for silicon dioxide concentration up to 4 %, the attenuation coefficient increased by 0.101 dB/cm-MHz for every 1 % increase of silicon dioxide concentration.

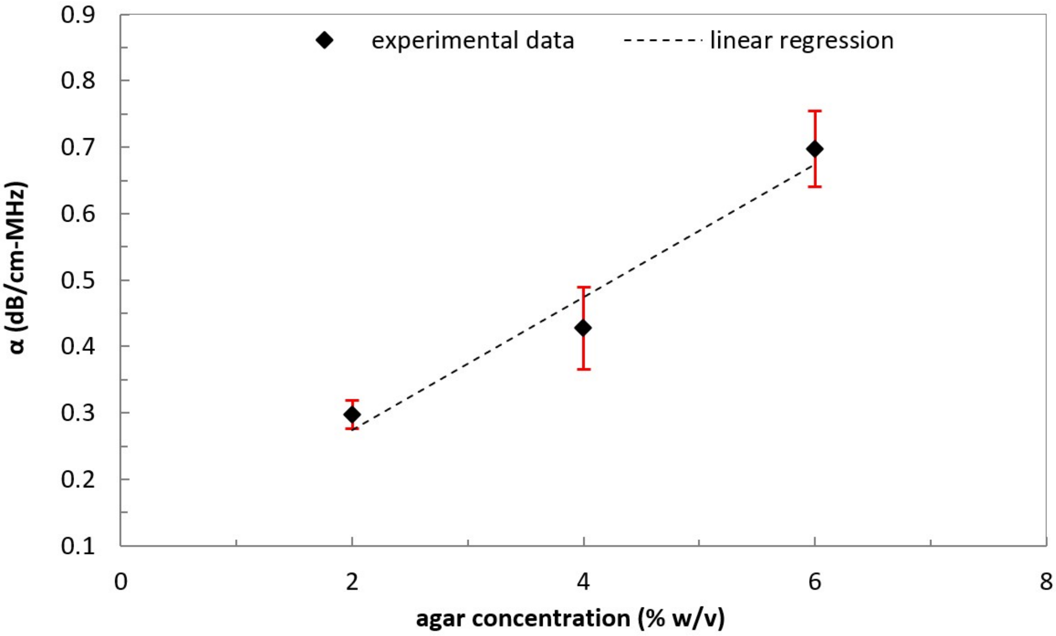

Figure 27 : Attenuation coefficient vs percentage of agar (n=10) for 0 % silicon dioxide and 0 % evaporated milk. Uncertainty bars represent standard deviations and the dashed line represents linear regression fitting (R2=0.961).

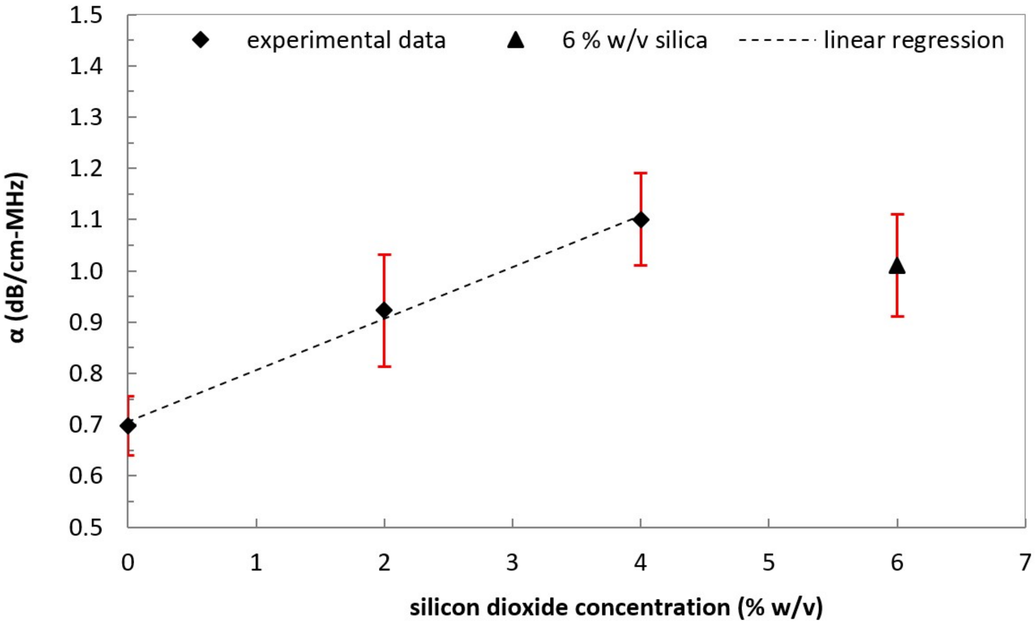

Figure 28 : Attenuation coefficient vs silicon dioxide (n=10) with 6 % agar and 0 % evaporated milk. Uncertainty bars represent standard deviations and the dashed line represents linear regression fitting (R2=0.995).

The effect of the variation of the evaporated milk amount on the attenuation coefficient of agar-based gels was also assessed. Figure 29 shows the attenuation coefficient versus the percentage of evaporated milk (n=10) for a preliminary agar and silicon dioxide concentration of 6 % and 4 % respectively. The sample lost its stiffness with an evaporated milk percentage of over 30 % as suggested in a previous study [134] and became too difficult to handle. Therefore, further investigation for higher evaporated milk concentrations was excluded. An attenuation coefficient increment of 0.013 dB/cm-MHz was observed for every 1 % increase of evaporated milk. The contribution of evaporated milk to the increment of ultrasonic attenuation was found to be significantly smaller than the one found for silicon dioxide.

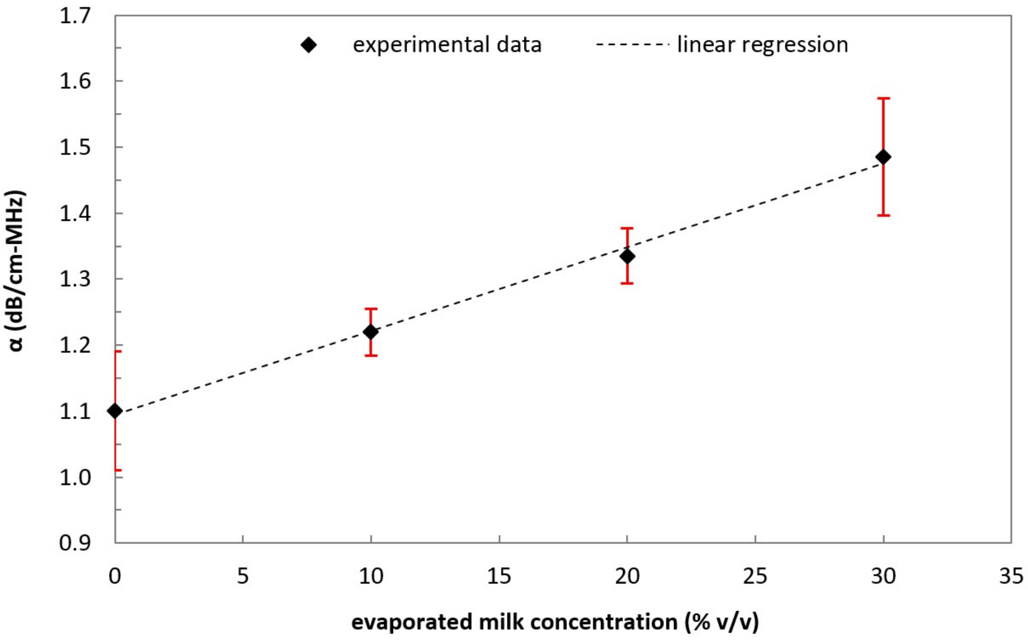

Figure 29 : Attenuation coefficient vs percentage of evaporated milk (n=10) for 4 % silicon dioxide and 6 % agar. Uncertainty bars represent standard deviations and the dashed line represents linear regression fitting (R2=0.996).

Further to the through-transmission method in which the signal through the reference (water) path is essential, the variable-thickness method was also used, in order to assess the insertion loss through the phantoms. As previously mentioned, using the specific technique, the signals through samples of different thicknesses were compared. Thereby, the ultrasonic attenuation due to the reflection phenomenon on the water/phantom interface was eliminated, and thus the results represented only the insertion losses (mostly absorption). The estimated attenuation coefficients were found to be smaller or very similar to the ones obtained by the through-transmission method previously used. This is mostly attributed to the fact that agar-based phantoms possess acoustic impendences similar to that of water [112], and thus the reflection on a water/agar-based gel interface is significantly small. The results obtained by both methods were compared as shown in Table 2, indicating a good agreement with the underlying theory.

Table 2 : The mean value of the attenuation coefficient and the corresponding standard deviation of each phantom, compared to the insertion loss obtained by the variable-thickness method.

Phantom Recipe			**Mean value of the attenuation coefficient (dB/cm-MHz)**	**Standard deviation (dB/cm-MHz)**	**Insertion loss (dB/cm-MHz)**	**Standard deviation (dB/cm-MHz)**
Agar (% w/v)	**Silicon dioxide (% w/v)**	**Evaporated milk (% v/v)**				
2	0	0	0.30	0.02	0.22	0.02
4	0	0	0.43	0.06	0.39	0.03
6	0	0	0.70	0.06	0.67	0.04
6	2	0	0.92	0.11	0.94	0.06
6	4	0	1.10	0.09	1.03	0.06
6	6	0	1.01	0.10	0.97	0.06
6	4	10	1.22	0.04	1.25	0.08
6	4	20	1.34	0.04	1.30	0.08
6	4	30	1.49	0.09	1.41	0.09

The sample with the optimum recipe (6 % w/v agar and 4 % w/v silicon dioxide) was scanned with a diagnostic ultrasound imaging system (UMT-150). The sample appeared with increased echogenicity due to the ability of silicon dioxide to scatter ultrasound waves as travel through the sample (Figure 30).

Figure 30 : Ultrasound image of the sample with the optimum recipe (6 % agar, 4 % silicon dioxide).

For the optimum recipe (6 % w/v agar and 4 % w/v silicon dioxide) further investigation was conducted for estimating the frequency dependence of attenuation. Figure 31 shows the estimated attenuation coefficient plotted against the probe frequency, in the frequency range of 1 to 2 MHz. The attenuation coefficient was found to varied from 0.97 (at 1.1 MHz) to 2.93 dB/cm-MHz (at 1.9 MHz). The least-squares method that was used to determine the line of best fit to data indicated a linear behavior (R^2 = 0.978), as shown in Figure 31.

The attenuation coefficient of freshly excised rabbit tissues was also estimated using the same experimental setup and formula used for the ultrasonic investigation of the agar-based phantoms. Overall, 10 measurements of the reference and attenuated (in the presence of the tissue) signal were made, approximately 1 hour after excision. The mean value of attenuation coefficient for samples of about 4 mm thickness, at 1.1 MHz, was found to be 0.86 ± 0.20, 1.18 ± 0.46, and 1.46 ± 0.44 dB/MHz-cm for the liver, muscle and kidney respectively. The estimated values for the soft tissues were compared to the ones obtained for the agar-based phantoms as shown in Table 3. The recipes with no evaporated milk were preferred due to their increased durability. An optimum amount of 6 % w/v agar, along with a silicon dioxide concentration of 0 to 4 % can be used to mimic the rabbit tissues. Generally, the phantom with 6 % and 4 % w/v agar and silicon dioxide concentration respectively was considered optimum for mimicking the rabbit tissue.

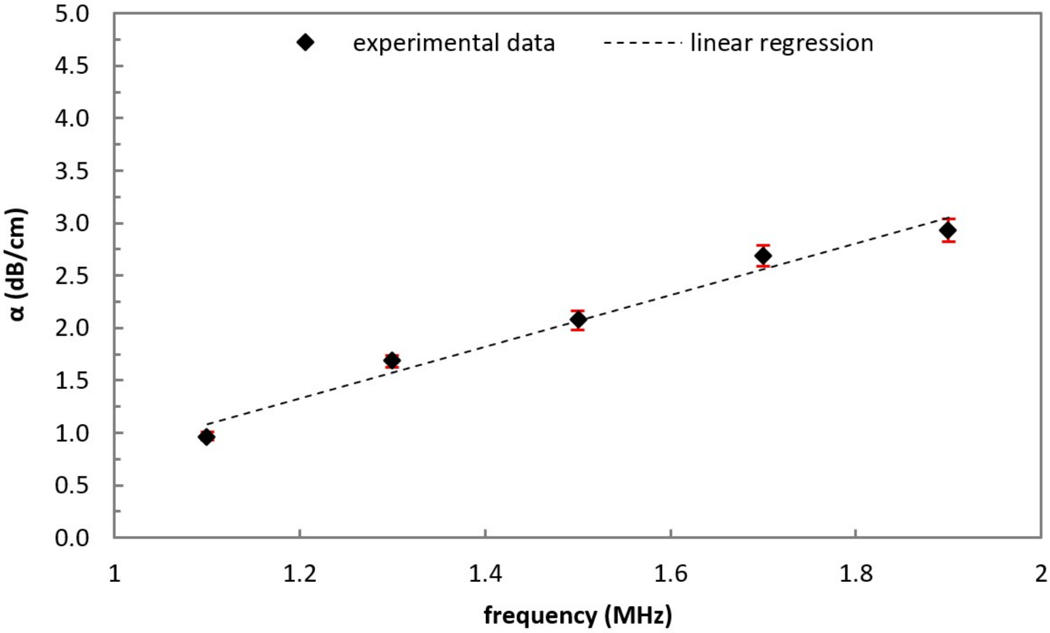

Figure 31 : The attenuation coefficient vs frequency of the phantom with the optimum recipe (6 % agar, 4 % silicon dioxide). Uncertainty bars represent standard deviations and the dashed line represents linear regression fitting (R2=0.9776).

Table 3 : The estimated mean value of the attenuation coefficient and the corresponding standard deviation of each rabbit tissue, and the phantom recipes that could be possibly used to mimic tissue.

Tissue	Mean value of attenuation coefficient (dB/cm-MHz)	Standard Deviation (dB/cm-MHz)	Phantom Recipe		
			Silicon dioxide (% w/v)	Agar (% w/v)	Evaporated milk (% w/v)
Liver	0.86	0.20	0-4	6	0
Muscle	1.18	0.46	2-4		
Kidney	1.46	0.44	2-4		

3.4 Conclusions

In this study, the variation of ultrasonic attenuation coefficient with different concentrations of evaporated milk, agar, and silicon dioxide was evaluated. A repeatability test (n=10) was performed for each one of the tested recipes and attenuation coefficients were acquired using the through-transmission method. Small day to day variability was observed for most of the agar-based gels, indicating the stability of the measurement system. The variable-thickness technique was also used and resulted in slightly lower values of attenuation coefficients, as expected, proving extra evidence of the accuracy of the estimated values.

Depending on the agar, silicon dioxide, and evaporated milk concentration, the attenuation coefficient varied in the range of 0.30-1.49 dB/cm-MHz. A linear increment of attenuation was observed with increasing agar (up to 6 %), silicon dioxide (up to 4 %), and evaporated milk (up to 30 %) concentration.

The attenuation contribution of agar percentage from 2 % to 4 % was 0.13 dB/cm-MHz, while a more significant (approximately double) contribution with a total attenuation increase of 0.27 dB/cm-MHz was found from 4 % to 6 %. Agar concentrations over 6 % resulted in stiff phantom and did not resemble realistically the stiffness of soft tissue, therefore agar was limited to 6 %.

It was noticed that the attenuation coefficient can best be regulated by varying the amount of silicon dioxide. The addition of 1 % w/v of silicon dioxide contributed to an increase of attenuation by 0.101 dB/cm-MHz up to a 4 % concentration. Although the scattering of the sample increased with the addition of silicon dioxide for an amount of over 4 % w/v, the contribution of silicon dioxide to absorption significantly decreased [134]. Thereby, it seems that for a silicon dioxide concentration of more than 4 % w/v, the attenuation is strongly affected by the decrement of absorption [134], rather than the enhancement of the scattering phenomenon.

The addition of 10 % v/v evaporated milk increased the attenuation by 0.127 dB/cm-MHz probably due to absorption. Evaporated milk was found to have a minimal contribution to attenuation (0.013 dB/cm-MHz for every 1 % v/v of evaporated milk), compared to the attenuation contribution of silicon dioxide (0.101 dB/cm-MHz for every 1 % w/v of silicon dioxide). The concentration of evaporated milk was limited to 30 % because although attenuation (and absorption as it was previously reported [134]) can be further raised with increased evaporated milk concentration, increased milk concentration results in loose phantom. Evaporated milk has been already suggested as a material that increases attenuation by Madsen et al [126].

Other materials such as glycerol (more than 5 %) and graphite powder have been reported to increase the attenuation of TMMs [131], [128]. The range values of the attenuation of agar/gelatin-based gels doped with glass bead scatterers were found in the lower range (0.35-0.46 dB/cm-MHz) of the attenuation results of this study [128]. Similar to the range of the estimated attenuation values are the gelatin-based gels doped with graphite [18]. The pure gelatin (with water and alcohol) gel demonstrates an attenuation in the range of 0.2-0.3 dB/cm-MHz. By adding a uniform amount of powdered graphite, the attenuation can be adjusted between 0.2-1.5 dB/cm-MHz (at 1.1 MHz) which is similar to the attenuation range values found in this work.

The ultrasonic attenuation coefficient of the sample with 4 % agar (0 % of silicon dioxide and evaporated milk) was found to be 0.43 ± 0.06 dB/cm-MHz which is close to the value found for human fat, liver, and cardiac tissue [138], [139]. In addition, the ultrasonic attenuation with an amount of agar of 6 % was found to be 0.70 ± 0.06 dB/cm-MHz which is almost equal to that of the human brain, according to [139]. The recipe with identical agar and silicon dioxide concentration of 2 % (0 % evaporated milk) was found to possess attenuation close to that of a bovine spleen (0.87 dB/cm-MHz), while a silicon dioxide concentration of 2-4 % w/v induced attenuation similar to the bovine brain (0.97 dB/cm-MHz) [140]. Mast et al [138]reported an attenuation coefficient of human muscle similar to the one obtained for the phantom with the optimum recipe of 6 % agar and 4 % silicon dioxide. Finally, using the recipe with 6 % agar, 4 % silicon dioxide and 10 % evaporated milk, the attenuation coefficient was found to be 1.22 ± 0.04 dB/cm-MHz which is close to the value of porcine liver (1.25 dB/cm-MHz) [140].

A linear relation between the attenuation coefficient and frequency was estimated for the phantom of the recipe (4 % agar, 6 % silicon dioxide). In agreement with our findings, other studies for tissue-mimicking phantoms, including polyacrylamide hydrogel-based phantoms [113], and gelatin-based phantoms doped with graphite [131], have reported a linear relationship between attenuation and frequency, in the range of 1 to 5 MHz.

Finally, the accuracy of the measurement system was confirmed by measuring the ultrasonic attenuation of freshly excised rabbit tissue, since our findings were in a very good agreement with the values reported in [141] for rabbit liver. The suitability of agar-based phantoms in mimicking real tissue was also assessed. Since the estimated values of the attenuation coefficient for both (the phantoms and liver tissues) lie within the same range, we can safely conclude that agar-based phantoms can be used to mimic rabbit tissue. Specifically, the optimum recipe of 6 % w/v agar and 4 % w/v silicon dioxide concentration, with an attenuation coefficient of 1.10 ± 0.09, was found to be suitable for mimicking rabbit tissue.

The findings of this study have been compared to the attenuation coefficient values found in the literature for human and animal tissues, as well as to the ones obtained for the freshly excised rabbit tissue in the current study. Our work has led us to conclude that agar-based phantoms with attenuation coefficient values similar to those of human and animal tissues can be developed with the proper selection of percentage of agar, silicon dioxide, and evaporated milk.

4 Determination of mechanical properties of agar, silicon dioxide, and evaporated milk gel phantoms

4.1 Introduction

Many studies have been conducted for defining the stiffness of various tissues of interest, particularly for cancer tissues and their differences in stiffness comparing to normal tissues [142]. Some examples are muscle and liver tissue ranging from 1 to 34 kPa in conjunction to cancerous tumors ranging between 112 and 638 kPa [143]. Figure 32 shows a comparison of the elastic modulus, size and time frames of different materials [144].

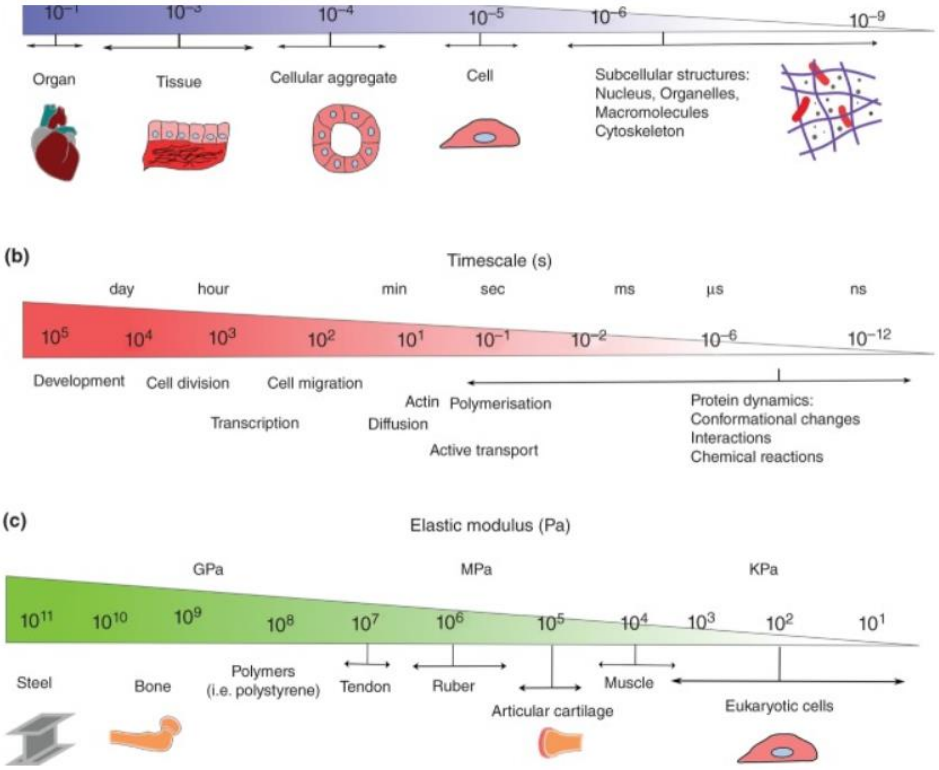

Figure 32 : Multiple scales of soft biomaterials. (a) Length scales from the molecular to the organ level; (b) timescales of different physiological processes; and (c) comparisons of the elastic modulus among different typical materials [143].

With the increase in interest for this area, many methods were developed for measuring the stiffness based on tissue deformation when applying a mechanical force. One of these methods is called nanoindentation. Nanoindentation is considered as a useful tool to analyse mechanically materials in the micro/ nano scale. This allows to concentrate on a specific area in a region, but also it has no restrictions in the morphology that a tissue must have in order to measure its stiffness [145]. The nanoindenter involves the application of a controlled load and depth to the surface to create a local deformation.

A study made by Van Dommelen et al [146] examined different parts of brain tissue and showcased their differences in terms of stiffness. Halves of porcine brains from 6-month-old pigs were formed into samples of 30 mm dimension. After performing indentation with 0.1 mm/s speed they observed that the shear moduli of the white matter (posterior, superior and anterior) gave higher values than the one of the grey matter. On the other hand, samples from the thalamus and midbrain were similar to the ones of the white matter.

Measurements completed in histological specimens show differences in the elastic modulus according to the layer of the material. Akhtar et al [147] studied the elastic modulus of the aorta and the vena cara. Large arteries, such as the aorta, balance the blood pressure differences using their elastic properties. The aorta showed significant changes in the elastic modulus from the outer layer (~30 MPa) to the inner layer (~8 MPa).

Hai et al [148] performed a different kind of study measuring the Young’s modulus both in agar phantoms and in human volunteers using the quantitative photoacoustic elastography (QPAE) method. They first created agar phantoms with concentrations of 20, 25, 30, 35 and 40 g/L added in gelatin background with 1 % intralipid. The cross sections of each phantom were around 3 mm. Then, they calculated the Young’s modulus, imaging the right arm of a healthy human volunteer by applying different loadings pulling his arm straight. Figures 33 and 34 show the results of this study.

Maccabi et al also did some comparative studies measuring the elastic modulus of phantoms and of animal tissues [149]. Specifically, they evaluated the viscoelastic properties of these materials, defining the elastic modulus (stiffness) and the long-term shear modulus (viscosity). They prepared three different types of phantoms: agar, polyvinyl alcohol (PVA) and gelatin. The selections were made in order to represent the acoustical and mechanical properties of human structures such as liver, breast and prostate. In parallel, they measured samples from porcine liver, rat liver and porcine gallbladder. Table 4 shows the results obtained for each sample.

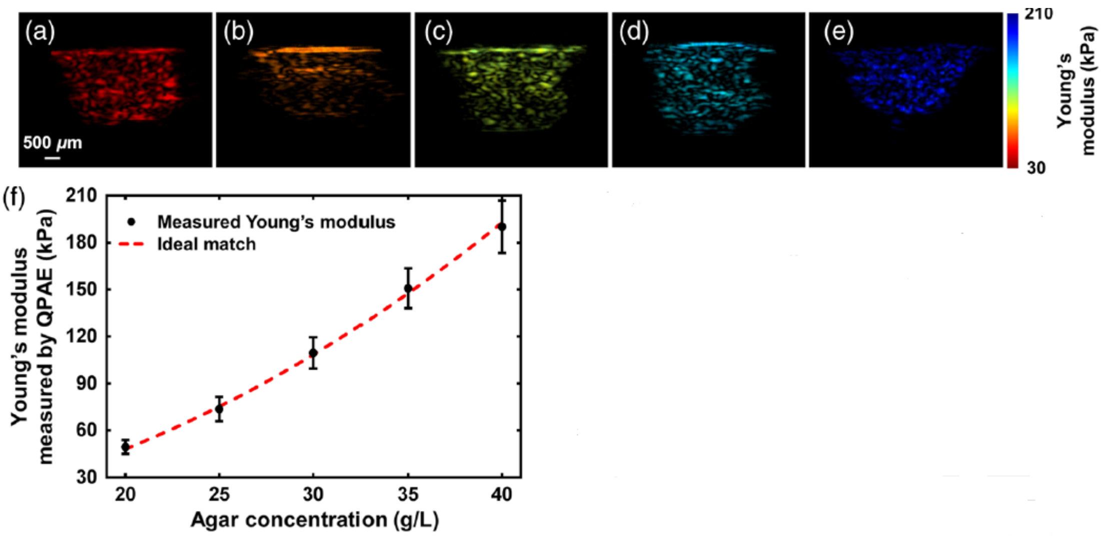

Figure 33 : QPAE of agar phantoms for increasing Agar concentrations (a-e), Young's modulus by QPAE related to agar concentrations (f) [148] .

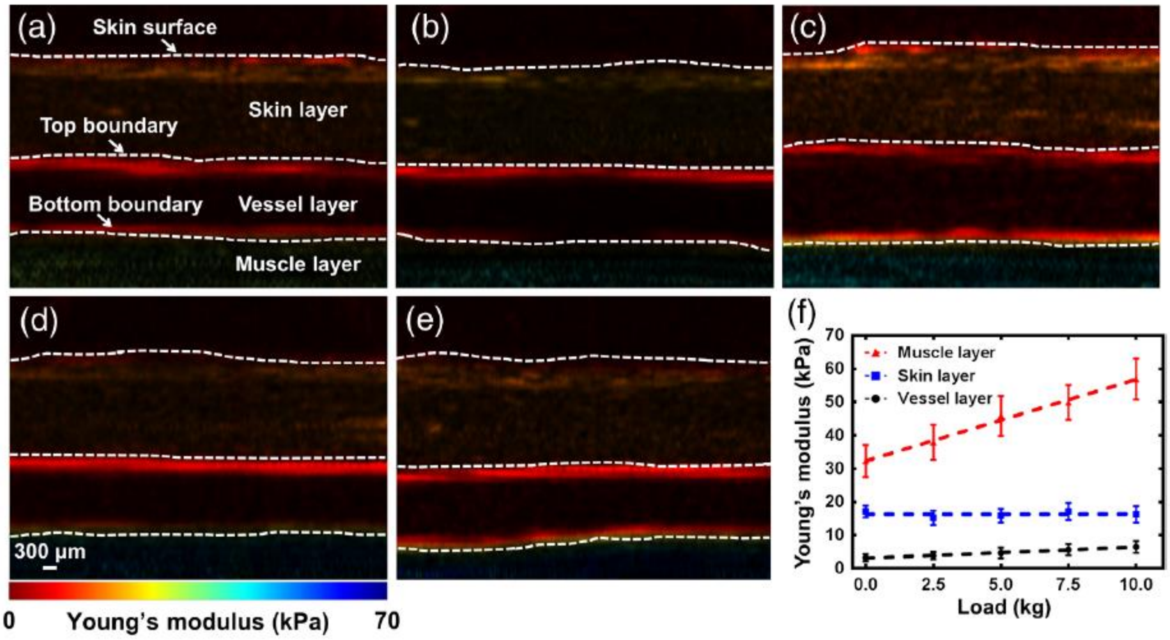

Figure 34 : QPAE of human biceps with different loadings a) 0.0 b) 2.5 c) 5.0 d) 7.5 and e) 10.0 Kg. Young's modulus value for each layer (f) [148].

According to Kaczmarek et al [150], the properties of an agar phantom depend on the pore size which varies along with the agar concentration. Higher agar concentration results in a decrease of the pore size, but the size increases with temperature due to melting of the weak junctions. The increase in agar concentration also produces stiffer materials giving a higher elastic modulus [150]. Manickam et al [151] investigated the elastic properties of agar phantoms varying the agar concentration from 1.7 % to 6.6 % w/w. The tested samples were of cylindrical shape with dimensions of 38 mm diameter and 70 mm height. The calculated Young's modulus ranged from 50 kPa to 450 kPa, where the increase in agar concentration again increased the shear modulus of the samples.

Table 4 : Mean Elastic Modulus values for each sample tested [149].

Sample	Mean Elastic Modulus (kPa)
14% PVA phantom	5.660
17% PVA phantom	9.435
20% PVA phantom	33.715
10% Gelatin Phantom	16.348
15% Gelatin Phantom	45.210
20% Gelatin Phantom	65.959
2% Agar Phantom	104.638
2.5% Agar Phantom	135.476
3% Agar Phantom	195.166
Porcine Liver	2.553
Rat Liver	2.758
Porcine Gallbladder	4.730

A similar study was conducted by Dwihapsari et al [152], calculating the shear modulus of agar phantoms of 2.5, 5 and 7.5% w/v concentrations. Agar was mixed with 50 ml distilled water, boiled for 20 min and poured in plastic tubes with 57 mm diameter and 75 mm height. The shear modulus of agar ranged from 130 – 180 kPa for 5% w/v and 300 – 380 kPa for 7.5 % w/v. The results confirmed the hypothesis that the shear modulus increases with higher agar concentrations.

Measurements for the determination of the hardness of hydrogels using nanoindentation were also done by Panteli et al [153]. The resistance to penetration by the nanoindenter was defined in five multiple network hydrogels and were correlated to the number of networks. The results showed that the nanoindentation hardness and elastic modulus increased with the increase in networks.

Other researchers, like Nayar et al [154], used nanoindentation to define the reduced modulus of agar phantoms varying agar concentration. They created phantoms containing agar dissolved phosphate buffered saline with agar concentrations of 0.5, 1.0, 2.0 and 5.0 % by weight. It was observed that the reduced modulus increased with agar concentrations resulting in values of reduced modulus equal to 30 kPa for 0.5 % concentrations to 700 kPa to 5.0 % concentrations. Also, the dynamic modulus was determined with varying load, frequency and amplitude. The results showed the same trend with values from 30 to 2300 kPa. An interesting observation made was the fact that constant hydration of the samples before each sampling, resulted in avoiding pores in the phantom structure.

On the other hand, Manickam et al [155] carried out a pilot study as part of a broader study, measuring the Young’s Modulus for phantoms containing agar, N-propanol and deionized water. The tested samples were of cylindrical shape with 38 mm diameter and 70 mm height. Confirming the findings of other studies, the results indicated an increase in the Young’s Modulus with increasing agar concentration. Agar ranged from 2 g (1.7 %) to 8 g (6.6 %) in the samples resulting in a Young’s Modulus from 50 kPa to 450 kPa covering the entire range of tissue stiffness. Figure 35 demonstrates the correlation between the concentration of agar and Young’s Modulus in the examined samples.

Other indications of the Young’s Modulus varying with agar concentrations gave a study made by Movahed et al [156]. Agar hydrogels were created including agar, water and dimethyl sulfoxide with dimensions 5.5 x 5.5 x 6 cm. The Young’s Modulus was measured using microindentometry and presented results of 105, 175 and 347 kPa for phantoms containing 1.5, 2.0 and 3.0% of agar.

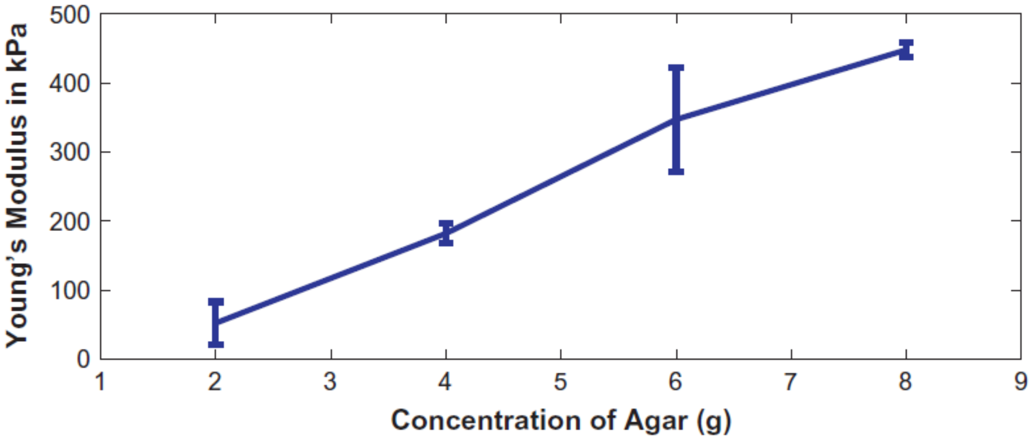

Figure 35 : Mean and standard deviation of Young's Modulus for samples with agar concentrations 2 - 8 g. [155]

McIlvain et al [157] created samples of agar phantoms which contained salt quantities. Among other measurements, they also observed the structure of samples varying one phantom preparation parameter each time. They varied the agar concentration, the salt concentration and the temperature. The observed the dependency of the phantom's mechanical properties from the preparation protocol, by examining the phantom structure with a microscope showcasing the microstructural changes of the gel. The baseline phantom was prepared at 90 °C, with 0.6% w/w salt and 1.0% w/w agar. Then they varied one parameter at a time with: temperatures 84 and 96 °C, salt concentration 0.3 and 0.9 % w/w and agar concentration 0.6 and 1.4 % w/w. Figure 36 shows the images they obtained for each sample.

A study made by Wrobel et al examined the morphology of a polydimethylsiloxane (PDMS) phantom using an Scanning Electron Microscope (SEM) [158]. They identified where the intrinsic scattering comes from while varying the concentration of glycerol in the phantom. Figure 36 shows the SEM images with the cavities in the phantom according to the glycerol concentration. The increase in glycerol causes the formation of increased and larger cavities. The chemical composition of the phantom showed that the two materials do not react with one another, but the PDMS working as a matrix with cavities and glycerol as a filler.

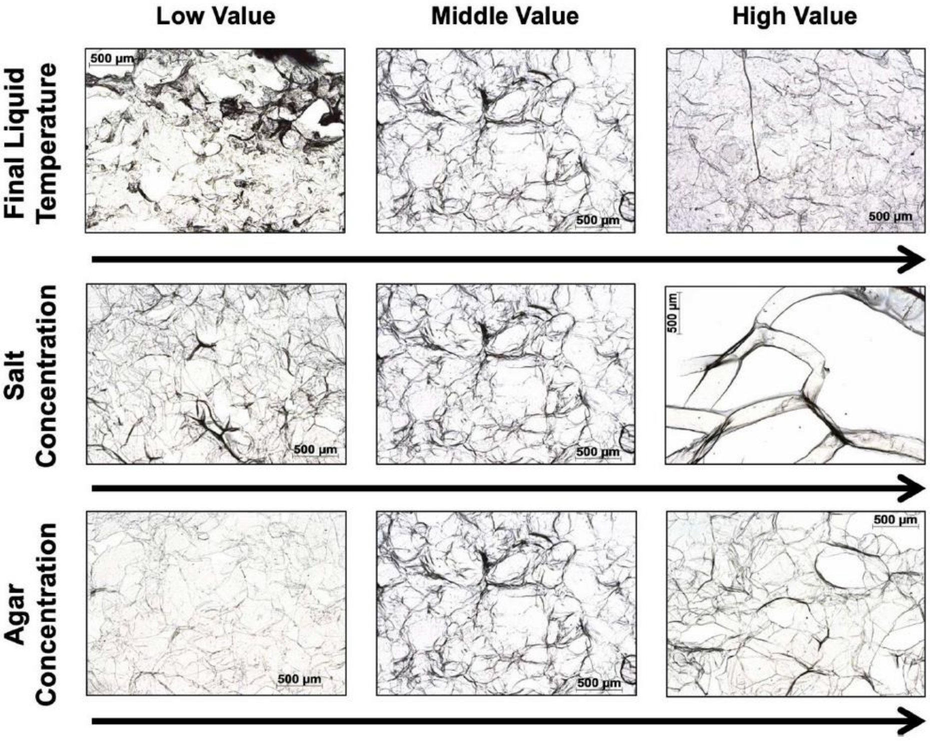

Figure 36 : Microscopy images of agar phantoms. Middle value images refer to the baseline gel [157].

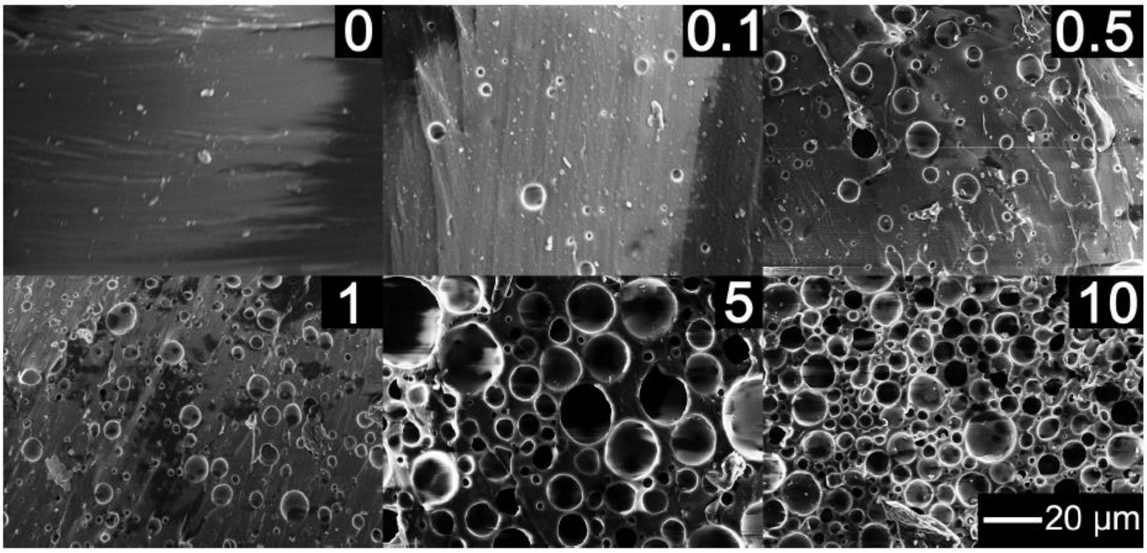

Figure 37 : SEM images of the internal structure of phantoms with glycerol concentrations from 0 to 10 parts per volume [158].

4.2 Materials and Methods

4.2.1 Samples preparation

As in previous study for attenuation, agar-based gels with different concentrations of agar (Merck KGaA, EMD Millipore Corporation, Darmstadt, Germany), silicon dioxide powder (Sigma-Aldrich, St. Louis, Missouri, United States), and evaporated milk (Nounou, Friesland Campina, Marousi, Greece) were formed [159].

The following ten samples were prepared: three samples with different w/v agar concentrations for each sample (2 %, 4 %, 6 %); three samples with different concentrations (w/v) of silicon dioxide (2 %, 4 %, 6 %) for agar concentration of 6 % w/v; and three samples with different v/v concentrations of evaporated milk (10 %, 20 %, 30 %) for 6 % w/v agar and 4 % w/v silicon dioxide. The last sample included 6 % of agar, 6 % of silicon dioxide but aged for 10 days before testing, to observe any alterations on the material through time.

The manufacturing process until the addition of agar was the same for all the samples. The procedure was slightly differentiated after the addition of agar and depended on the number of materials used. Initially, ultrapure degassed/deionized water was slowly heated and continuously stirred using a magnetic stirrer (SBS, A160, Steinberg Systems, Germany) for a period of 10 minutes until its temperature reached 50 ^{o}C. During the procedure, the temperature increase was monitored using an electronic thermometer (Omega Thermometer, HH806AU, Omega Engineering, Norwalk, Connecticut, USA).

For every batch, the agar content was added slowly in degassed/deionized water to mitigate aggregation. It is worth mentioning that since agar was in granular form with a particle size of approximately 1400 μm, it was first ground into powder before mixing with water to promote homogeneous jellification in the absence of impurities. In case no other material was added, the mixture was let to heat until it reached 90 ^{o}C and then to cool down to 50 ^{o}C. High temperatures allowed agar’s bonds to break and bind to the rest of the mixture (in case other materials were added). During the cooling period, the mixture was continuously stirred with the magnetic stirrer. The mixture started to solidify when the temperature dropped at around 50 ^{o}C. The amount of water that evaporated during boiling was replaced. The evaporation of the water was estimated by following the same procedure without the insertion of the solid materials. The evaporated water was calculated by subtracting the remaining volume of water from the initial volume. Care was taken by stirring the solution gently to avoid the creation of air bubbles that are known to reflect ultrasound waves. When other materials were added to the mixture, the silicon dioxide was first added 2-3 minutes after the agar insertion. The mixture including both the agar and silicon dioxide was heated until it reached 90 ^{o}C. Afterward, the mixture was left to natural cool down to 50 ^{o}C. Following this, the evaporated milk (v/v) was heated to 50 ^{o}C and added to the rest of the mixture. For a final step, the whole mixture was stirred well to allow full dissolvement of all ingredients.

The preparation procedure for each phantom was simple and did not last more than 20 minutes. The mixture was poured into a Polylactic Acid (PLA)-designed mold and was let to jellify overnight at room temperature. The dimensions of each mold were 40 mm in height, 26 mm in width, and 32 mm in length with 3 mm thickness.

4.2.2 Scanning Electron Microscope

Images of the phantoms have been acquired using a SEM (FEI, Quanta 200). Prior to the investigation, all samples were sputter coated with a thin (<10 nm) silver layer to reduce electron charging effects. Images were collected at 5 kV to 20 kV accelerating voltages in various magnifications.

4.2.3 Nanoindentation and Elastic Modulus

Nanoindentation on all samples was performed using a NanoTest Platform (Micromaterials Ltd, UK), using a three-sided pyramidal diamond indenter (Berkovich type) with an angle between its central axis and one of its faces of 65.3°, and a tip curvature of about 10 nm was used. The samples were subjected to a maximum load of 0.53 mN, the loading time was set to 5 s, the hold time at maximum load was set to 30 s, and the unloading time was set to 2 s. Figure 38 demonstrates the geometry of the indenter in the phantom. During the test the load (P) and depth of penetration (h) was continuously monitored, in order to measure the mechanical responses of the materials in load-displacement curves. For each sample, a total of 6 indentation experiments were performed. The hardness (H) and reduced elastic modulus (E_r) of the materials were extracted from the nanoindentation load-displacement curves using:

$$H = \frac{Pmax}{A} \qquad (3)$$

$$Er = \frac{\frac{\sqrt{\pi}}{2} S}{\sqrt{A}} \qquad (4)$$

where Pmax is the maximum applied load, A is the projected contact area at maximum load, $1/E_r = (1 - \nu_s^2)/E_s + (1 - \nu_i^2)/E_i$, vs is the Poisson's ratio of the sample, vi is the Poisson's ratio for the diamond indenter (0.07), E_s is the sample elastic modulus, E_i is the indenter elastic modulus (1141 GPa), and S is the contact stiffness found from the slope of the unloading portion (dP/dh) of the load-displacement curve at Pmax.

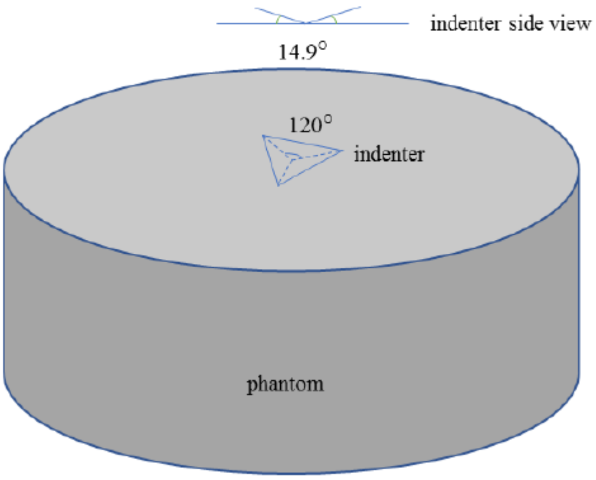

Figure 38 : Geometry of the Berkovich type pyramidal indenter and the phantom.

4.3 Results

All ten phantoms were analysed using the SEM comparing the structure of the phantoms while varying the concentration of one element each time. As mentioned before, prior to the analysis the samples were sputter coated with a silver layer as shown in Figure 39.

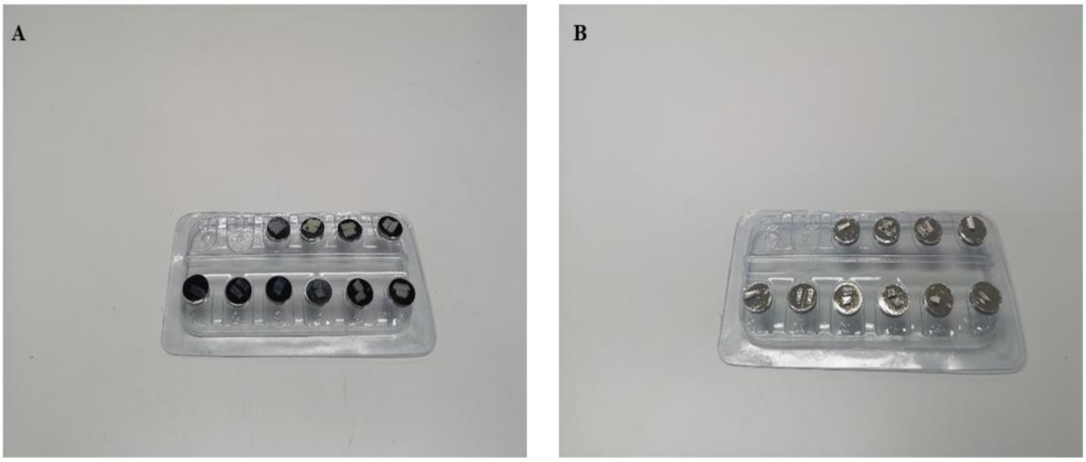

Figure 39 : Picture of the samples before (A) and after (B) the sputter coating.

The following figures present the SEM images while analysing the different phantoms. Figure 40 shows the images obtained for phantoms with 2 %, 4 % and 6 % w/v of agar. It is observed that the increase in the agar concentration results to a denser, harder and smoother phantom. Figure 41 demonstrates the variation of images when increasing the concentration of silicon dioxide. The pictures include the internal structure of phantoms with 6 % w/v agar and 0 %, 2 %, 4 % and 6 % of silicon dioxide. The silicon dioxide affects the roughness of the texture, while increasing its concentration. Figure 42 includes the SEM captions while varying the evaporated milk concentration. Concentrations used were 6 % agar, 4 % silicon dioxide w/v and 0 %, 10 %, 20 % and 30 % v/v of evaporated the phantoms.

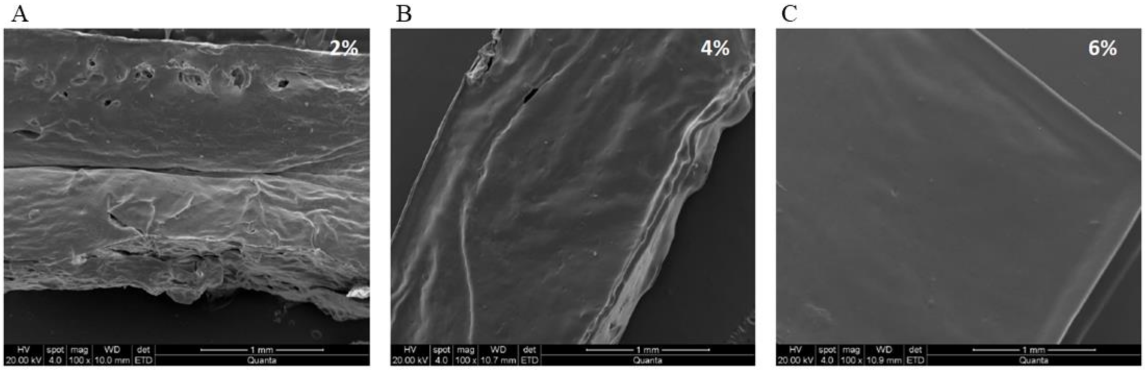

Figure 40 : SEM images of the internal structure of agar phantoms containing agar A) 2 % w/v B) 4% w/v and C) 6% w/v

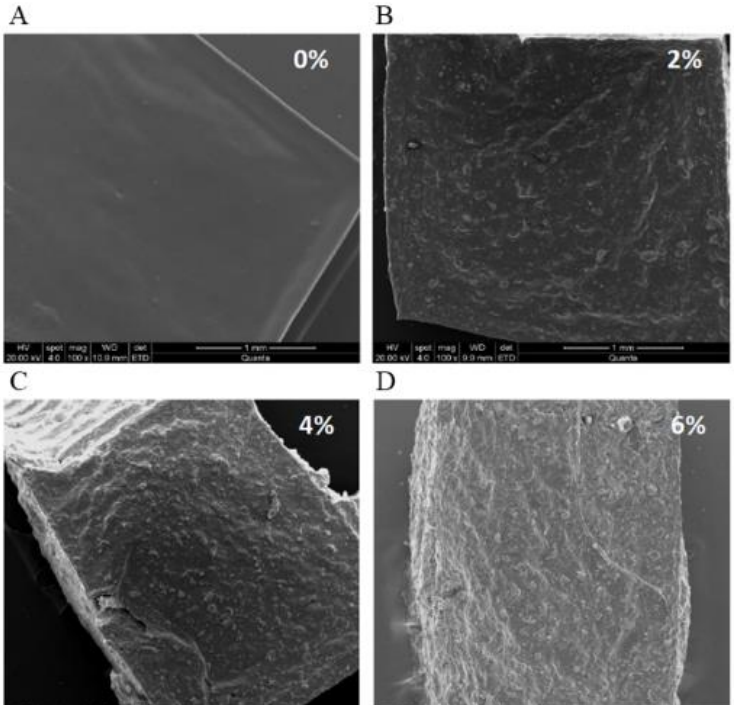

Figure 41 : SEM images of the internal structure of agar phantoms containing agar 6% w/v and silicon dioxide A) 0 % w/v, B) 2% w/v, C) 4% w/v and D) 6% w/v.

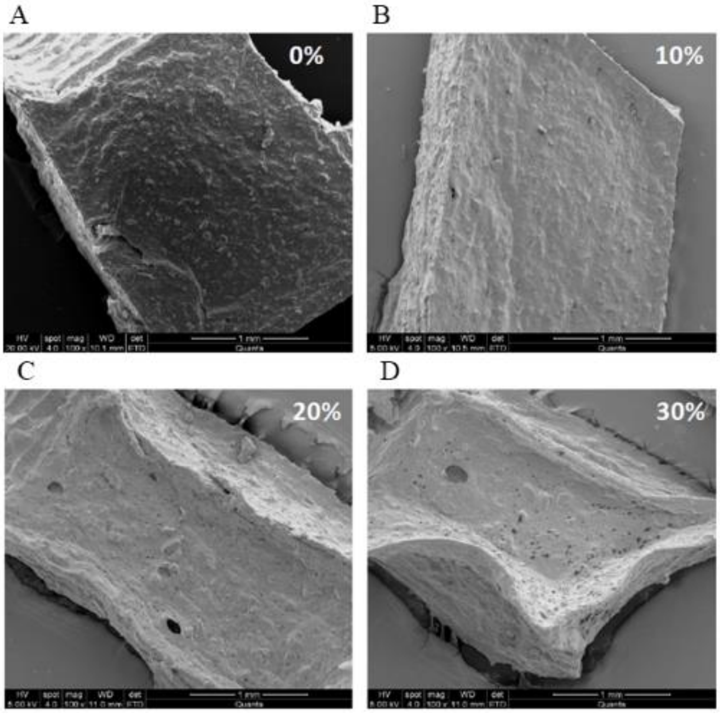

Figure 42 : SEM images of the internal structure of agar phantoms containing 6% w/v agar, 4% w/v silicon dioxide and evaporated milk A) 0 % v/v, B) 10% v/v, C) 20% v/v and D) 30% v/v.

The effect of phantom ageing was also investigated by obtaining SEM images for two samples with same concentrations (6 % agar, 6 % silicon dioxide) but one tested at four days after preparation and the second one at 10 days. Based on the images, no significant microstructural changes were observed among the two specimens. Figure 43 includes the SEM images for these two specimens.

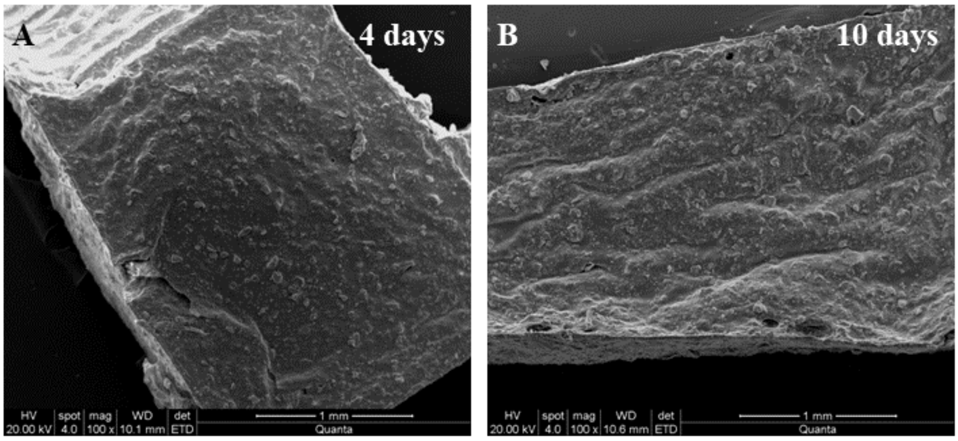

Figure 43 : SEM images of the internal structure of phantoms with 6 % w/v agar, 6 % w/v silicon dioxide and different day of preparation A) at four days and B) at ten days after preparation.

As mentioned before, for all the samples the elactic modulus was also defined using the nanoindentation method. As observed by the SEM images, the increase in the agar percentage gave denser and tougher phantoms. This is also confirmed by the values of the elastic modulus where higher agar concentrations lead to stiffer materials. Figure 44 shows the mean and standard deviation of the phantoms with ranging agar percentage from 2 to 6 % w/v. On the contrary when the agar concentration was kept constant and the percentage of silicon dioxide increased, the elastic modulus was increasing up to a certain point but for samples with 4 and 6 % w/v of silicon dioxide, the values dropped. This is probably due to fact that higher concentration of silicon dioxide become harder to mix and dissolve in the phantom mixture but also voids could be created during mixing. Figure 45 demonstrates the values of elastic modulus obtained for the four samples. Finally, the elastic modulus was calculated also in correlation to the evaporated milk concentrations which confirmed the findings of the SEM images. An increase of the evaporated milk reduces the elastic modulus as shown in Figure 46.

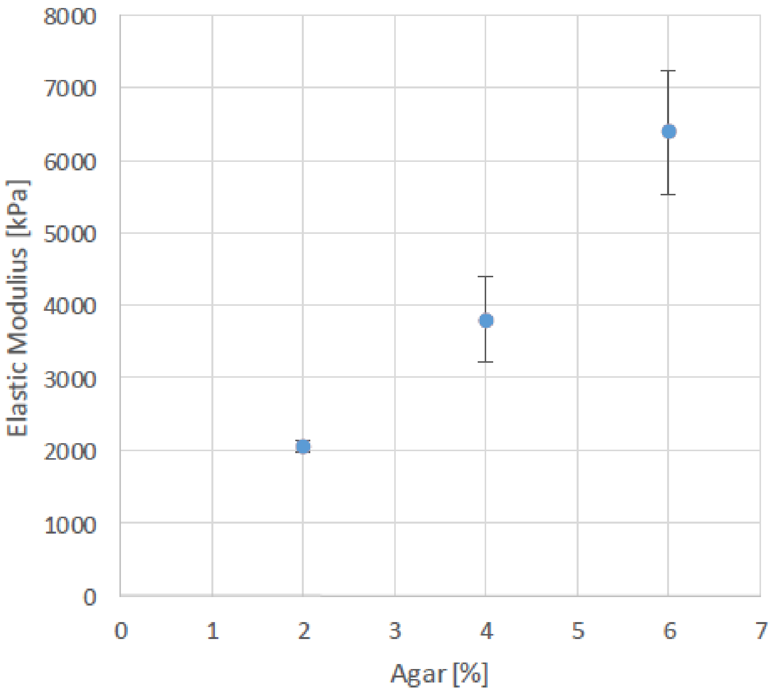

Figure 44 : Correlation of the elastic modulus (kPa) with agar concentrations of 2 %, 4 % and 6 % w/v.

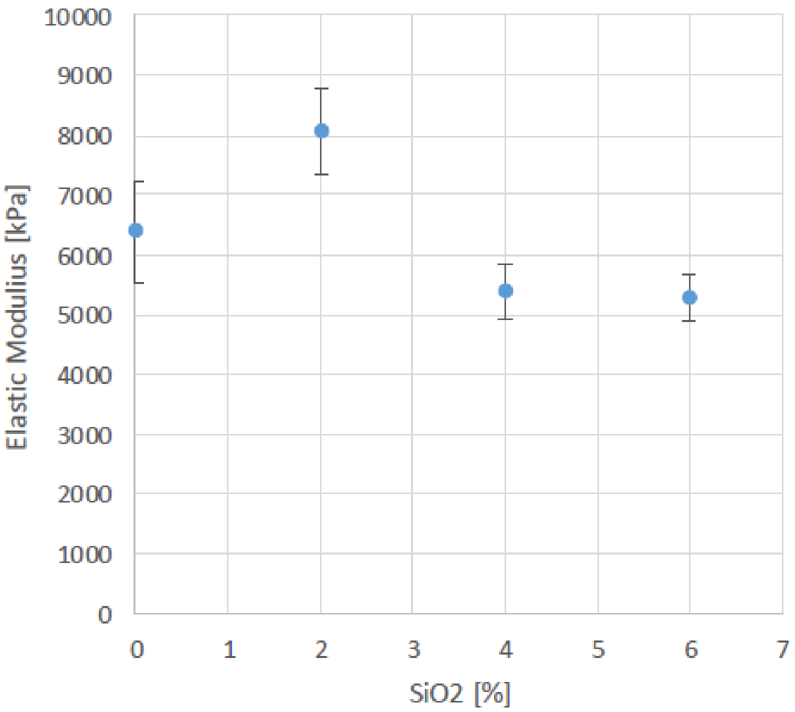

Figure 45 : Correlation of the elastic modulus (kPa) with silicon dioxide concentrations of 0 %, 2 %, 4 % and 6 % w/v.

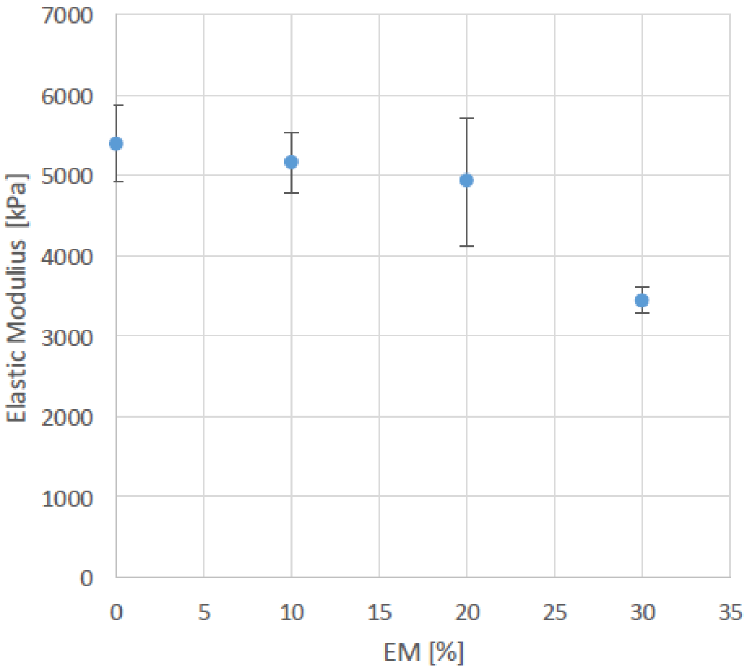

Figure 46 : Correlation of the elastic modulus (kPa) with evaporated milk concentrations of 0 %, 10 %, 20 % and 30 % v/v.

4.4 Conclusions

These experiments aimed in investigating the mechanical properties of the widely used agar phantoms and their correlation to each of the phantom's components. There are various phantom formulations used among researchers each providing a different characteristic to the phantom. Our laboratory uses agar phantoms in combination with silicon dioxide. Evaporated milk is added in some cases. Since the mechanical effects of these phantoms were not measured before, this study presents the structure of the phantoms using SEM and the estimated elastic modulus, for each combination of composition.

It was observed that each of the three components of the phantom, have a major effect on the structure of the phantom itself. By increasing the agar percentage, the phantoms become denser, smoother and stiffer. When the agar concentration was kept constant and the percentage of silicon dioxide changed, the phantoms became rougher in terms of texture and the elastic modulus increased until it reached its peak. One possible cause for this fact is the increase in bubbles when preparing the phantom, while mixing and dissolving the larger quantities of silicon dioxide becomes more difficult. Additionally, the increase in evaporated milk showed a significant decrease in the stiffness of these phantoms since milk is a less rough material. Finally, the aging parameter was also investigated while examining the structure of two phantoms with similar composition but different day of preparation. The phantoms were stored in refrigeration and tested for microstructural changes in specimens aged at four and ten days respectively. There were no significant changes in the structure between the two phantoms.

5 Evaluation of the effect of preservative addition and storing conditions in the shelf life of agar phantoms

5.1 Introduction

As previously mentioned, HIFU research is widely based on the use of gel phantoms for performing experiments. Phantoms consist a valuable tool for gaining knowledge and for further development of HIFU applications. There are different materials used to create a phantom which mimics tissue and its acoustic properties. Phantoms can be made from various materials: gelatin [101]–[103], agar [104]–[106], polyurethane [107], polyacrylamide [21]- [22], N-isopropylacrylamide [110] and polyvinyl alcohol cryogel [111]. Agar phantoms are cheap and easy to produce, durable in high temperatures, nontoxic, disposable and with a melting point of 65 ^{o}C [112]. On the downside they lack of long term stability [112]. Agar is generally used for representing biological tissues since it has similar mechanical characteristics but also because these characteristics vary according to concentration [154]. Additionally, agar phantoms are reusable and resist melting [160].

The storing conditions play a key role in the durability of the agar phantom. There are no studies investigating the life span of agar phantoms in different storage conditions. Manickam et al [155] noticed as part of another study that agar phantoms stored in distilled water for 3 months showed no signs of alteration of their properties. Earle et al. [160] studied several phantoms for their properties and durability. They created phantoms with agar concentrations ranging from 2.5 % to 10 % of agar and compared them with gelatin phantoms of 5% and 10 % concentrations using diagnostic ultrasound. Also, some of the phantoms included different additives (flour and red dye) to investigate any increase in opacity, ethanol for bubbles removal, liquid latex as a skin alternative. The durability of the phantoms was examined by repeatedly punching with a needle a small area of the phantom until the later lost its resistance and fragmented. They observed that the red dye increased the opacity, but the flour increased the echogenicity and its correlation to real tissue. Ethanol was effective in removing bubbles but reducing the echogenicity and liquid latex created skin resemblance but needed four days to set on the sample. They also noticed that agar phantoms that were left for one week in room temperature did not show any alteration in the appearance, except from some shrinking.

Agar phantoms that were stored in refrigeration did not show any signs of change at all. This was not the case for the gelatin phantoms they tested, where the phantoms developed moulds in room temperatures by the fourth day. Regarding durability, agar phantoms resisted in more needle punctuations before fragmenting compared to gelatin phantoms. Another interesting observation from this study, is the fact that agar phantoms were recycled, by melting them and reusing the material for creating a new phantom. The properties were similar to the original phantoms but the new phantoms were denser, probably due to water loss.

Another study conducted by Ntombela et al. [161] aimed in creating agar phantoms that would represent the optical properties of brain, bladder wall and lung tissue. Agar was combined with aluminium oxide and India ink to improve scattering. The resulting phantoms were wrapped and stored in refrigeration to evaluate their stability. There were no degradation signs of the samples for up to three weeks, in conjunction with samples that were stored in room temperatures that desiccated after one week.

Souza et al. [162] created a standard operation procedure for fabricating agar phantoms providing clear manufacturing steps for the specific tissue mimicking phantoms. The phantom includes glycerol, benzalkonium chloride, silicon carbide, aluminium oxide, and agar. The researchers mention that the resulting phantom should be stored in a closed container in a water/glycerol mixture in room temperature to avoid contact with air. In this way, the specific phantom can last up to one year. Also, it is mentioned that with the addition of benzalkonium chloride acting as an antifungal agent the phantom shelf life could be extended to two years.

It is obvious that researchers are investigating the addition of different additives to improve the performance of their phantoms. For the agar phantoms, the addition of an effective preservative would improve the phantom's biggest drawback which is its durability. Preservatives are compounds that postpone or protect from the microorganisms' action, providing chemical stability and durability. One type of preservative widely used in food and pharmaceutical industry to avoid fungal growth is sodium benzoate [163]. Quantities of sodium benzoate directly tested in the growth of fungus in suspensions presented a high activity in preventing fungal growth and this activity increased with increased concentrations of the preservative [164]. Sodium benzoate with a chemical formula of $C6H5COONa$, is a synthetic preservative that is safe and one of the first food preservatives applied to prevent food spoilage as approved by FDA [165]. While this compound provides a water soluble and safe option for microbial growth, high doses can cause toxicity. Studies made in rats showed weight loss, increase in creatinine, urea, uric acid and decrease of white blood cells when administered with high doses of benzoic acid [165]. For the effects of its use in humans, numerous studies indicate both its benefits and its potential threats but still no conclusions can be safely assumed regarding its use [166].

This study aims in investigating the effect of sodium benzoate when added in the formulation of agar phantoms in combination with the phantom’s storing conditions. It is an attempt to observe any changes in the durability of the agar phantom with the use of sodium benzoate in combination with evaporated milk, but also to confirm the effect of the storing conditions in the phantoms trying to define the optimum conditions for longer phantom life span.

5.2 Materials and Methods

For the purpose of this study sixteen agar phantoms were formulated using the usual method of preparation. Agar (Merck KGaA, EMD Millipore Corporation, Darmstadt, Germany), silicon dioxide powder (Sigma-Aldrich, St. Louis, Missouri, United States), and evaporated milk (Nounou, Friesland Campina, Marousi, Greece), sodium benzoate (Sigma-Aldrich, St. Louis, Missouri, United States) and glycerol with 99 % purity (Sigma-Aldrich, St. Louis, Missouri, United States) were used.

The agar and silicon dioxide concentrations were kept constant for all samples and equal to 6 % w/v of agar and 4 % w/v of silicon dioxide. From the sixteen samples, eight of them contained 30 % v/v of evaporated milk and eight of them contained 0.4 % w/v of sodium benzoate. The concentration of sodium benzoate was chosen based on the most commonly used ranges used in the pharmaceutical and food industry as preservative but selecting the maximum percentage since the phantoms are not intended for human use and since is stated that its preservative action increases with an increase in its concentration [167] [164].

The manufacturing process until the addition of agar was the same for all the samples. The procedure was slightly differentiated after the addition of agar and depended on the number of materials used. Initially, ultrapure degassed/deionized water was slowly heated and continuously stirred using a magnetic stirrer (SBS, A160, Steinberg Systems, Germany) for a period of 10 minutes until its temperature reached 50 ^oC. During the procedure, the temperature increase was monitored using an electronic thermometer (Omega Thermometer, HH806AU, Omega Engineering, Norwalk, Connecticut, USA).

For every batch, the agar content was added slowly in degassed/deionized water to mitigate aggregation. It is worth mentioning that since agar was in granular form with a particle size of approximately 1400 μm, it was first ground into powder before mixing with water to promote homogeneous jellification in the absence of impurities. The silicon dioxide was first added 2-3 minutes after the agar insertion. For the samples containing sodium benzoate, this was added 2-3 minutes after the silicon dioxide insertion. The mixture was let to heat until it reached 90 ^oC and then to cool down to 50 ^oC. High temperatures allowed agar's bonds to break and bind to the rest of the mixture (in case other materials were added). During the cooling period, the mixture was continuously stirred with the magnetic stirrer. The mixture started to solidify when the temperature dropped at around 50 ^oC. The amount of water that evaporated during boiling was replaced. The evaporation of the water was estimated by following the same procedure without the insertion of the solid materials. The evaporated water was calculated by subtracting the remaining volume of water from the initial volume. Care was taken by stirring the solution gently to avoid the creation of air bubbles that are known to reflect ultrasound waves. Following this for the samples that contained milk, the evaporated milk (v/v) was heated to 50 ^oC and added to the rest of the mixture. For a final step, the whole mixture was stirred well to allow full dissolvement of all ingredients.

The preparation procedure for each phantom was simple and did not last more than 20 minutes. The mixtures were poured into Polylactic Acid (PLA)-designed molds and were let to jellify overnight at room temperature. Due to the high number of samples prepared, mold of different dimensions were used according to availability. The following day the phantoms were removed from their molds and separated to four different storing conditions which were: room temperature, refrigeration, in 12/88 % glycerol/water solution in room temperature and in 12/88 % glycerol/water solution in refrigeration. Table 5 shows the composition and storing condition of each produced sample. The samples that were not kept in a glycerol/water solution, were wrapped to minimize the contact with air that would enhance microbial growth. The 12/88 % glycerol/water solution was selected based on the study made by Souza et al [162] which mentioned that agar phantoms can be preserved for longer periods of time in this type of environment. Each sample was monitored visually for changes in its appearance and dimensions. Pictures of each sample were taken approximately every two weeks until fungal growth was observed and the sample for discarded.

Table 5 : Composition and storing conditions of produced phantoms.

Sample No	% Agar	% Silicon Dioxide	% Evap. Milk	% Sodium Benzoate	Storing Conditions
1	6	4	30	0	4 ^{o}C
2	6	4	30	0.4	4 ^{o}C
3	6	4	0	0	4 ^{o}C
4	6	4	0	0.4	4 ^{o}C
5	6	4	30	0	25^{o}C
6	6	4	30	0.4	25^{o}C
7	6	4	0	0	25^{o}C
8	6	4	0	0.4	25^{o}C
9	6	4	30	0	4^{o}C Glycerol/Water
10	6	4	30	0.4	4^{o}C Glycerol/Water
11	6	4	0	0	4^{o}C Glycerol/Water
12	6	4	0	0.4	4^{o}C Glycerol/Water
13	6	4	30	0	25^{o}C Glycerol/Water
14	6	4	30	0.4	25^{o}C Glycerol/Water
15	6	4	0	0	25^{o}C Glycerol/Water
16	6	4	0	0.4	25^{o}C Glycerol/Water

5.3 Results

From the first group of samples with different compositions that were wrapped and stored in refrigeration at 4 ^{o}C it was observed that although the phantoms were stored in low temperature, the contact with air allowed the growth of fungus on all four samples. It is noted that the sample containing evaporated milk presented fungal growth at a great extent comparing to samples that did not contain any quantities of milk. This is because milk provides suitable environment and nutrients that encourage microorganisms to develop. On the other hand, samples 3 and 4 presented fungal growth at the same period, but to a smaller extent due to the absence of milk. It is also observed that sample 4 showed fewer fungal areas compared to sample 3, which might indicate that the addition of sodium benzoate had an effect in preventing to some extent the fungus to develop further. For the four samples of this group no alteration in the dimensions of the samples occurred. Figures 47 – 50 show the progress of each of the samples 1, 2, 3 and 4 with photos taken at week 0, week 1 and week 3 in which the samples were discarded.

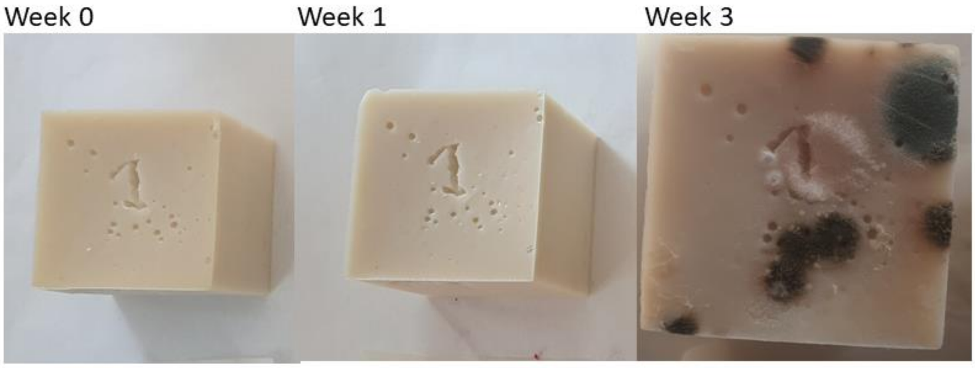

Figure 47 : Sample 1; progress from week 0 to week 3 (containing 30 % evaporated milk and 0 % sodium benzoate, stored at 4ºC)

Figure 48 : Sample 2; progress from week 0 to week 3 (containing 30 % evaporated milk and 0.4 % sodium benzoate, stored at 4ºC)

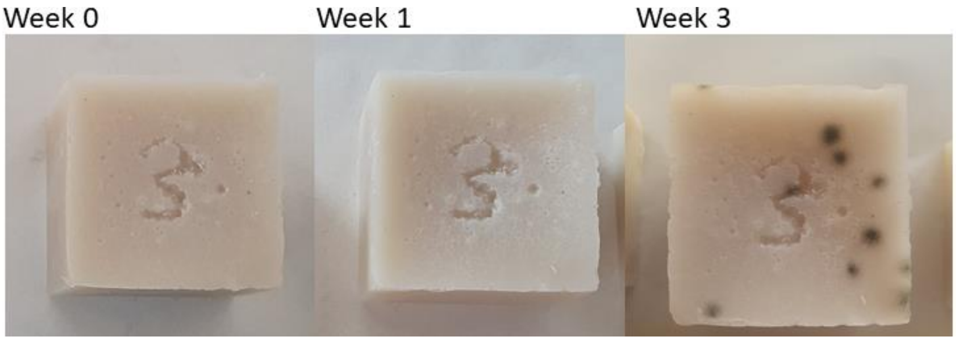

Figure 49 : Sample 3; progress from week 0 to week 3 (containing 0 % evaporated milk and 0 % sodium benzoate, stored at 4ºC)

Figure 50 : Sample 4; progress from week 0 to week 3 (containing 0 % evaporated milk and 0.4 % sodium benzoate, stored at 4°C)

The second group of phantoms were wrapped to minimize exposure to the environment and stored in room temperature of 25°C. All four samples presented fungal growth after one week, while their structure was severely shrank and deformed. Samples 5 and 6 that contained 30 % of evaporated milk, showed more intense signs of fungus and shrinkage, with their dimensions being alternated by 1 cm. In this case, the presence of the preservative in sample 6 did not have a positive effect on the fungal growth. Samples 7 and 8 also indicated fungal growth but in less extent, mainly due to the absence of milk in their composition. Deforming and shrinkage of 0.5 cm was also observed. When visually inspected, sample 8, which contained the preservative quantity, showed less fungus count on its surface compared to sample 7. This confirms the hypothesis from the first group of phantoms that the existence of the preservative in the composition might have a slight effect on preventing or delaying fungal growth. This quantity though was not enough to completely prevent the fungal growth in these storing conditions. Figures 51 to 54 demonstrate the progress of samples 5, 6, 7 and 8 for week 0 and week 1 in which the samples developed fungal growth and were discarded.

Figure 51 : Sample 5; progress from week 0 to week 3 (containing 30 % evaporated milk and 0 % sodium benzoate, stored at 25°C)

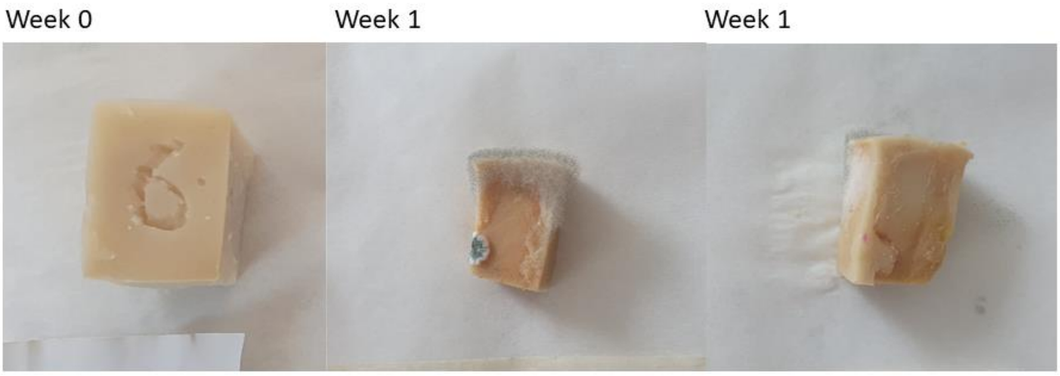

Figure Sample 6; progress from week 0 to week 3 (containing 30 % evaporated milk and 0.4 % sodium benzoate, stored at 25ºC)52 : Sample 6; progress from week 0 to week 3

Figure 53 : Sample 7; progress from week 0 to week 3 (containing 0 % evaporated milk and 0 % sodium benzoate, stored at 25ºC)

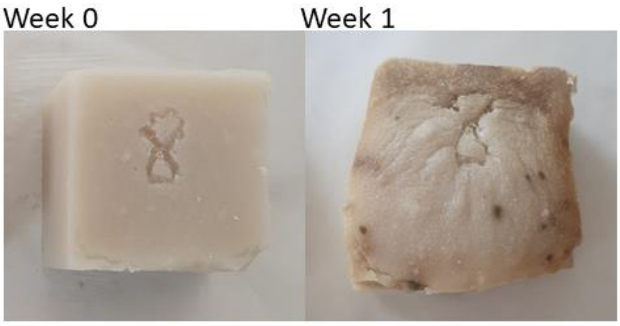

Figure 54 : Sample 8; progress from week 0 to week 3 (containing 0 % evaporated milk and 0.4 % sodium benzoate, stored at 25ºC)

The third group of phantoms contained the four phantoms with respective compositions but stored in glycerol/water 12/88 % solution and placed in refrigeration at 4ºC. The four samples were monitored for a period of 21 weeks with no signs of fungal growth, shrinkage or deformation occurring. Figures 55 to 58 show the progress of samples 9, 10, 11 and 12 from week 0 and up to week 21 when the experiment concluded.

It is visible that the phantoms were preserved intact in the glycerol/water solution at temperature 4ºC for a period of 21 weeks. There were no visible signs of difference between the samples containing the preservative or the samples that contained milk. All four samples remained in the original visual condition.

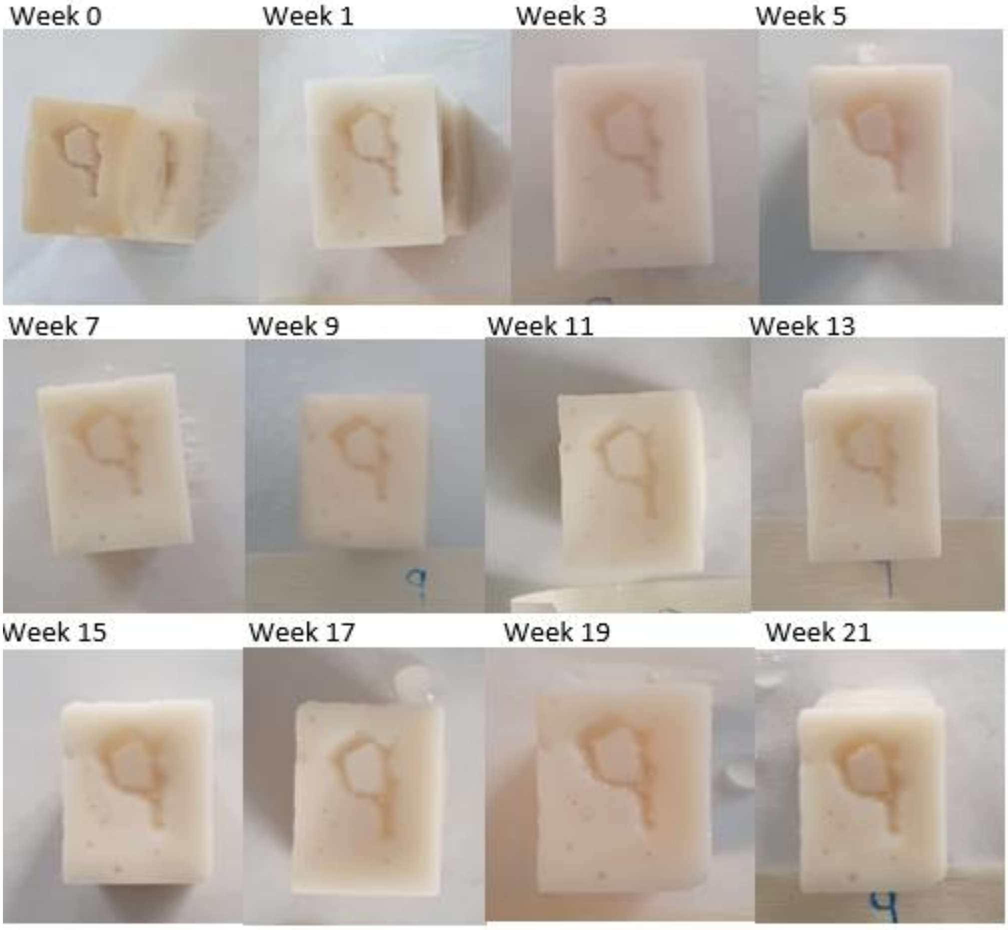

Figure 55 : Sample 9; progress from week 0 to week 21 (containing 30 % evaporated milk and 0 % sodium benzoate, stored in glycerol/water at 4ºC)

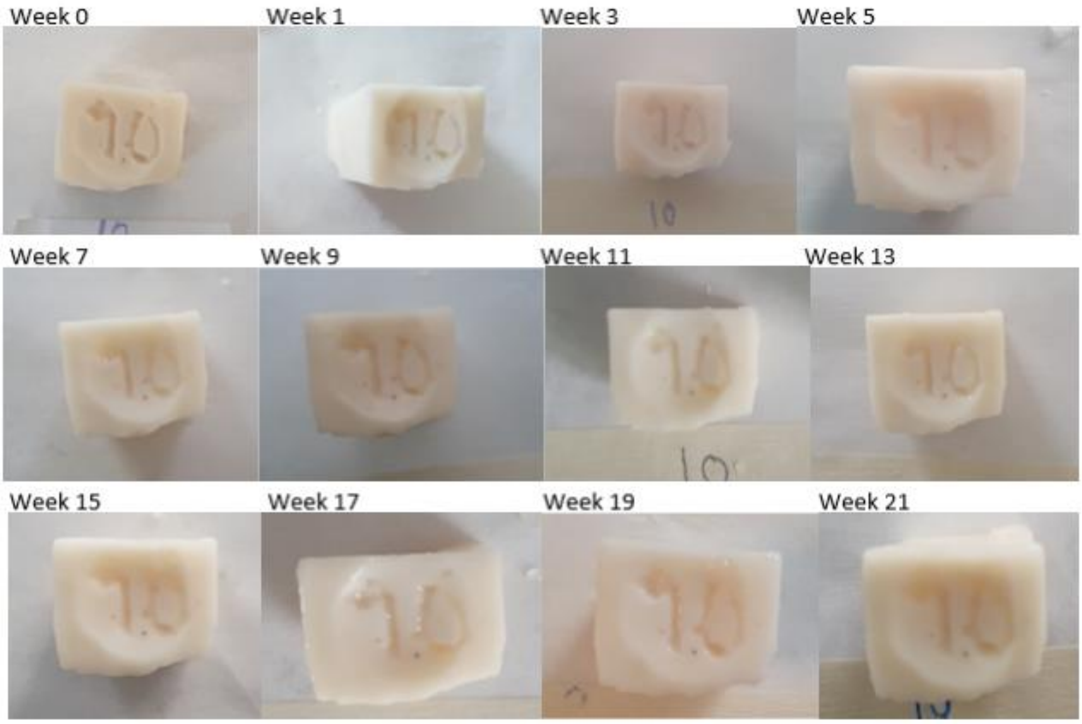

Figure 57 : Sample 10; progress from week 0 to week 21 (containing 30 % evaporated milk and 0.4 % sodium benzoate, stored in glycerol/water at 4ºC)

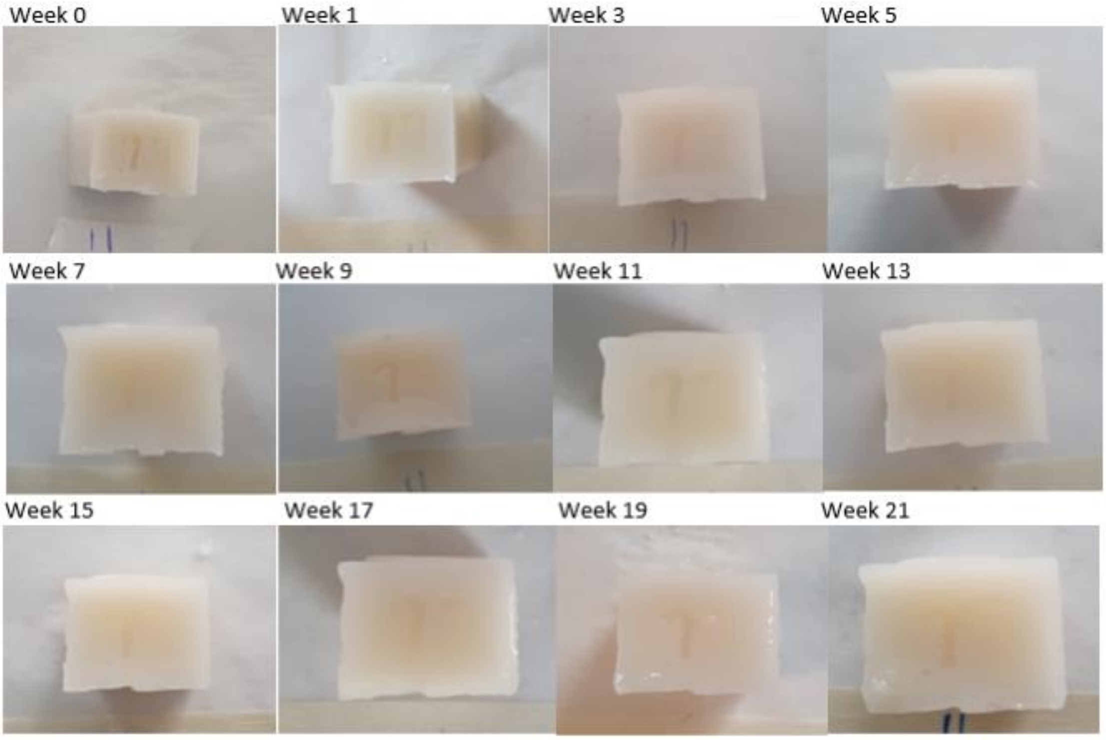

Figure 56 : Sample 11; progress from week 0 to week 21 (containing 0 % evaporated milk and 0 % sodium benzoate, stored in glycerol/water at 4ºC)

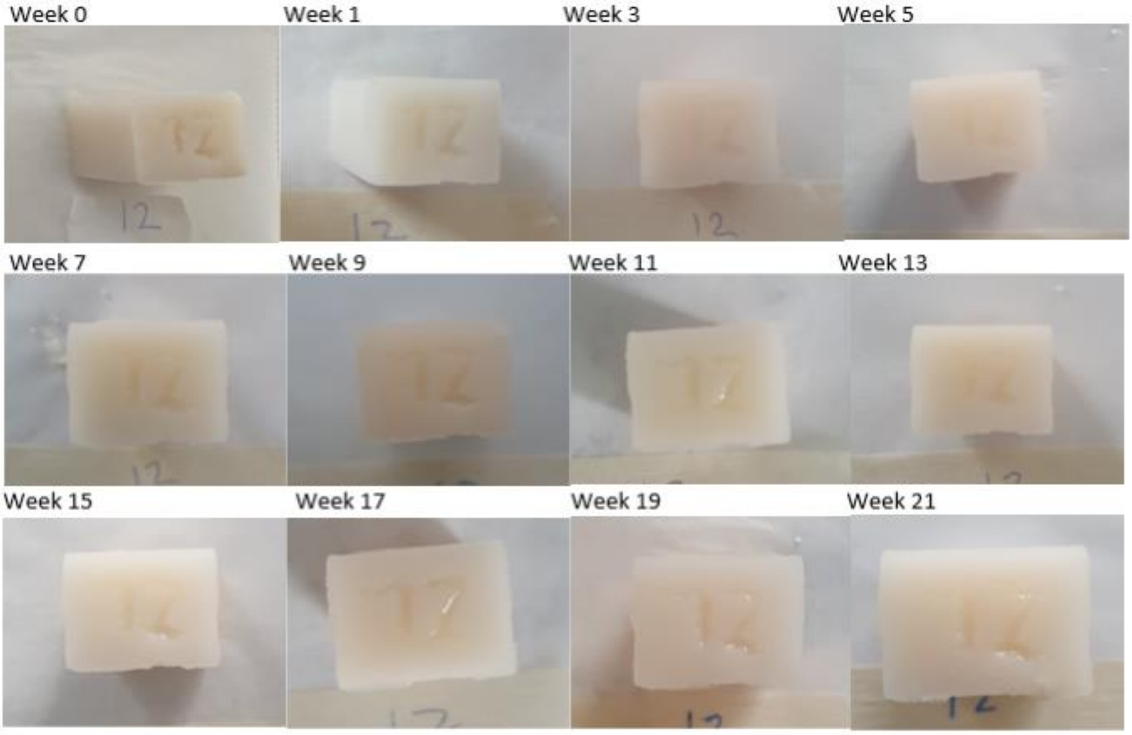

Figure 58 : Sample 12; progress from week 0 to week 21 (containing 0 % evaporated milk and 0.4 % sodium benzoate, stored in glycerol/water at 4ºC)

Finally, the fourth group of phantoms contained the four phantoms with respective compositions but stored in glycerol/water 12/88 % solution in room temperature at 25ºC. The samples initially showed no signs of fungal growth, but at week 3, fungus developed on the surface of the solution. In fact, the solution's surface was the only part that came into contact with air. It is not clear if nutrients from only one phantom caused the fungal growth on the surface of the solution, since the four phantoms were stored together. When the phantoms were removed from the solution, there were no indications of fungal growth on the surface of the phantoms. Therefore, the solution contamination cannot be attributed to one single phantom, but probably to nutrients existing in all phantoms. In addition, there was no difference between the samples containing sodium benzoate or evaporated milk. It is visible that the glycerol/water solution does not provide a suitable environment for long-term storage of phantoms in room temperatures. Figures 59 to 62 show each of the samples 14, 15, 16 and 17 for week 0 to week 3.

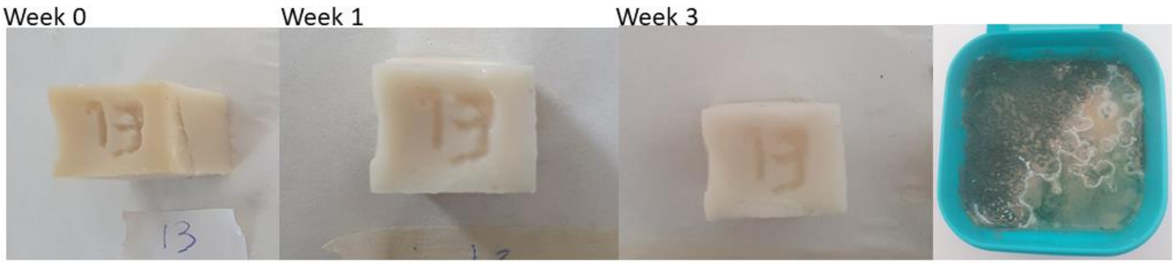

Figure 60 : Sample 13; progress from week 0 to week 3 (containing 30 % evaporated milk and 0 % sodium benzoate, stored in glycerol/water at 25ºC)

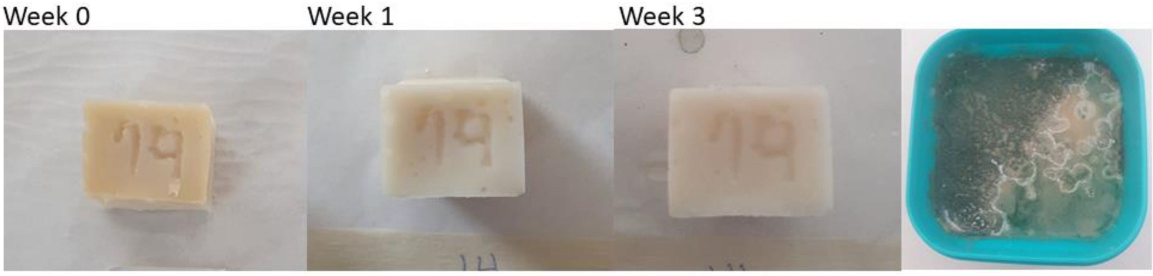

Figure 61 : Sample 14; progress from week 0 to week 3 (containing 30 % evaporated milk and 0.4 % sodium benzoate, stored in glycerol/water at 25ºC)

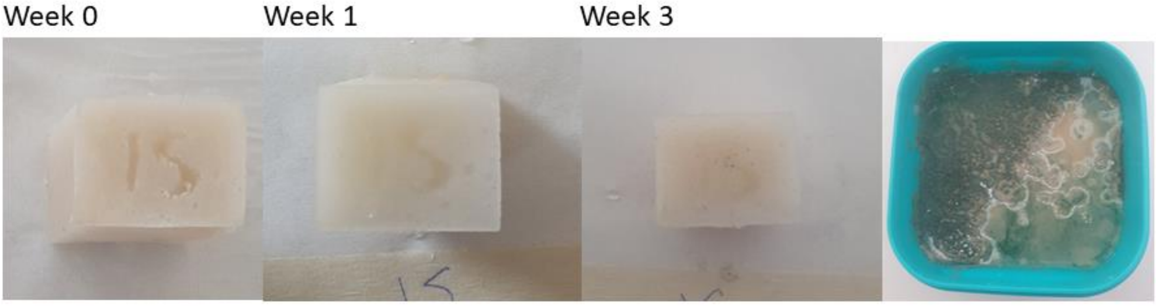

Figure 59 : Sample 15; progress from week 0 to week 3 (containing 0 % evaporated milk and 0 % sodium benzoate, stored in glycerol/water at 25ºC)

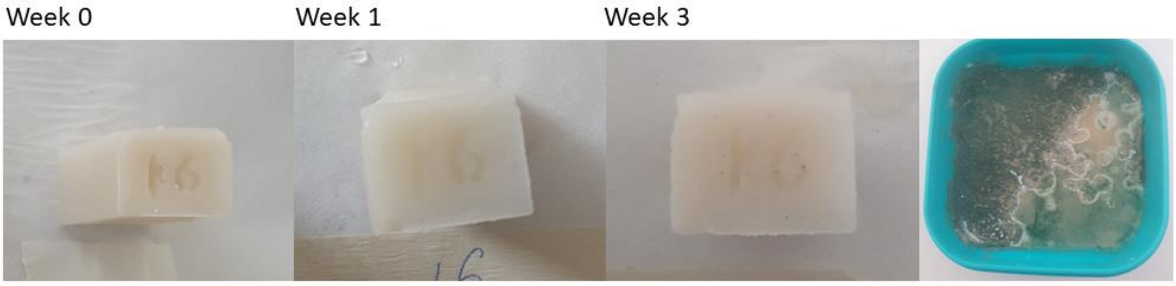

Figure 62 : Sample 16; progress from week 0 to week 3 (containing 0 % evaporated milk and 0.4 % sodium benzoate, stored in glycerol/water at 25ºC)

5.4 Conclusions

This study's main objective to investigate the effect of the addition of a widely used preservative such as sodium benzoate into a well-tested composition of agar phantom. In parallel, the influence of the storing conditions were examined and correlated with the use of the preservative. Based on the results of this study some conclusions can be made about the whole process. At first, the presence of evaporated milk in the composition holds a key role for its preservation. The milk provides the perfect ground for fungus to grow with all the necessary nutrients for further development. In addition, the existence of sodium benzoate in some of the phantoms provided indications of a mild fungal growth prevention but not enough to avoid the growth completely. A detrimental role in the stability and life span of the phantoms holds the storing conditions. A phantom cannot be preserved in room temperatures without spoiling even if it is not in contact with air. On the contrary, phantoms that were stored in glycerol/water solution and in refrigeration remained intact for the entire course of this study. Therefore, this way of storing is an effective way to store the produced agar phantoms for longer periods of time.

A future development of this study could be the measurement of the pH of the agar phantom and its correlation with a more suitable preservative. Each preservative varies its effect according to the pH of the environment, making some more suitable for certain cases. Eventually, if the pH of the phantoms is defined, then a preservative could be selected and investigate the effect it would have on the durability of the phantom.

6 Amyloid β plaque reduction with antibodies crossing the blood brain barrier opened in 3 sessions with focused ultrasound in a rabbit model.

6.1 Introduction

Alzheimer Disease (AD) is a major form of Dementia. There were an estimated 46.8 million people with dementia worldwide in 2015 [168] . This number will increase to an estimated 75 million in 2030, and 131.5 million in 2050. Much of the increase will be in developing countries. There are 9.9 million new cases of dementia each year, implying that there is a new case of dementia globally every four seconds. The total estimated worldwide cost of dementia was 818 billion US$ in 2015 [168].

Among the brain changes believed to contribute to the development of Alzheimer's disease is the accumulation of Amyloid β (Aβ) peptide outside neurons. Aβ is generated from β-amyloid precursor protein (β-APP). Another change is the accumulation of an abnormal form of the protein tau inside neurons (called tau tangles). In Alzheimer's disease, information transfer at synapses begins to fail, the number of synapses decline, and neurons eventually die. AD is a complex and serious neurodegenerative disorder, with no established treatment, and therefore there are enormous research efforts worldwide for therapeutics of AD. Our study focuses on the feasibility of using repeated pulsed focused ultrasound (FUS) in combination with antibodies as a new potential therapeutic modality.

Part of this study was immunotherapy which is one of the promising therapeutic approaches focused on using antibodies to facilitate clearance of the Aβ peptide [169]. One mechanism that could explain the process is the soluble equilibrium mechanism which is based on antibodies neutralizing soluble Aβ and shifting the equilibrium to favor dissolution [169]. This mechanism of action usually takes place in both the periphery and central compartments. However, one limitation of delivering antibodies in the brain is the blood-brain barrier (BBB). It has been reported that that only 0.1% of exogenous antibodies administered endovascularly enter the brain [170]. Direct administration of antibodies to the brain of transgenic mice has been shown to reduce Aβ plaques [171], because more antibodies reached the affected region. However, these methods are invasive since the injection is administered through the skull [172].

The nature of the BBB makes it the most significant obstacle to the transport of drugs into the brain. This obstacle prohibits all large-molecules and most small molecules from entering the brain. This is a limiting factor for the application of therapies in the brain. In the last decade, important studies in animal models (rabbit, mice, monkeys) have shown that pulsed ultrasound administered with ultrasound contrast agent can open the BBB for a short period with minimal side effects [29], [48], [173], [53], [174], [175], [176]. The opening of BBB using FUS can be utilized as a noninvasive method for delivering drugs to the brain.

Relevant studies for AD treatment using FUS by Jordao et al [177],[100] have shown that endogenous antibodies entered the brain after BBB opening using magnetic resonance imaging guided FUS (MRgFUS) and eliminated cortical Aβ plaques in the transgenic TgCRND8 mice. Moreover, in the study by Jordao et al [177] exogenous antibodies were used (BC-10) as a therapeutic agent against Aβ plaque destruction. This transgenic animal model was chosen because it exhibits abundant plaque load.

In another study by Burgess et al [178] it has been shown that repeated MRgFUS led to spatial memory improvement in a transgenic mouse model of AD. The behavior changes could be attributed to decreased amyloid pathologic abnormalities and increased neuronal plasticity. Recently, Leinenga and Götz [179] removed Aβ with repeated scanning ultrasound (SUS) using similar pulsed exposure as other groups in mouse brain, without any therapeutic agent. Plaque burden was reduced in SUS-treated AD mice compared to sham-treated animals, and cleared plaques were observed in 75% of SUS-treated mice. The Leinenga and Götz [179] study, which was conducted concurrently with our study, reported an additional treatment session one month after the first treatment.

In order to test this new therapy, an animal model for AD was needed. A rabbit model fed with high cholesterol diet was utilized, which creates Aβ plaques in the brain. The first study to report that high cholesterol diet in rabbits results to accumulation of Aβ plaques has been demonstrated by Sparks et al [180]. The Aβ plaques were created with a 2% cholesterol-enriched diet for the duration of up to 8 weeks. The mechanism of developing Aβ plaques is not fully understood yet. The rabbits were sacrificed at the end of the experiment because the 2% cholesterol diet caused hypercholesterolemic side effects, at 8 weeks [180].

Our proposed study includes the following major tasks:

Utilize an existing reliable rabbit model that creates AD plaques in the brain. This is achieved by delivering high cholesterol diet in rabbits, a concept that was inspired mostly by the Sparks et al study [180]. Multi session (3 times) BBB opening was applied, either with FUS only or with FUS in synergy with antibodies. Finally, a comparison of the effects of treating with FUS only and with FUS and antibodies was provided [181]. Since there was evidence that the BBB opening was sustained for about 3 hours [64], and based on the evidence of the therapeutic effect of endogenous and exogenous antibodies reported by Jordao et al [177], then it can be claimed that by opening the BBB in 3 successive sessions, increased therapeutic effect due to the repeated entrance of these antibodies can be achieved. The rabbit AD model offered larger brain volume and larger plaque size, therefore it could serve as a better model than mouse.

6.2 Material and Methods

6.2.1 Animals and diet

The animal experimental protocol was approved by the national body in Cyprus responsible for animal studies (Ministry of Agriculture, Animal Services). A total of 52 New Zealand rabbits (3.4–4.1 kg) were used during the experiments. The rabbits were divided randomly into the following groups: In group A (n=3) the rabbits were fed with normal chow. The purpose of this group was to demonstrate the histology of brain without Amyloid beta plaques. In the following groups, the animals were fed a 2 % high cholesterol diet (T2030, Harlan laboratories SRL, Udine, Italy) for 4 months. The daily average consumption of this specialized diet was 200 g per rabbit. Three rabbits (group B) were sacrificed without any treatment in order to be used as a reference for measuring the initial plaque load. Two rabbits (group C) received only antibody treatment. Two rabbits (group D) were exposed only to BBB opening with FUS in order to assess the effect of diffusion into the brain possibly by endogenous antibodies or other proteins. Two rabbits (group E) were exposed to BBB opening with FUS and exogenous antibodies in order to assess the effect of both endogeneous antibodies or other proteins, and exogenous antibodies. In Group F, 16 rabbits were treated with only FUS and antibodies in order to study the effect of time on plaque clearance. In Group G twelve rabbits were treated with only FUS (1, 2 and 3 sessions with n=4 per session). In Group H twelve rabbits were treated with FUS and antibodies (1, 2 and 3 sessions with n=4 per session). Since the staining used required the animal to be sacrificed, the contralateral side of the brain served as a control. Additionally, group B received no treatment and therefore gave an indication of the initial plaque density load. The brain of three rabbits underwent Enzyme-Linked Immunosorbent Assay (ELISA) evaluation in order to confirm the creation of Amyloid beta plaques (Aβ-42). Table 6 summarizes the various groups used during this feasibility study. All animals that received the high cholesterol diet were sacrificed in 4 months, because severe side effects appeared (hypercholesteremic side effects such as weight loss, appetite loss, and jaundice). In addition, these rabbits at this stage demonstrated significant cognitive deficits. After delivering high cholesterol diet for 4 months, the creation of Aβ plaques was present in all animals.

Table 6 : Various groups used during the study for the disruption of Amyloid beta plaques in rabbits

Group	n	Condition	Treatment	Purpose
A	3	Normal diet	None	Demonstrated histology of brain without Amyloid beta plaques.
B	3	2 % high cholesterol diet	None	Real control. Use to measure initial plaque load.
C	2	2 % high cholesterol diet	No FUS. Antibodies only.	Prove that without BBB opening, the injection of antibodies is not so useful.
D	2	2 % high cholesterol diet	FUS only.	Effect of endogenous antibodies or other proteins.
E	2	2 % high cholesterol diet	FUS and antibodies.	Effect of exogenous antibodies.
F	16	2 % high cholesterol diet	FUS and antibodies.	Effect of time in days in clearing Amyloid beta plaques (1, 2, 3, and 4 days).
G	12	2 % high cholesterol diet	FUS only. 1, 2 and 3 sessions with n=4 per session	Effect of endogenous antibodies or other proteins with multiple sessions.
H	12	2 % high cholesterol diet	FUS and antibodies. 1, 2 and 3 sessions with n=4 per session	Effect of exogenous antibodies with multiple sessions.

6.2.2 Focused ultrasound system

The focused ultrasound system was composed of a signal generator (HP 33120A, Agilent technologies, Englewood, CO, USA), an RF amplifier (150 W, AR, Souderton, PA, USA), and a spherically shaped bowl transducer made from piezoelectric ceramic of low magnetic susceptibility (Etalon, Lebanon, IN, USA). The transducer operates at 1 MHz, had a focal length of 10 cm and a diameter of 4 cm. The welfare of the animal was monitored by an MRI compatible camera (MRC Systems GmbH, Heidelberg, Germany).

The positioning device had 3 computer controlled axes (X, Y, and Z). All the parts of the positioning device were manufactured using a 3D printer (FDM400, Stratasys, 7665 Commerce Way, Eden Prairie, Minnesota, 55344, USA). The positioning device can be placed on the table of any MRI scanner. The range of the robot was: X: 120 mm, Y: 80 mm, and Z: 50 mm. The positioning device was manufactured by MEDSONIC LTD, Limassol, Cyprus. Figure 63 shows the placement of the rabbit in the positioning device for performing in vivo experiments.

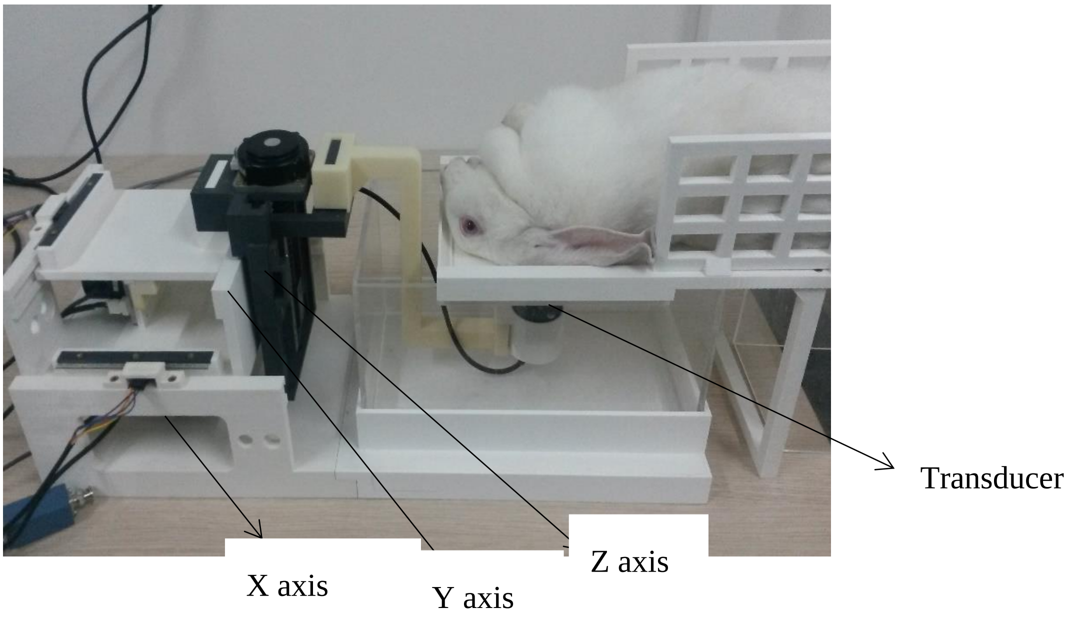

Figure 63 : Placement of the rabbit in the positioning device for performing in vivo experiments.

The FUS system was utilized in an MRI scanner (Signa 1.5 T, by General Electric, Fairfield, CT, USA). A spinal coil (USA instruments, Cleveland, OH, USA) was used to acquire the MRI signal. The opening of the BBB was imaged using MRI contrast-enhanced T1-weighted fast spin echo: Repetition time (TR): 500 ms, Echo time (TE): 18

ms, Echo train length (ETL): 4, Bandwidth (BW): 16 kHz; matrix size: 256 X 256; Number of excitations (NEX): 4; Field of view (FOV): 10 cm; slice thickness: 3 mm; interslice spacing: 0.3 mm). The MRI contrast was achieved using a contrast agent (Magnevist®, Berlex Laboratories, Inc., Wayne, NJ), which was injected intravenously at a dose of 0.125 mmol per kg of body weight as a bolus injection. The contrast agent was injected roughly 5 mins after sonication, and imaging was initiated 5 mins after the injection of the contrast agent.

6.2.3 Antibodies

A dose of 40 μg/kg of anti β amyloid protein antibody (BC-10, Sigma Aldrich, St Louis, MO, USA) with molecular weight of 100 KDa was delivered through the ear vein. It has been shown by Bard et. al., 2000 [182] that antibodies delivered peripherally bind to the Aβ plaques. The antibodies were delivered about 5 minutes before BBB opening.

6.2.4 Cholesterol measurement

The cholesterol of the rabbits was measured by extracting blood from the ear vein after overnight fasting immediately before sacrificing the species using the enzymatic cholesterol oxidase method (kit by Sigma Aldrich, Saint Louis, MI, USA).

6.2.5 Histopathological techniques

Coronal frozen sections (20 μm) were cut from the excised brains, and cut at the level of the hippocampus from treated rabbits. The sections were air-dried, fixed in 10% formalin for 10 min, and treated with 1% hydrogen peroxide in PBS. Then the sections were incubated with blocking solution of 1.5% normal serum (Vector Laboratories, Peterborough, UK). For the estimation of amyloid plaque load sagittal sections of 20 μm thicknesses spanning all the hippocampal formation were chosen for Thioflavine-S staining (Sigma Aldrich, Saint Louis, MI, USA). Sections were incubated for 8 minutes in aqueous solution of Thioflavine-S (1% w/v). The sections were then differentiated with 80 % Ethanol for 3 minutes, and with 95% Ethanol for 3 minutes. Sections were rinsed three times with double distilled water. Imaging for Thioflavine-S was performed on an Olympus microscope (BX 50, Tokyo, Japan).

The plaque load was measured using the freeware software imageJ, which counted dots in histological slides which were stored in digital format. The software measured dots either in automatic mode or, in the case of dots that were very close, in manual mode.

6.2.6 Measurement of acoustic pressure

The peak negative pressure was measured in a tank filled with degassed water. The measurement was performed using a calibrated hydrophone (HGL series, ONDA Corporation, Sunnyvale, CA 94089 USA). The free-field pressure field produced by the FUS transducer was measured using a 3-D positioning device with the needle hydrophone (ONDA Corporation). The spatial resolution was 0.1 mm in the radial direction (X- and Y -axes) and 0.5 mm in the axial direction (Z-axis), with measured distance of 40 and 120 mm in the Z axis and 3 mm in the radial direction. The maximum peak negative acoustic pressure measured at the focus was 0.8 MPa, which was equivalent to 190 W of electrical power. The half-pressure length of the acoustic field measured with a hydrophone (ONDA corporation), was 21 mm and the corresponding half-pressure width was 1.5 mm. The value reported for the rabbit experiments was estimated in the brain based on ultrasound attenuation of 5 Np/m/MHz [183] through a 1 cm path. A loss of 14 dB/cm-MHz was considered for the 3 mm skull, based on the data reported Pinton et. al. [184]. The total power delivered by the transducer was measured before the beginning of each experiment with an ultrasound power meter (Model UPM-DT-100N, Ohmic Instruments, Easton, MD, USA).

6.2.7 Hematoxylin and Eosin (H&E)

Histologic examination using H&E was performed in 3 rabbit brains. After sacrifice, the brains were removed and formalin-fixed, and paraffin-embedded sections were prepared with a thickness of 20 μm. Sections were stained with H&E for histologic evaluation of the effects of the FUS exposure. There are many papers discussing the pressure threshold for hemorrhage during BBB opening, but these papers either used different frequency, or the pressure indicated might not be the minimum. Therefore, the H&E test was used to ensure that no hemorrhage was caused by the acoustic pressure used (0.8 MPa).

6.2.8 ELISA analysis

The rabbit Beta Amyloid 1-42 (Aβ42) ELISA kit (Thermo Fisher Scientific) was used for the quantitative determination of Aβ42 in brain tissue using a 96-well plate and a microplate reader. The assay recognizes rabbit Aβ42. The Aβ antigen binds to the immobilized (capture) antibody. Bound rabbit antibody was detected by the use of a horseradish peroxidase-labeled anti-rabbit antibody. After removal of excess anti-rabbit antibody, a substrate solution was added, which acted upon by the bound enzyme to produce color. The intensity of this colored product was directly proportional to the concentration of rabbit Aβ42 present in the original specimen. Treated and untreated brain tissue from 3 rabbits was homogenized in a 20 mM Tris-buffered solution. Soluble Aβ was extracted using DEA/NaCl solution, followed by centrifugation. The supernatant was removed and neutralized for soluble Aβ analysis. The total fraction was solubilized in cold formic acid, followed by sonication and centrifugation. The supernatant was similarly collected and neutralized.

6.2.9 In vivo experiments

The rabbits were anaesthetized using a mixture of 500 mg of ketamine (100 mg/mL, Aveco, Ford Dodge, IA), 160 mg of xylazine (20 mg/mL, Loyd Laboratories, Shenandoah, IA), and 20 mg of acepromazine (10 mg/mL, Aveco, Ford Dodge, IA) at a dose of 1 mL/kg.

The rabbits were sacrificed at different timing depending on the study group (ranging from 1 to 4 days) in order to allow enough time for exogenous antibodies to bind to the plaques. There is evidence that the BBB after FUS exposure remains open for 3 hours [64].

The total time of sonication was 20 s. The pulse length was 10 ms with pulse repetition period of 1 s. One pulse sonication was needed to open the BBB. The decision of using these parameters was based on the study by McDannold et al 2005 [174], and Hynynen et al 2001 [64]. The power used was adjusted so that the peak negative pressure was set to 0.8 MPa.

The ultrasound contrast agent used was SonoVue **(**Bracco Imaging France SAS, Courcouronnes, France). The injection was administered 10 seconds before sonication. The method of delivering the contrast agent was intravenous from the ear vein as a bolus injection. The dosage used was 50 µl/kg of body weight [174], which is the dose used in humans.

6.2.10 Statistical Analysis

Data were analyzed for statistical significance using one-way analysis of variance (ANOVA). All values in each group were expressed as mean value ± SEM. All group comparisons were considered significant at $p < 0.05$.

6.3 Results

Serum total cholesterol concentrations varied from 40 to 85 mg/dL in control rabbits (n=4) and from 659 to 1600 mg/dL in the cholesterol-fed rabbits (n=28). The mean in the 28 cholesterol-fed rabbits was 955 mg/dL (standard deviation was 226 mg/dL).

The opening of the BBB was demonstrated as shown in Figure 64A with MRI contrast-enhanced T1-W fast spin echo. The contrast agent was injected 5 mins after sonication, and imaging was initiated 5 mins after the injection of the contrast agent. The contrast-enhanced area (with enhanced signal) corresponds to the area sonicated by the transducer (4 X 4 grid with step of 2 mm). Therefore, the volume of the BBB opening was approximately 1 cm X 1 cm X 2 cm (2 cm^3). This was calculated based on the size of the 10 mm X 10 mm grid (plane perpendicular to the transducer beam) and the 20 mm penetration depth (plane parallel to the transducer beam) which basically covered almost the entire brain of the rabbit. The targeting of the site shown was achieved by navigating the transducer using the positioning device. The temperature change in the brain tissue during BBB opening did not exceeded 2 ^{o}C. The beam was identified using the technique of applying low acoustic intensity, and thus detecting the beam spot using MR thermometry. In this particular figure, the target was placed in the right lobe. Figure 64B shows HE staining of the FUS exposure used in Figure 64A (ie BBB opening) demonstrating no haemorrhage due to the level of applied pressure.

Fig 65A shows a coronal section of a rabbit brain, cut in the hippocampus of a control rabbit with no diet (Group A) showing no plaque accumulation. Figure 65B shows a coronal section of a rabbit brain (Group B), cut in the hippocampus of a high cholesterol-fed rabbit with no treatment. Fig 65D shows a coronal section of a rabbit brain, cut in the hippocampus with treatment with antibodies only (Group D) showing no visible destruction of plaques. Fig 65C shows a coronal section of a rabbit brain, with BBB opening using FUS (Group C) demonstrating some visible reduction of plaques in the right hemisphere.

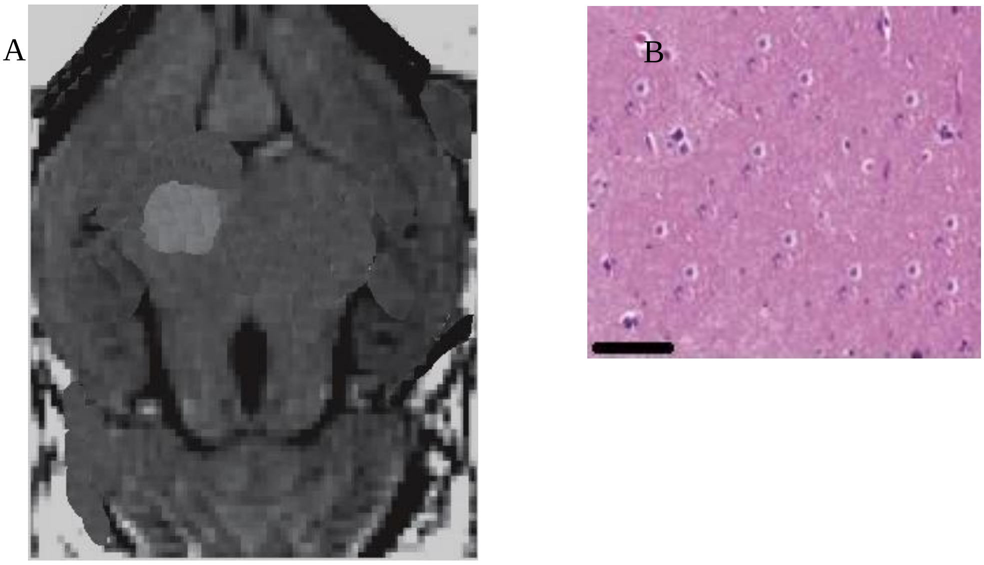

Figure 64 : A) Demonstration of BBB disruption using MRI contrast-enhanced T1-Weighted fast spin echo. B) HE staining of the FUS exposure used in Figure 64A

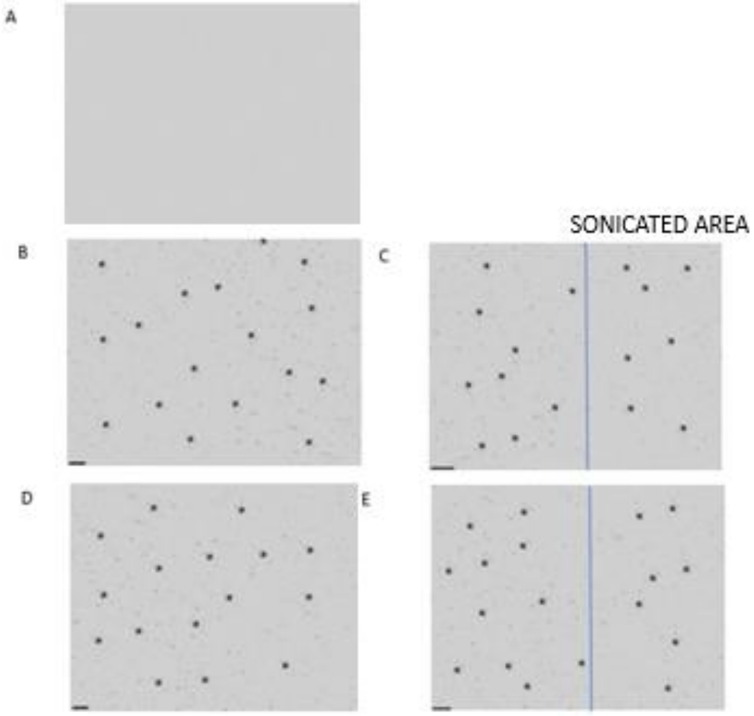

Figure 65 : A) Coronal section of a rabbit brain, cut in the hippocampus of a rabbit with no diet (group A), B) Coronal section of a rabbit brain, cut in the hippocampus of a control rabbit with no treatment at all (group B). C) Coronal section of a rabbit brain, with BBB opening using FUS only (group D). D) coronal section of a rabbit brain, cut in the hippocampus with no BBB opening and treatment with antibodies only (group C). E) Coronal section of a rabbit brain, with BBB opening using FUS and antibodies (group E). Bar=100 µm.

The plaque load decreased from $200/cm^2$ (control of group B) to $190/cm^2$. Fig 65E shows a coronal section of a rabbit brain, with BBB opening using FUS and antibodies (Group E) demonstrating some visible reduction of plaques in the right hemisphere. The plaque load decreased from $200/cm^2$ (control of group B) to $133/cm^2$. Test performed in selected rabbits using ELISA kits confirmed that these plaques were Aβ-42 plaques.

Fig 66 shows the plaque load in rabbit brain measured at different days after treated with FUS and antibodies and only one session. This result showed that the full effect of antibodies on plaque reduction was reached after 3 days.

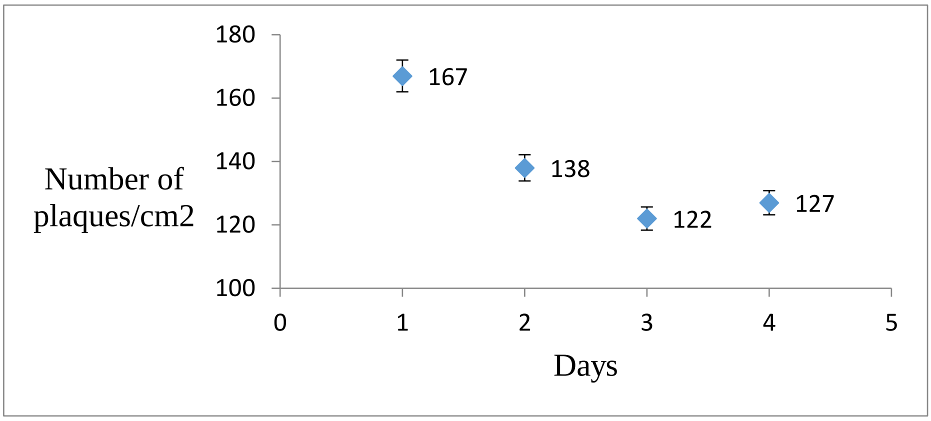

Figure 66 : Plaque load in rabbit brain measured at different days after treated with FUS and exogenous antibodies.

Figure 67A shows a coronal section of a rabbit brain, cut in the hippocampus treated with exogenous antibodies and 1 session of BBB opening using FUS. The left part of the brain included severe accumulation of Aβ 42-plaques. The right part of the brain showed substantial reduction of Aβ plaques. Figure 67B shows a coronal section of a rabbit brain, cut in the hippocampus treated with exogenous antibodies and 2 sessions of BBB opening using FUS. Each session was 3 days apart. The right part of the brain showed reduction of Aβ plaques compared to the case of 1 session FUS with $p<0.001$. Figure 67C shows a coronal section of a rabbit brain, cut in the hippocampus treated with exogenous antibodies and 3 sessions of BBB opening. Each session was 3 days apart. The right part of the brain showed reduction of Aβ plaques compared to the case of 1 session FUS with $p<0.001$. In all animal groups injected with exogenous antibodies, a significant reduction in plaques was observed ($p<0.05$, $p<0.001$ and $p<0.001$ for 1, 2 and 3 sessions, respectively).

These preliminary findings motivated us to acquire some more data from the histological sections in order to get quantitative measurements of the reduction in the number of plaques for the two different treatments (FUS only and FUS and antibodies).

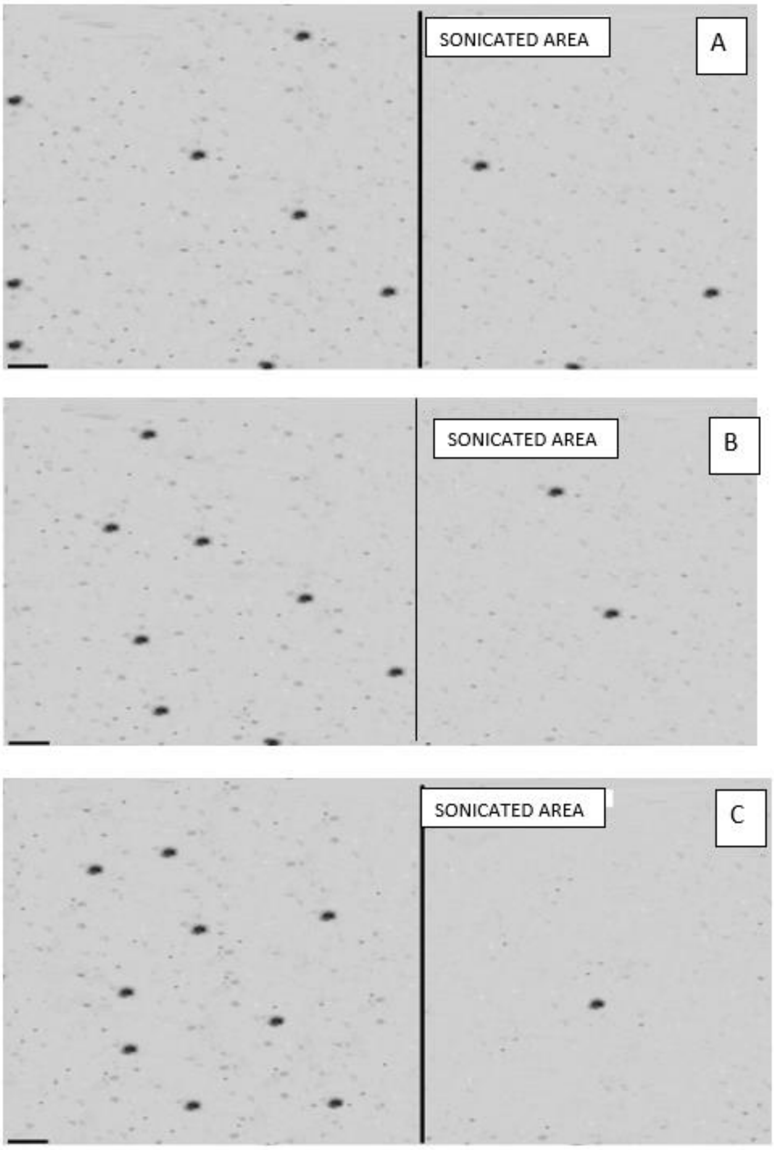

Figure 67 : A). Coronal section of a rabbit brain, cut in the hippocampus treated with exogenous antibodies and 1 session of BBB opening using FUS. B) Coronal section of a rabbit brain, cut in the hippocampus treated with exogenous antibodies and 2 sessions of BBB opening using FUS. C) Coronal section of a rabbit brain, cut in the hippocampus treated with exogenous antibodies and 3 sessions of BBB opening using FUS.

Figure 68 shows the distribution of plaque sizes in rabbits fed with high cholesterol diet, with 1 session (Figure 68A), with 2 sessions (Figure 68B), and with 3 sessions (Figure 68C). Plaques larger than 10 µm in diameter represents only 4 % (8/200) of the total plaques (based on the untreated area for session 1). Most of the plaques (145/200) were of diameter between 2-10 µm. Finally, small plaques (< 1µm) represent 22.5 % (45 out of 200) plaques. The number of plaques for this animal model was approximately 200 plaques/cm2 with surprisingly small variability (standard deviation is 9). The plaque size in humans with AD could be larger, and therefore it was possible that the efficacy of the proposed method was overestimated in this small animal model.

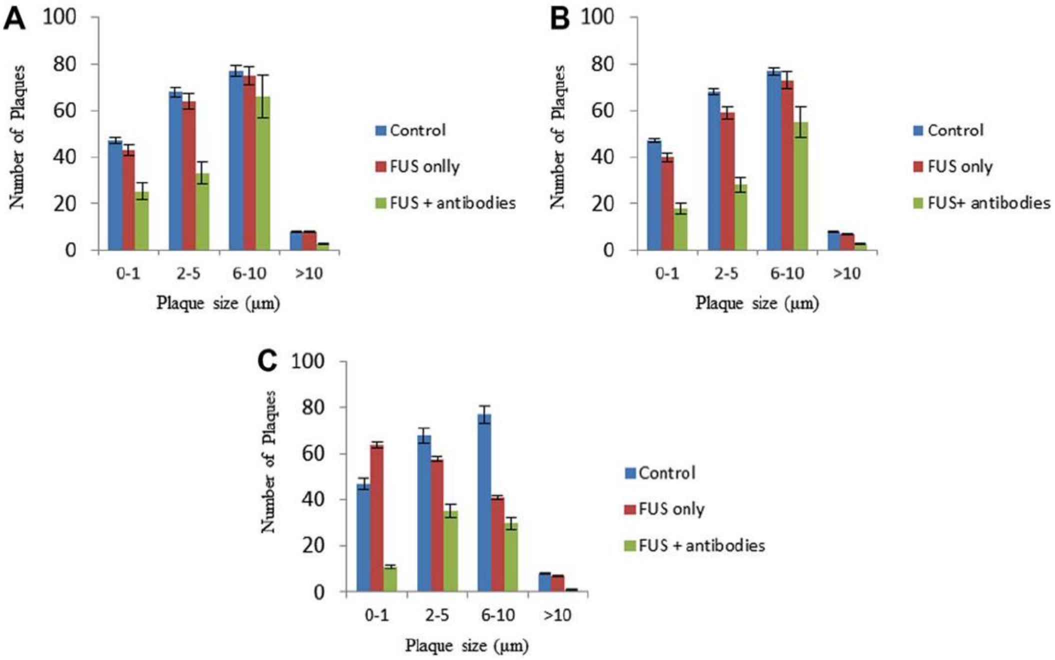

Figure 68 : Distribution of plaque size using the high cholesterol diet in rabbits with 1 session (Figure 68A), with 2 sessions (Figure 68B), and with 3 sessions (Figure 68C).

The reduction of the number of plaques due to the two methods (FUS only and FUS with antibodies) is summarized in Table 7. This table shows the average number of plaques/cm^2 with standard deviation vs treatment method at different instances (control, after opening the BBB once, twice and three times).

Table 7 : Average Number of plaques/cm2 (standard deviation) vs. treatment method (FUS only, FUS and antibodies) at different instances (control, after 1 BBB opening, 2 BBB openings and 3 BBB openings) with statistical indicators included.

	Average Number of plaques per cm^2 (standard deviation)			
	Control N=3	One BBB session N=4	Two BBB sessions N=4	Three BBB sessions N=4
FUS only	200 (9)	190 (12) p=0.07	179 (11) p=0.02	177 (9) p=0.03
FUS and antibodies	200 (9)	127 (7) p=0.05	104 (14) p=0.001	78 (14) p=0.001

6.4 Discussion

High-cholesterol-enriched diet produced Aβ plaques in the rabbit brain as it was shown previously by Sparks et. al 2004 [185]. This useful animal model was also confirmed in this study. The molecular mechanism by which high cholesterol diet produces Aβ like plaques is not fully understood yet. This animal model has been also used by other groups for other applications. One example was atherosclerosis which had been reported to positively correlate with the cerebral deposition of Aβ plaques in the B6Tg2576 mouse model for Alzheimer's disease [186]. In this article the goal was to develop an animal model for the evaluation of FUS for reducing Aβ plaques.

Our study showed that the maximum size of plaque was 30 μm (see Figure 65B). The size of Aβ plaques in mice as reported from the study by Yan et. al. 2009 [187] was 20 μm. In the study by Prasanthi et. al. 2008 [188] the plaques in rabbit were approximately 10 μm and in another study by Sharma et.al. 2008 [189] the maximum plaque size in rabbit was close to 20 μm. We cannot confirm whether the maximum plaque size was achieved, because we had to sacrifice the animal after 4 months, to avoid distress of the rabbit. It was suggested by Serrano-Pozo et. al. 2012 [190] that plaques in humans reached a stable size distribution and did not substantially grew over decades. Therefore, we are not certain whether maximum plaque size and quantity was reached.

Although dietary cholesterol has no effect on the processing of β-APP or on the production of Aβ in the brain, high cholesterol diets results in the production of Aβ plaques in the brain. This was demonstrated from studies of cholesterol-fed animals [169], [170], [191], [192], and also confirmed by our study. Similar effect was also seen in mice-fed with high cholesterol diets [191]. A primary goal of the proposed study was the delivery of a therapy with multiple BBB openings (called sessions). Each session was three days apart, and a maximum of 3 sessions were used. The major conclusion is that by increasing the number of sessions, the number of plaques decreased (both for FUS only approach and for the FUS and antibodies approach). With FUS only, the number of plaques dropped from 200 plaques/cm^2 (average) to 170 plaques/cm^2 (average). The overall drop of 30 plaques/cm^2 (average) was possibly caused by the endogenous antibodies and it was comparable to the numbers reported by Jordao et. al. 2010 [177] and Jordao et. al. 2013 [100]. From Figure 68 one can observe that not all large plaques (> 10 μm) were eliminated with FUS only. The reason that the number of plaques decreased due to the multiple sessions with FUS and bubbles only is possibly attributed to the fact that the body produced endogenous antibodies [177] and thus by opening the BBB frequently contributed to plaque reduction. The rate plaque elimination due to FUS alone which was close to 10 /cm^2 per session is considered slow. In the future if a patient with serious AD is treated with a phased array transducer non-invasively with multiple opening of the BBB (e.g. for 5-10 sessions) it may be possible to reduce the plaques for this patient without the need of any drugs.

The effect of exogenous antibodies was more drastic. With 3 sessions the average number of plaques/cm^2 was reduced from 200 to 78. As we know part of this reduction (nearly 30 plaques/cm^2) was possibly due to the endogenous antibodies [177], [100] which entered the brain due to BBB opening. The rest of the reduction is attributed to the exogenous antibodies. Jordao et. al. 2010 [177] showed that in some mice a reduction in the number of plaques of almost 20 % was achieved due to exogenous antibodies. The larger drop observed in our results is attributed to the multiple sessions delivered (3 sessions). If endogenous antibodies affected the results, then with multiple BBB openings (3 in our study) then this effect was possibly additive. It is possible to enhance the proposed treatment further, by prolonging the opening of the BBB by using repeated FUS as proposed by Yang et. al. 2011 [193]. The prolongation of the BBB will allow more time for the antibodies to enter the brain.

Thus, the proposed study demonstrated that by opening the BBB, it will be possible to deliver exogenous antibodies to the brain, which reduces Aβ plaques. More importantly by opening the BBB frequently (3 times in this study) the reduction in the number of plaques was accelerated. Therefore, FUS has the potential to be used non-invasively for the treatment of AD. The response seen in plaque elimination in rabbits needs to be investigated also in humans. This dramatic response observed for rabbits might not be as prominent in humans, but even a less drastic response could be very beneficial for this neurodegenerative disease. FUS has been already proven successful for treating patients with essential tremor [194], therefore it may also play a role in other neurological diseases.

According to Mould and Sweeney [195] the half-time of the various antibody isotopes in humans varies between 2 and 6 days (exception is IgG which is 23 days). It is logical to assume that the manufacturers of animal antibodies try to produce antibodies with half-times close to humans. It was observed in our experiments that the antibodies must be allowed to react with amyloid beta plaques for at least 3 days. Therefore, 3 days must elapse until a new session of FUS is initiated.

Since the animals had to be sacrificed it was impossible to assess whether the plaque reduction restored the neurological deficits. This is a very important study that has to be done in the future. It must be proven, that by reducing the plaque load, the neurological deficits are hopefully restored.

By opening the BBB frequently more time was allowed for the exogenous antibodies to react with the plaques and therefore better therapeutic result was achieved. If this application is proven successful, it may be possible in the future that patients visit a hospital frequently on an outpatient basis and receive FUS/antibody therapy (similar to Dialysis patients).

The main advantage of the rabbit model compared to the mouse model is the bigger size of the brain which provides larger brain and therefore possibly better focusing. Also, the plaque size in rabbits is probably larger than the plaques produced in mice. However, there are several drawbacks with the production of the rabbit model. The skull thickness for the rabbits we used varies from 2-3 mm. If thermal ablation was the targeted modality, this would have required high energies in order to create ablative temperatures in the brain. This would have resulted to severe skull heating. However, for the purpose of BBB opening, the high power used for few ms was sufficient to open the BBB. Nevertheless, regarding ultrasound transmission the mouse model is superior because its skull thickness is smaller. Additionally, the cost of implementing the rabbit model is five times bigger than the mouse model (mostly attributed to the expensive diet). Furthermore, the rabbit model requires 3 months to be fully developed, whereas the mouse model requires approximately 2 weeks. Finally, the possibility of producing Amyloid beta plaques in the mouse is quite high. From our experience some rabbits did not produce the expected plaques.

In the future it is planned to perform experiments for a larger group of animals, thus producing sufficient statistical evidence. A longterm study, outside the scope of the current study, is required to evaluate whether this decrease of amyloid β plaque restores neurological deficits. Another improvement is to realize the attachment of antibody to amyloid plaques using antibody labeling. This attachment was shown by Jordao et al. 2010 [177], but needs to be demonstrated also for the delivery of multiple sessions using FUS. Finally, another important issue is to evaluate the effect of any other protein that could possibly enter through the BBB. This requires extensive experimental work using proper protein labeling.

6.5 Conclusions

The main objective of the study was to remove Amyloid beta plaques using multiple sessions of FUS-induced BBB opening using microbubbles with and without antibodies in a rabbit model. An animal model using high cholesterol diet in rabbits for 4 months was used. With this model plaques of 30 μm in diameter were produced. By increasing the number of sessions, the number of plaques decreased (both for FUS only and with FUS and antibodies). With FUS only the average number of plaques/cm^2 dropped from 200 (before treatment) to 170 plaques/cm^2. The effect of FUS with exogenous antibodies was more drastic. With 3 BBB opening sessions the average number of plaques/cm^2 was reduced from 200 to 78. This study demonstrated that by opening the BBB, it will be possible to deliver exogenous antibodies to the brain, which eliminates Amyloid β plaques. More importantly by opening the BBB frequently (3 times in this study) the reduction in the number of plaques was accelerated.

7 Conclusions

This doctoral dissertation has examined various challenges for the use of HIFU in a brain application. The study was separated into four different sub-studies in the area of agar phantoms and brain applications. The first study was concentrated on the design and creation of a suitable agar phantom to be used in HIFU application on the blood brain barrier. A model that currently is not available to researchers, whereas all experiments are performed on animal models. The second objective of this dissertation was the evaluation of the attenuation is agar phantoms with various concentrations. The next study included the evaluation of the mechanical effects of agar phantoms such as the structure and the stiffness since these data will help in understanding better the effect in the structure of the phantom according to its composition. The third study included the evaluation of an alteration in the composition of an agar phantom with the use of a preservative and its effect in the life of the phantom in combination with the storing conditions. Finally, the last study examined an application for the reduction of amyloid β plaques in a rabbit model with the use of antibodies crossing the blood brain barrier.

The first study was inspired by the fact that all of the experiments performed for BBB disruption are usually done on animal models thus the need for a model of BBB opening is important in order for HIFU protocols to be easily tested. This made experiments in this area expensive and time consuming. Therefore, trials have been made in order to create a suitable phantom model that would represent the BBB function and disruption during HIFU applications, showcasing the leakage that actually occurs during this disruption. An initial model was achieved, showcasing a liquid flow in a closed system under normal conditions and a liquid leakage after HIFU application, just like what happens during BBB disruption applications of HIFU. This model was comprised by a set of tubes properly sealed that allowed fluid circulation with no leakage in steady state. When a common HIFU protocol for BBB disruption in animal models was applied, this system allowed liquid leakage.

This model can be used as a base for advancing and developing an accurate and innovative phantom model that will replace some animal models. In this way researchers will be able to perform more accurate and cost-effective experiments using a phantom, testing several different protocols and parameters and gaining valuable knowledge for BBB disruption.

The proposed model is simplistic regarding its physical structure. The intention with this study is to inspire researchers to develop more advanced models that mimic BBB opening. The attenuation of the agar phantom did not allow liquid leakage with the current equipment. This model though can be used as a basis for others to advance further and create a more complex model.

The second study involved the evaluation of the variation of ultrasonic attenuation coefficient with different concentrations of evaporated milk, agar, and silicon dioxide. A repeatability test was performed for each one of the tested recipes and attenuation coefficients were acquired using the through-transmission method. Small day to day variability was observed for most of the agar-based gels, indicating the stability of the measurement system. The variable-thickness technique was also used and resulted in slightly lower values of attenuation coefficients, as expected, proving extra evidence of the accuracy of the estimated values.

Depending on the agar, silicon dioxide, and evaporated milk concentration, the attenuation coefficient varied in the range of 0.30-1.49 dB/cm-MHz. A linear increment of attenuation was observed with increasing agar (up to 6 %), silicon dioxide (up to 4 %), and evaporated milk (up to 30 %) concentration. It was also noticed that the attenuation coefficient can best be regulated by varying the amount of silicon dioxide. The addition of 1 % w/v of silicon dioxide contributed to an increase of attenuation by 0.101 dB/cm-MHz up to a 4 % concentration. The addition of 10 % v/v evaporated milk increased the attenuation by 0.127 dB/cm-MHz probably due to absorption. Evaporated milk was found to have a minimal contribution to attenuation (0.013 dB/cm-MHz for every 1 % v/v of evaporated milk), compared to the attenuation contribution of silicon dioxide (0.101 dB/cm-MHz for every 1 % w/v of silicon dioxide).

The findings of this study have been compared to the attenuation coefficient values found in the literature for human and animal tissues, as well as to the ones obtained for the freshly excised rabbit tissue in the current study. This work has led to the conclusion that agar-based phantoms with attenuation coefficient values similar to those of human and animal tissues can be developed with the proper selection of percentage of agar, silicon dioxide, and evaporated milk.

The third study aimed in investigating the mechanical properties of the widely used agar phantoms and their correlation to each of the phantom's components. There are various phantom formulations used among researchers each providing a different characteristic to the phantom. Since the mechanical effects of these phantoms were not measured before, this study revealed the structure of the phantoms using SEM and estimated their elastic modulus, for each combination of composition.

It was observed that each of the three components of the phantom, have a major effect on the structure of the phantom itself. By increasing the agar percentage, the phantoms become denser, smoother and stiffer. When the agar concentration was kept constant and the percentage of silicon dioxide changed, the phantoms became rougher in terms of texture and the elastic modulus increased until it reached its peak. One possible cause for this fact is the increase in bubbles when preparing the phantom, while mixing and dissolving the larger quantities of silicon dioxide becomes more difficult. Additionally, the increase in evaporated milk showed a significant decrease in the stiffness of these phantoms since milk is a less rough material. Finally, the aging parameter was also investigated while examining the structure of two phantoms with similar composition but different day of preparation. The phantoms were stored in refrigeration and tested for microstructural changes in specimens aged at four and ten days respectively. There were no significant changes in the structure between the two phantoms.

The fourth study had as its main objective to investigate the effect of the addition of a widely used preservative such as sodium benzoate into a well-tested composition of agar phantom. In parallel, the influence of the storing conditions were examined and correlated with the use of the preservative. Based on the results of this study key conclusions were made revolving the whole process. At first, the presence of evaporated milk in the composition holds a key role for its preservation. The milk provides the perfect ground for fungus to grow with all the necessary nutrients for further development. In addition, the existence of sodium benzoate in some of the phantoms provided indications of a mild fungal growth prevention but not enough to avoid the growth completely. A detrimental role in the stability and life span of the phantoms plays the storing condition of the phantom. A phantom cannot be preserved in room temperatures without spoiling even if it is not in contact with air. On the contrary, phantoms that were stored in glycerol/water solution and in refrigeration remained intact for the entire course of this study. Therefore, this storing method is an effective way to store the produced agar phantoms for longer periods of time.

A future development of this study could be the measurement of the pH of the agar phantom and its correlation with a more suitable preservative. Each preservative varies its effect according to the pH of the environment, making some more suitable for certain cases. Eventually, if the pH of the phantoms is defined, then a preservative could be selected and investigate the effect it would have on the durability of the phantom.

Finally, the last study focused in removing Amyloid beta plaques using multiple sessions of FUS-induced BBB opening using microbubbles with and without antibodies in a rabbit model. An animal model using high cholesterol diet in rabbits for 4 months was used. With this model plaques of 30 μm in diameter were produced. By increasing the number of sessions, the number of plaques decreased (both for FUS only and with FUS and antibodies). With FUS only the average number of plaques/cm2 dropped from 200 (before treatment) to 170 plaques/cm2. The effect of FUS with exogenous antibodies was more drastic. With 3 BBB opening sessions the average number of plaques/cm2 was reduced from 200 to 78. This study demonstrated that by opening the BBB, it will be possible to deliver exogenous antibodies to the brain, which eliminates Amyloid β plaques. More importantly by opening the BBB frequently (3 times in this study) the reduction in the number of plaques was accelerated.

These five studies are only a small part of the studies and investigations performed in the Therapeutic Ultrasound Laboratory of Cyprus University of Technology. The lab completed numerous studies involving robotic systems and positioning devices used in various areas of therapeutic ultrasound [115], [196]–[202]. Also a wide range of phantoms has been developed, each of them focusing on a different tissue and application [112], [114], [203]–[205] In addition, studies in vitro and in vivo were conducted using also applications in animal models [181], [206]–[209]. The investigations examine multiple diseases that humanity deals with in daily life such as cancer, Alzheimer's Disease, atherosclerosis, fibroids etc, providing possible treatments using therapeutic ultrasound.

8 REFERENCES

[1] J. G. Lynn, R. L. Zwemer, A. J. Chick, and A. E. Miller, “a New Method for the Generation and Use of Focused Ultrasound in Experimental Biology.,” *J. Gen. Physiol.*, vol. 26, no. 2, pp. 179–93, 1942.

[2] H. E. Cline, J. F. Schenck, K. Hynynen, R. D. Watkins, S. P. Souza, and F. A. Jolesz, “MR-Guided Focused Ultrasound Surgery,” *Journal of Computer Assisted Tomography*, vol. 16. pp. 956–965, 1992.

[3] K. Hynynen, A. Darkazanli, E. Unger, and J. F. Schenck, “MRI-guided noninvasive ultrasound surgery,” *Med. Phys.*, vol. 20, no. 1, pp. 107–115, Jan. 1993.

[4] K. Hynynen, A. Darkazanli, C. A. Damianou, E. Unger, and J. F. Schenck, “The usefulness of a contrast agent and gradient-recalled acquisition in a steady-state imaging sequence for magnetic resonance imaging-guided noninvasive ultrasound surgery.,” *Invest. Radiol.*, vol. 29, pp. 897–903, 1994.

[5] C. M. C. Tempany, E. a Stewart, N. McDannold, B. J. Quade, F. a Jolesz, and K. Hynynen, “MR imaging-guided focused ultrasound surgery of uterine leiomyomas: a feasibility study.,” *Radiology*, vol. 226, pp. 897–905, 2003.

[6] M. E. Ikink *et al.*, “Ultrasound with Direct Skin Cooling for the Treatment of Symptomatic Uterine Fibroids : Proof-of-Concept Study,” vol. 2015, 2015.

[7] F. Orsi *et al.*, “High-Intensity Focused Ultrasound Ablation: Effective and Safe Therapy for Solid Tumors in Difficult Locations,” no. September, pp. 245–252, 2010.

[8] Y. Hsiao, S. Kuo, H. Tsai, M. Chou, and G. Yeh, “Journal of Cancer Clinical Application of High-intensity Focused Ultrasound in Cancer Therapy,” vol. 7, 2016.

[9] A. P. Malietzis G., Monzon L., Hand J., Wasan H., Leen E., Abel M., Muhammad A., Price P., “High-intensity focused ultrasound : advances in technology and experimental trials support enhanced utility of focused ultrasound surgery in oncology,” no. January, 2013.

[10] M. A. Abcdefg, M. Z. Mahmoud, K. S. A. Abcdefg, A. S. Abcdef, and M. A. F. Abcdef, “High-Intensity Focused Ultrasound (HIFU) in Localized Prostate Cancer Treatment,” pp. 131–141, 2015.

[11] A. Napoli *et al.*, “Real-time magnetic resonance-guided high-intensity focused ultrasound focal therapy for localised prostate cancer: Preliminary experience,” *Eur. Urol.*, vol. 63, pp. 395–398, 2013.

[12] G. Hatiboglu, I. V Popeneciu, M. Deppert, B. Hadaschik, M. Hohenfellner, and D. Teber, “Quality of life and functional outcome after infravesical desobstruction and HIFU treatment for localized prostate cancer,” *BMC Urol.*, pp. 1–7, 2017.

[13] F. Wu *et al.*, “A randomised clinical trial of high-intensity focused ultrasound ablation for the treatment of patients with localised breast cancer,” *Br. J. Cancer*, vol. 89, no. 12, pp. 2227–2233, 2003.

[14] P. E. Huber *et al.*, “A New Noninvasive Approach in Breast Cancer Therapy Using Magnetic Resonance Imaging-guided Focused Ultrasound Surgery A New Noninvasive Approach in Breast Cancer Therapy Using Magnetic Resonance Imaging-guided Focused Ultrasound Surgery 1,” pp. 8441–8447, 2001.

[15] H. Furusawa *et al.*, “The evolving non-surgical ablation of breast cancer: Mr Guided focused ultrasound (MRgFUS),” *Breast Cancer*, vol. 14, no. 1, pp. 55–58, 2007.

[16] E. C. Gombos, D. F. Kacher, H. Furusawa, and K. Namba, “Breast focused ultrasound surgery with magnetic resonance guidance.,” *Top. Magn. Reson. Imaging*, vol. 17, pp. 181–188, 2006.

[17] K. Hynynen *et al.*, “MR imaging-guided focused ultrasound surgery of fibroadenomas in the breast: a feasibility study.,” *Radiology*, vol. 219, no. 11, pp. 176–185, 2001.

[18] C. Zavaglia, A. Mancuso, A. Foschi, and A. Rampoldi, “High-intensity focused ultrasound (HIFU) for the treatment of hepatocellular carcinoma : is it time to abandon standard ablative percutaneous treatments ?,” vol. 2, no. 4, pp. 184–187, 2013.

[19] L. Liu *et al.*, “Potential enhancement of intravenous nano - hydroxyapatite in high

- intensity focused ultrasound ablation for treating hepatocellular carcinoma in a rabbit model," pp. 1485–1492, 2014.

[20] L. Zhang *et al.*, "High-intensity focused ultrasound (HIFU): Effective and safe therapy for hepatocellular carcinoma adjacent to major hepatic veins," *Eur. Radiol.*, vol. 19, pp. 437–445, 2009.

[21] R. W. Ritchie *et al.*, "Extracorporeal high intensity focused ultrasound for renal tumours: a 3-year follow-up," pp. 1004–1009, 2010.

[22] H. J. Jang, J. Lee, D. Lee, W. Kim, and J. H. Hwang, "Current and Future Clinical Applications of High-Intensity Focused Ultrasound (HIFU) for Pancreatic Cancer," vol. 4, no. September, pp. 57–61, 2010.

[23] S. Dababou, C. Marrocchio, J. Rosenberg, R. Bitton, K. B. Pauly, and A. Napoli, "A meta-analysis of palliative treatment of pancreatic cancer with high intensity focused ultrasound," *J. Ther. Ultrasound*, 2017.

[24] T. D. Khokhlova and J. H. Hwang, "HIFU for palliative treatment of pancreatic cancer," vol. 2, no. 3, 2011.

[25] E. E. Konofagou, Y.-S. Tung, J. Choi, T. Deffieux, B. Baseri, and F. Vlachos, "Ultrasound-induced blood-brain barrier opening.," *Curr. Pharm. Biotechnol.*, vol. 13, no. 7, pp. 1332–45, 2012.

[26] N. McDannold, N. Vykhodtseva, and K. Hynynen, "Blood-Brain Barrier Disruption Induced by Focused Ultrasound and Circulating Preformed Microbubbles Appears to Be Characterized by the Mechanical Index," *Ultrasound Med. Biol.*, vol. 34, no. 5, pp. 834–840, 2008.

[27] N. Vykhodtseva, N. McDannold, and K. Hynynen, "Progress and problems in the application of focused ultrasound for blood-brain barrier disruption," *Ultrasonics*, vol. 48, no. 4, pp. 279–296, 2008.

[28] N. McDannold, N. Vykhodtseva, and K. Hynynen, "Effects of Acoustic Parameters and Ultrasound Contrast Agent Dose on Focused-Ultrasound Induced Blood-Brain Barrier Disruption," *Ultrasound Med. Biol.*, vol. 34, no. 6, pp. 930–937, 2008.

[29] J. J. Choi, M. Pernot, S. A. Small, and E. E. Konofagou, "Noninvasive, transcranial

and localized opening of the blood-brain barrier using focused ultrasound in mice," *Ultrasound Med. Biol.*, vol. 33, no. 1, pp. 95–104, 2007.

[30] J. J. Choi, S. Wang, Y. S. Tung, B. Morrison, and E. E. Konofagou, "Molecules of Various Pharmacologically-Relevant Sizes Can Cross the Ultrasound-Induced Blood-Brain Barrier Opening in vivo," *Ultrasound Med. Biol.*, vol. 36, no. 1, pp. 58–67, 2010.

[31] T. Deffieux and E. E. Konofagou, "Numerical Study of a Simple Transcranial Focused Ultrasound System Applied to Blood-Brain Barrier Opening," *IEEE Trans Ultrason Ferroelect Fre Control*, vol. 57, no. 12, pp. 2637–2653, 2010.

[32] F. Marquet, Y.-S. Tung, and E. E. Konofagou, "Feasibility Study of a Clinical Blood-Brain Barrier Opening Ultrasound System," *Nano Life*, vol. 1, pp. 309-, 2010.

[33] F. Marquet, Y. S. Tung, T. Teichert, V. P. Ferrera, and E. E. Konofagou, "Noninvasive, transient and selective Blood-Brain barrier opening in Non-Human primates in vivo," *PLoS One*, vol. 6, no. 7, pp. 1–7, 2011.

[34] C. Sonne, F. Xie, J. Lof, J. Oberdorfer, P. Phillips, And C. Everbach, "Differences in definity and optison microbubble destruction rates at a similar mechanical index with different real-time perfusion systems," *J. Am. Soc. Echocardiogr.*, vol. 16, no. 11, pp. 1178–1185, Nov. 2003.

[35] R. Tente, *Investigation of microbubble-cell interaction and development of an ultrasound delivery system Raniska Tente A thesis submitted for the degree of Doctor of Philosophy The University of Edinburgh*. 2009.

[36] S. Wang, G. Samiotaki, O. Olumolade, J. a Feshitan, and E. E. Konofagou, "Microbubble type and distribution dependence of focused ultrasound-induced blood-brain barrier opening.," *Ultrasound Med. Biol.*, vol. 40, no. 1, pp. 130–137, Jan. 2014.

[37] N. J. McDannold, C. D. Arvanitis, N. Vykhodtseva, and M. S. Livingstone, "Temporary disruption of the blood-brain barrier by use of ultrasound and microbubbles: safety and efficasy evaluation in rhesus macaques," *Cancer Res.*, vol. 72, no. 14, pp. 3652–3663, 2012.

[38] H. Liu *et al.*, “Design and Experimental Evaluation of a Phased-Array System for Transcranial Blood – Brain Barrier Opening and Brain Drug Delivery,” *IEEE Trans. Biomed. Eng.*, vol. 61, no. 4, pp. 1350–1360, 2014.

[39] W. C. Huang, X. Y. Wu, and H. L. Liu, “System Design of Ultrasonic Image-guided Focused Ultrasound for Blood Brain Barrier disruption,” in *13th International Conference on Biomedical Engineering: ICBME 2008 3--6 December 2008 Singapore*, C. T. Lim and J. C. H. Goh, Eds. Berlin, Heidelberg: Springer Berlin Heidelberg, 2009, pp. 435–438.

[40] H.-L. Liu *et al.*, “Design and Experimental Evaluation of a 256 -Channel Dual-Frequency Ultrasound Phased-Array System for Transcranial Blood-Brain Barrier Opening and Brain Drug Delivery,” *IEEE Trans Biomed Eng.*, vol. 61, no. 4, pp. 1350–60, 2014.

[41] F.-Y. Yang *et al.*, “Pulsed high-intensity focused ultrasound enhances the relative permeability of the blood-tumor barrier in a glioma-bearing rat model,” *IEEE Trans. Ultrason. Ferroelectr. Freq. Control*, vol. 58, no. 5, pp. 964–970, 2011.

[42] F. Y. Yang, H. E. Wang, G. L. Lin, H. H. Lin, and T. T. Wong, “Evaluation of the increase in permeability of the blood-brain barrier during tumor progression after pulsed focused ultrasound,” *Int. J. Nanomedicine*, vol. 7, pp. 723–730, 2012.

[43] P. C. Chu *et al.*, “Pharmacodynamic analysis of magnetic resonance imaging-monitored focused ultrasound-induced blood-brain barrier opening for drug delivery to brain tumors,” *Biomed Res. Int.*, vol. 2013, 2013.

[44] F. Y. Yang, C. E. Ko, S. Y. Huang, I. F. Chung, and G. S. Chen, “Pharmacokinetic changes induced by focused ultrasound in glioma-bearing rats as measured by dynamic contrast-enhanced MRI,” *PLoS One*, vol. 9, no. 3, 2014.

[45] P. Y. Chen *et al.*, “Novel magnetic/ultrasound focusing system enhances nanoparticle drug delivery for glioma treatment,” *Neuro. Oncol.*, vol. 12, no. 10, pp. 1050–1060, 2010.

[46] F. Y. Yang *et al.*, “Treating glioblastoma multiforme with selective high-dose liposomal doxorubicin chemotherapy induced by repeated focused ultrasound,” *Int. J. Nanomedicine*, vol. 7, pp. 965–974, 2012.

[47] H. L. Liu, C. H. Fan, C. Y. Ting, and C. K. Yeh, “Combining microbubbles and ultrasound for drug delivery to brain tumors: Current progress and overview,” *Theranostics*, vol. 4, no. 4, pp. 432–444, 2014.

[48] K. Hynynen, N. McDannold, N. Vykhodtseva, and F. A. Jolesz, “Noninvasive MR imaging-guided focal opening of the blood-brain barrier in rabbits.,” *Radiology*, vol. 220, no. 4, pp. 640–646, 2001.

[49] F. Schlachetzki *et al.*, “Observation on the integrity of the blood-brain barrier after microbubble destruction by diagnostic transcranial color-coded sonography,” *J. Ultrasound Med.*, vol. 21, no. 4, pp. 419–429, 2002.

[50] N. Sheikov, N. McDannold, N. Vykhodtseva, F. Jolesz, and K. Hynynen, “Cellular mechanisms of the blood-brain barrier opening induced by ultrasound in presence of microbubbles,” *Ultrasound Med. Biol.*, vol. 30, no. 7, pp. 979–989, 2004.

[51] K. Hynynen, N. McDannold, N. A. Sheikov, F. A. Jolesz, and N. Vykhodtseva, “Local and reversible blood-brain barrier disruption by noninvasive focused ultrasound at frequencies suitable for trans-skull sonications,” *Neuroimage*, vol. 24, no. 1, pp. 12–20, 2005.

[52] N. McDannold, N. Vykhodtseva, S. Raymond, F. A. Jolesz, and K. Hynynen, “MRI-guided targeted blood-brain barrier disruption with focused ultrasound: Histological findings in rabbits,” *Ultrasound Med. Biol.*, vol. 31, no. 11, pp. 1527–1537, 2005.

[53] F.-Y. Yang, W.-M. Fu, R.-S. Yang, H.-C. Liou, K.-H. Kang, and W.-L. Lin, “Quantitative Evaluation of Focused Ultrasound with a Contrast Agent on Blood-Brain Barrier Disruption,” *Ultrasound Med. Biol.*, vol. 33, no. 9, pp. 1421–1427, 2007.

[54] N. McDannold, N. Vykhodtseva, and K. Hynynen, “Use of ultrasound pulses combined with Definity for targeted blood-brain barrier disruption: a feasibility study.,” *Ultrasound Med. Biol.*, vol. 33, no. 4, pp. 584–90, Apr. 2007.

[55] N. Sheikov, N. McDannold, S. Sharma, and K. Hynynen, “Effect of Focused Ultrasound Applied With an Ultrasound Contrast Agent on the Tight Junctional Integrity of the Brain Microvascular Endothelium,” *Ultrasound Med. Biol.*, vol.

34, no. 7, pp. 1093–1104, 2008.

[56] R. Chopra, N. Vykhodtseva, and K. Hynynen, “Influence of exposure time and pressure amplitude on blood-brain-barrier opening using transcranial ultrasound exposures,” *ACS Chem. Neurosci.*, vol. 1, no. 5, pp. 391–398, 2010.

[57] E. E. Cho, J. Drazic, M. Ganguly, B. Stefanovic, and K. Hynynen, “Two-Photon Fluorescence Microscopy Study of Cerebrovascular Dynamics in Ultrasound-Induced Blood—Brain Barrier Opening,” *J. Cereb. Blood Flow Metab.*, vol. 31, no. 9, pp. 1852–1862, 2011.

[58] M. A. O'Reilly, A. C. Waspe, M. Ganguly, and K. Hynynen, “Focused-Ultrasound Disruption of the Blood-Brain Barrier Using Closely-Timed Short Pulses: Influence of Sonication Parameters and Injection Rate,” *Ultrasound Med. Biol.*, vol. 37, no. 4, pp. 587–594, 2011.

[59] J. J. Choi, K. Selert, Z. Gao, G. Samiotaki, B. Baseri, and E. E. Konofagou, “Noninvasive and Localized Blood—Brain Barrier Disruption using Focused Ultrasound can be Achieved at Short Pulse Lengths and Low Pulse Repetition Frequencies,” *J. Cereb. Blood Flow Metab.*, vol. 31, no. 2, pp. 725–737, 2011.

[60] K.-C. Wei *et al.*, “Neuronavigation-guided focused ultrasound-induced blood-brain barrier opening: a preliminary study in swine.,” *AJNR. Am. J. Neuroradiol.*, vol. 34, no. 1, pp. 115–20, Jan. 2013.

[61] S. Wang, G. Samiotaki, O. Olumolade, J. A. Feshitan, and E. E. Konofagou, “Microbubble type and distribution dependence of focused ultrasound-induced blood-brain barrier opening,” *Ultrasound Med. Biol.*, vol. 40, no. 1, pp. 130–137, 2014.

[62] A. Burgess, H. H. Kullervo, and M. Biophysics, “Drug delivery across the blood-brain barrier using focused ultrasound,” vol. 11, no. 5, pp. 711–721, 2015.

[63] V. Frenkel, “Ultrasound mediated delivery of drugs and genes to solid tumors,” *Adv. Drug Deliv. Rev.*, vol. 60, no. 10, pp. 1193–1208, 2008.

[64] K. Hynynen, N. McDannold, N. Vykhodtseva, and F. A. Jolesz, “Noninvasive MR Imaging–guided Focal Opening of the Blood-Brain Barrier in Rabbits,” *Radiology*, vol. 220, no. 3, pp. 640–646, 2001.

[65] S. B. Raymond, L. H. Treat, J. D. Dewey, N. J. McDannold, K. Hynynen, and B. J. Bacskai, “Ultrasound enhanced delivery of molecular imaging and therapeutic agents in Alzheimer’s disease mouse models,” *PLoS One*, vol. 3, no. 5, pp. 1–7, 2008.

[66] H.-L. Liu, Hsu, and P.-C. Chu, “Magnetic resonance imaging enhanced by superparamagnetic iron oxide particles: usefulness for distinguishing between focused ultrasound-induced blood-brain barrier disruption and brain hemorrhage,” *J Mag Reson Imaging.*, no. 29, p. 31:8, 2009.

[67] H.-L. Liu, W. Y-Y., and H. P.H, “In vivo assessment of macrophage CNS infiltration during disruption of the blood-brain barrier with focused ultrasound: a magnetic resonance imaging study,” *J Cereb Blood Flow Metab.*, no. 30, pp. 177–86, 2010.

[68] H.-L. Liu, C.-H. Fan, C.-Y. Ting, and C.-K. Yeh, “Combining microbubbles and ultrasound for drug delivery to brain tumors: current progress and overview.,” *Theranostics*, vol. 4, no. 4, pp. 432–44, Jan. 2014.

[69] F.-Y. Yang *et al.*, “Focused ultrasound and interleukin-4 receptor-targeted liposomal doxorubicin for enhanced targeted drug delivery and antitumor effect in glioblastoma multiforme.,” *J. Control. Release*, vol. 160, no. 3, pp. 652–8, Jun. 2012.

[70] F. Y. Yang *et al.*, “Pharmacokinetic Analysis of 111In-Labeled Liposomal Doxorubicin in Murine Glioblastoma after Blood-Brain Barrier Disruption by Focused Ultrasound,” *PLoS One*, vol. 7, no. 9, pp. 1–7, 2012.

[71] F. Y. Yang *et al.*, “Focused ultrasound and interleukin-4 receptor-targeted liposomal doxorubicin for enhanced targeted drug delivery and antitumor effect in glioblastoma multiforme,” *J. Control. Release*, vol. 160, no. 3, pp. 652–658, 2012.

[72] M. Aryal, N. Vykhodtseva, Y.-Z. Zhang, J. Park, and N. McDannold, “Multiple treatments with liposomal doxorubicin and ultrasoundinduced disruption of blood-tumor and blood-brain barriers improves outcomes in a rat glioma model,” *J Control Release*, vol. 169, no. 0, pp. 103–111, 2013.

[73] L. H. Treat, N. McDannold, Y.-Z. Zhang, N. Vykhodtseva, and K. Hynynen,

"Improved anti-tumor effect of liposomal doxorubicin after targeted blood-brain barrier disruption by MRI-guided focused ultrasound in rat glioma," *Ultrasound Med. Biol.*, vol. 38, no. 10, pp. 1716–1725, 2012.

[74] H. L. Liu, C. Y. Huang, J. Y. Chen, H. Y. J. Wang, P. Y. Chen, and K. C. Wei, "Pharmacodynamic and therapeutic investigation of focused ultrasound-induced blood-brain barrier opening for enhanced temozolomide delivery in glioma treatment," *PLoS One*, vol. 9, no. 12, pp. 1–19, 2014.

[75] K. C. Wei *et al.*, "Focused Ultrasound-Induced Blood-Brain Barrier Opening to Enhance Temozolomide Delivery for Glioblastoma Treatment: A Preclinical Study," *PLoS One*, vol. 8, no. 3, pp. 1–10, 2013.

[76] M. Kinoshita, N. McDannold, F. a Jolesz, and K. Hynynen, "Noninvasive localized delivery of Herceptin to the mouse brain by MRI-guided focused ultrasound-induced blood-brain barrier disruption.," *Proc. Natl. Acad. Sci. U. S. A.*, vol. 103, no. 31, pp. 11719–23, Aug. 2006.

[77] E.-J. Park, Y.-Z. Zhang, N. Vykhodtseva, and N. McDannold, "Ultrasound-mediated blood-brain/blood-tumor barrier disruption improves outcomes with trastuzumab in a breast cancer brain metastasis model.," *J. Control. Release*, vol. 163, no. 3, pp. 277–84, Nov. 2012.

[78] S. K. Wu *et al.*, "Short-time focused ultrasound hyperthermia enhances liposomal doxorubicin delivery and antitumor efficacy for brain metastasis of breast cancer," *Int. J. Nanomedicine*, vol. 9, pp. 4485–4494, 2014.

[79] A. Ranjan *et al.*, "Image-guided drug delivery with magnetic resonance guided high intensity focused ultrasound and temperature sensitive liposomes in a rabbit Vx2 tumor model," *J. Control. Release*, vol. 158, no. 3, pp. 487–494, 2012.

[80] M. J. Park *et al.*, "Pulsed High-Intensity Focused Ultrasound Therapy Enhances Targeted Delivery of Cetuximab to Colon Cancer Xenograft Model in Mice," *Ultrasound Med. Biol.*, vol. 39, no. 2, pp. 292–299, 2013.

[81] A. B. Etame *et al.*, "Enhanced delivery of gold nanoparticles with therapeutic potential into the brain using MRI-guided focused ultrasound," *Nanomedicine Nanotechnology, Biol. Med.*, vol. 8, no. 7, pp. 1133–1142, 2012.

[82] W. De-Jong, W. Hagens, P. Krystek, M. Burger, A. Slips, and R. Geertsman, "Particle size-dependent organ distribution of gold nanoparticles after intravenous administration," *Biomaterials*, vol. 29, pp. 1912–9, 2008.

[83] M. R. M. Surendra Devarakonda, M. Lanier, C. Dumoulin, and R. K. Banerjee, "Assessment of Gold Nanoparticle-Mediated-Enhanced Hyperthermia Using MR-Guided High-Intensity Focused Ultrasound Ablation Procedure," *Nano Lett.*, vol. 17, no. 4, pp. 2532–2538, 2017.

[84] J. Xi *et al.*, "Au nanoparticle-coated, PLGA-based hybrid capsules for combined ultrasound imaging and HIFU therapy," *J. Mater. Chem. B*, vol. 3, pp. 4213–4220, 2015.

[85] X. Wang *et al.*, "Au-nanoparticle coated mesoporous silica nanocapsule-based multifunctional platform for ultrasound mediated imaging, cytoclasis and tumor ablation," *Biomaterials*, vol. 34, no. 8, pp. 2057–2068, 2013.

[86] R. J. Diaz *et al.*, "Focused ultrasound delivery of Raman nanoparticles across the blood-brain barrier: Potential for targeting experimental brain tumors," *Nanomedicine Nanotechnology, Biol. Med.*, vol. 10, no. 5, pp. 1075–1087, 2014.

[87] H.-L. Liu *et al.*, "Magnetic resonance monitoring of focused ultrasound/magnetic nanoparticle targeting delivery of therapeutic agents to the brain," *Proc. Natl. Acad. Sci.*, vol. 107, no. 34, pp. 15205–15210, 2010.

[88] K. S. Oh *et al.*, "Effect of HIFU treatment on tumor targeting efficacy of docetaxel-loaded Pluronic nanoparticles," *Colloids Surfaces B Biointerfaces*, vol. 119, pp. 137–144, 2014.

[89] X. Zhang *et al.*, "Methotrexate-loaded PLGA nanobubbles for ultrasound imaging and Synergistic Targeted therapy of residual tumor during HIFU ablation," *Biomaterials*, vol. 35, no. 19, pp. 5148–5161, 2014.

[90] J. Unga and M. Hashida, "Ultrasound induced cancer immunotherapy," *Adv. Drug Deliv. Rev.*, vol. 72, pp. 144–153, 2014.

[91] Shohet *et al.*, "Echocardiographic destruction of albumin microbubbles directs gene delivery to the myocardium," *Circ. 101*, pp. 2554–2556, 2000.

[92] Pislaru, Kinnick, Singh, Gulati, Greenleaf, and Simari, "Optimization of

ultrasound-mediated gene transfer: comparison of contrast agents and ultrasound modalities,” *Eur. Hear. J.*, pp. 1690–1698, 2003.

[93] Mo, C. Coussios, Seymour, and Carlisle, “Ultrasound-enhanced drug delivery for cancer,” *Expert Opin. Drug Deliv.*, pp. 1525–1538, 2012.

[94] C. Bing, M. Ladouceur-Wodzak, C. R. Wanner, J. M. Shelton, J. A. Richardson, and R. Chopra, “Trans-cranial opening of the blood-brain barrier in targeted regions using a stereotaxic brain atlas and focused ultrasound energy,” *J. Ther. Ultrasound*, vol. 2, no. 1, p. 13, 2014.

[95] J. J. Choi, S. Wang, T. R. Brown, S. A. Small, K. E. K. Duff, and E. E. Konofagou, “Noninvasive and transient blood-brain barrier opening in the hippocampus of Alzheimer’s double transgenic mice using focused ultrasound.,” *Ultrason. Imaging*, vol. 30, no. 3, pp. 189–200, 2008.

[96] N. McDannold, N. Vykhodtseva, and K. Hynynen, “Use of ultrasound pulses combined with definity for targeted blood-brain barrier disruption,” *AIP Conf. Proc.*, vol. 911, no. 4, pp. 547–553, 2007.

[97] A. Burgess and K. Hynynen, “Noninvasive and targeted drug delivery to the brain using focused ultrasound,” *Neuropharmacology*, 2016.

[98] T. D. Azad, J. Pan, I. D. Connolly, A. Remington, M. Christy, and G. A. Grant, “Therapeutic strategies to improve drug delivery across the blood-brain barrier,” *Neurosurg Focus*, vol. 38, no. 7, 2015.

[99] B. Marty *et al.*, “Dynamic study of blood – brain barrier closure after its disruption using ultrasound : a quantitative analysis,” pp. 1948–1958, 2012.

[100] J. F. Jordão *et al.*, “Amyloid-β plaque reduction, endogenous antibody delivery and glial activation by brain-targeted, transcranial focused ultrasound.,” *Exp. Neurol.*, vol. 248, pp. 16–29, Oct. 2013.

[101] E. Madsen, J. Zagzebski, R. Banjavie, and R. Jutila, “Tissue mimicking materials for ultrasound phantoms,” *Med. Phys.*, vol. 5, no. 55, pp. 391–4, 1978.

[102] J. Cook, R. Bouchard, and S. Emelianov, “Tissue-mimicking phantoms for photoacoustic and ultrasonic imaging,” *Biomed Opt Express*, vol. 2, no. 11, pp. 3193–206, 2011.

[103] R. Bude and R. Adler, “An easily made, low-cost, tissue-like ultrasound phantom material,” *J Clin Ultrasound*, vol. 23, pp. 271–3, 1995.

[104] E. Madsen, G. Frank, and F. Dong, “Liquid or solid ultrasonically tissue-mimicking materials with very low scatter,” *Ultrasound Med. Biol.*, vol. 24, no. 4, pp. 535–42, 1998.

[105] H. C. Zell K, Sperl JI, Vogel MW, Niessner R, “Acoustical properties of selected tissue phantom materials for ultrasound imaging,” *Phys Med Biol*, vol. 52, no. 20, pp. 475–84, 2007.

[106] V. T. Partanen A, Mougenot C, “Feasibility of Agar-Silica Phantoms in Quality Assurance of MRgHIFU,” *8TH Int*, vol. 1113, no. 1, pp. 296–300, 2009.

[107] K. H. Kondo T, Kitatuji M, “New tissue mimicking materials for ultrasound phantoms,” *IEEE Ultrason. Symp.*, vol. 3, pp. 1664–7, 2005.

[108] M. J. Choi, S. R. Guntur, K. I. L. Lee, D. G. Paeng, and A. Coleman, “A Tissue Mimicking Polyacrylamide Hydrogel Phantom for Visualizing Thermal Lesions Generated by High Intensity Focused Ultrasound,” *Ultrasound Med. Biol.*, vol. 39, no. 3, pp. 439–448, 2013.

[109] A. F. Prokop, S. Vaezy, M. L. Noble, P. J. Kaczkowski, R. W. Martin, and L. A. Crum, “Polyacrylamide gel as an acoustic coupling medium for focused ultrasound therapy,” *Ultrasound Med. Biol.*, vol. 29, no. 9, pp. 1351–1358, 2003.

[110] C. W.-S. Sun M-K, Shieh J, Lo C-W, Chen C-S, Chen B-T, Huang C-W, “Reusable tissue-mimicking hydrogel phantoms for focused ultrasound ablation,” *Ultrason Sonochem*, vol. 23, pp. 399–405, 2015.

[111] A. H. Surry K, “Poly (vinyl alcohol) cryogel phantoms for use in ultrasound and MR imaging,” *Phys Med*, vol. 49, no. 24, pp. 5529–46, 2004.

[112] G. Menikou and C. Damianou, “Acoustic and thermal characterization of agar based phantoms used for evaluating focused ultrasound exposures,” *J. Ther. Ultrasound*, vol. 5, no. 1, p. 14, 2017.

[113] C. Lafon *et al.*, “Gel phantom for use in high-intensity focused ultrasound dosimetry,” *Ultrasound Med. Biol.*, vol. 31, no. 10, pp. 1383–1389, 2005.

[114] T. Alekou, M. Giannakou, and C. Damianou, “Focused ultrasound phantom model

for blood brain barrier disruption," *Ultrasonics*, vol. 110, p. 106244, 2021.

[115] C. Yiallouras, K. Ioannides, T. Dadakova, M. Pavlina, M. Bock, and C. Damianou, "Three-axis MR-conditional robot for high-intensity focused ultrasound for treating prostate diseases transrectally," *J. Ther. Ultrasound*, vol. 3, no. 1, pp. 1–10, 2015.

[116] C. R. Hill, "Optimum acoustic frequency for focused ultrasound surgery," *Ultrasound Med. Biol.*, vol. 20, no. 3, pp. 271–277, 1994.

[117] M. S. Nolle AW, "Measurement of ultrasonic bulk-wave propagation in high polymers," *J. Acoust. Soc. Am.*, vol. 20, no. 4, pp. 432–439, 1948.

[118] McSkimin HJ, "Ultrasonic methods for measuring mechanical properties of liquids and solids," *Physical Acoustics, Academic Press*, pp. 271–334, 1964.

[119] Umchid S, "Frequency dependent ultrasonic attenuation coefficient measurement," in *3rd International Symposium on Biomedical Engineering*, 2008, pp. 234–238.

[120] He P and Z. J, "Acoustic dispersion and attenuation measurement using both transmitted and reflected pulses," *Ultrasonics*, vol. 39, pp. 27–32, 2001.

[121] C. A. N. and W. C. A. P. G. Cortela, L. E. Maggi, M. A. Von Kruger, "Ultrasonic attenuation and speed in phantoms made of polyvinyl chloride-plasticol (PVCP) and graphite powder," *Proc. Meet. Acoust.*, vol. 19, no. 1, 2013.

[122] N. Parmar and M. C. Kolios, "An investigation of the use of transmission ultrasound to measure acoustic attenuation changes in thermal therapy," *Med. Biol. Eng. Comput.*, vol. 44, no. 7, pp. 583–591, 2006.

[123] L. E. M. and C.-F. P. B. R. D. Oliveira, T. Q. Santos, "Ultrasound propagation velocity and acoustic attenuation on agarose phantoms in three different manufacture techniques," in *Pan American Health Care Exchanges*, 2014.

[124] E. K. and M. B. B. Gambin, "Relationships between acoustical properties and stiffness of soft tissue phantoms," *Hydroacoustics*, vol. 19, pp. 111–120, 2011.

[125] L. AIUM Technical Standards Committee, "Standards methods for measuring performance of pulse-echo ultrasound imaging equipment," in *American Institute of Ultrasound in Medicine Standard*, 1990.

[126] D. F. Madsen EL, Frank GR, “Liquid or solid ultrasonically tissue-mimicking materials with very low scatter,” *Ultrasound Med. Biol.*, vol. 24, no. 4, pp. 535–42, 1998.

[127] C. H. E. and C. M. M. C. Sun, S. D. Pye, J. E. Browne, A. Janeczko, B. Ellis, M. B. Butler, V. Sboros, A. J. W. Thomson, M. P. Brewin, “The speed of sound and attenuation of an IEC agar-based tissue-mimicking material for high frequency ultrasound applications,” *Ultrasound Med. Biol.*, vol. 38, no. 7, pp. 1262–1270, 2012.

[128] T. V. and G. R. F. E. L. Madsen, M. A. Hobson, H. Shi, “Tissue-mimicking agar/gelatin materials for use in heterogeneous elastography phantoms,” *Phys. Med. Biol.*, vol. 50, pp. 5597–5618, 2005.

[129] A. M. and L. R. A. Cafarelli, A. Verbeni, A. Poliziani, P. Dario, “Tuning acoustic and mechanical properties of materials for ultrasound phantoms and smart substrates for cell cultures,” *Acta Biomater.*, vol. 16, 2016.

[130] R. A. B. and S. W. S. M. M. Burlew, E. L. Madsen, J. A. Zagzebski, “A new ultrasound tissue-equivalent material,” *Radiology*, vol. 134, no. 2, pp. 517–520, 1980.

[131] J. R. Madsen EL, Zagzebski JA, Banjavie RA, “Tissue mimicking materials for ultrasound phantoms,” *Med. Phys.*, vol. 5, no. 5, pp. 391–4, 1978.

[132] A. F. and T. M. P. K. J. M. Surry, H. J. B. Austin, “Poly(vinyl alcohol) cryogel phantoms for use in ultrasound and MRI imaging,” *Phys. Med. Biol.*, vol. 49, pp. 5529–5546, 2004.

[133] “HIFU phantoms,” *Onda Corporation*. [Online]. Available: www.ondacorp.com/products_hifusol_phantoms.shtml. [Accessed: 26-Mar-2020].

[134] C. I. and C. D. T. Drakos, M. Giannakou, G. Menikou, “An improved method to estimate ultrasonic absorption in agar-based gel phantom using thermocouples and MR thermometry,” *Ultrasonics*, vol. 103, 2020.

[135] J. A. Z. and G. R. F. E. L. Madsen, “Oil-in-gelatin dispersions for use as ultrasonically tissue-mimicking materials,” *Ultrasound Med. Biol.*, vol. 8, no. 3,

pp. 277–287, 1982.

[136] I. Reinertsen and D. L. Collins, “A realistic phantom for brain-shift simulations,” *Med. Phys.*, vol. 33, no. 9, pp. 3234–3240, 2006.

[137] R. G. and V. Y. F. A. Keshavarzi, S. Vaezy, P. J. Kaczkowski, G. Keilman, R. Martin, E. Y. Chi, “Attenuation coefficient and sound speed in human myometrium and uterine fibroid tumors,” *J. Ultrasound Med.*, vol. 20, pp. 473–480, 2001.

[138] L. M. H. and M. J. O. T. D. Mast, “Simulation of ultrasonic pulse propagation through the abdominal wall,” *J. Acoust. Soc. Am.*, vol. 102, no. 2, pp. 1177–1190, 1997.

[139] M. Bethesda, “Tissue substitutes, phantoms and computational modelling in medical ultrasound,” 1998.

[140] C. R. H. and F. D. J. C. Bamber, M. J. Fry, “Ultrasonic attenuation and backscattering by mammalian organs as a function of time after excision,” *Ultrasound Med. Biol.*, vol. 3, pp. 15–20, 1977.

[141] O. M. Ghoshal G, Lavarello RJ, Kemmerer JP, Miller RJ, “Ex vivo study of quantitative ultrasound parameters in fatty rabbit livers,” *Ultrasound Med. Biol.*, vol. 38, no. 12, pp. 2238–2248, 2012.

[142] T. H. T A Krouskop 1, T M Wheeler, F Kallel, B S Garra, “Elastic moduli of breast and prostate tissues under compression,” *Ultrason Imaging* ., vol. 20, no. 4, pp. 260–74, 1998.

[143] G. Lamouche *et al.*, “Review of tissue simulating phantoms with controllable optical , mechanical and structural properties for use in optical coherence tomography,” vol. 3, no. 6, pp. 1381–1398, 2012.

[144] E. Moeendarbary and A. R. Harris, “Cell mechanics : principles , practices , and prospects,” vol. 6, no. October, pp. 371–388, 2014.

[145] L. Qian and H. Zhao, “Nanoindentation of Soft Biological Materials,” 2018.

[146] J. A. W. Van Dommelen, T. P. J. Van Der Sande, M. Hrapko, and G. W. M. Peters, “Mechanical properties of brain tissue by indentation : Interregional variation,” *J. Mech. Behav. Biomed. Mater.*, vol. 3, no. 2, pp. 158–166, 2010.

[147] R. Akhtar *et al.*, “Nanoindentation of histological specimens: Mapping the elastic properties of soft tissues,” *J. Mater. Res.*, vol. 24, no. 3, pp. 638–646, Mar. 2009.

[148] P. Hai and L. V Wang, “Quantitative photoacoustic elastography in humans,” vol. 21, no. 6, 2016.

[149] A. Maccabi *et al.*, “Quantitative characterization of viscoelastic behavior in tissue-mimicking phantoms and ex vivo animal tissues,” pp. 1–18, 2018.

[150] K. Kaczmarek, R. Mrowczynski, T. Hornowski, R. Bielas, and A. Jozefczak, “The Effect of Tissue-Mimicking Phantom Compressibility on Magnetic Hyperthermia,” *Nanomaterials*, 2019.

[151] K. Manickam, R. Reddy, and S. Seshadri, “Characterization of biomechanical properties of agar based tissue mimicking phantoms for ultrasound stiffness imaging techniques,” *J. Mech. Behav. Biomed. Mater.*, vol. 35, pp. 132–143, 2014.

[152] Y. Dwihapsari *et al.*, “The Study of Mechanical Properties and Relaxation Time of Agar Hydrogel for Tissue Mimicking Phantom Material in Magnetic Resonance Imaging The Study of Mechanical Properties and Relaxation Time of Agar Hydrogel for Tissue Mimicking Phantom Material in Ma.”

[153] P. A. Panteli, C. S. Patrickios, and M. Constantinou, “Multiple Network Hydrogels : A Study of Their Nanoindentation Hardness,” vol. 1800201, pp. 1–6, 2019.

[154] V. T. Nayar, J. D. Weiland, C. S. Nelson, and A. M. Hodge, “Elastic and viscoelastic characterization of agar,” *J. Mech. Behav. Biomed. Mater.*, vol. 7, pp. 60–68, 2012.

[155] K. Manickam, R. Reddy, and S. Seshadri, “Study of ultrasound stiffness imaging methods using tissue mimicking phantoms,” *Ultrasonics*, vol. 54, no. 2, pp. 621–631, 2014.

[156] P. Movahed, W. Kreider, A. D. Maxwell, B. Dunmire, and B. Freund, “Ultrasound-induces bubble clusters in tissue-mimicking agar phantoms,” *Ultrasound Med. Biol.*, vol. 43, no. 10, pp. 2318–2328, 2017.

[157] G. McIlvain, E. Ganji, C. Cooper, M. L. Killian, B. A. Ogunnaike, and C. L. Johnson, “Reliable preparation of agarose phantoms for use in quantitative

magnetic resonance elastography," *J. Mech. Behav. Biomed. Mater.*, 2019.

[158] M. S. Wróbel, A. P. Popov, A. V Bykov, and V. V Tuchin, "Nanoparticle-free tissue-mimicking phantoms with intrinsic scattering," vol. 7, no. 6, pp. 2088–2094, 2016.

[159] T. Drakos *et al.*, "Ultrasonic attenuation of an agar, silicon dioxide and evaporated milk gel phantom," *J. Ultrasound Med.*, Epub ahead, 2021.

[160] M. Earle, G. De Portu, and E. Devos, "Agar ultrasound phantoms for low-cost training without refrigeration," *African J. Emerg. Med.*, vol. 6, no. 1, pp. 18–23, 2016.

[161] L. Ntombela, B. Adeleye, and N. Chetty, "Low-cost fabrication of optical tissue phantoms for use in biomedical imaging," *Heliyon*, vol. 6, no. October 2019, p. e03602, 2020.

[162] R. M. Souza, T. Q. Santos, D. P. Oliveira, R. M. Souza, A. V Alvarenga, and R. P. B. Costa-Felix, "Standard operating procedure to prepare agar phantoms," *J. Phys. Conf. Ser.*, vol. 733, p. 012044, Jul. 2016.

[163] H. . Krebs, D. Wiggins, M. Stubbs, A. Sols, and F. Bedoya, "Studies on the mechanism of the antifungal action of benzoate," *Biochem*, vol. 214, pp. 657–663, 1983.

[164] A. A. Alsudani, "In vitro antifungal effect of potassium sorbate and sodium benzoate on the growth of fungi causing sinusitis," *African J. Microbiol. Res.*, vol. 11, no. 6, pp. 232–236, 2017.

[165] M. Shahmohammadi, M. Javadi, and M. Nassiri-Asl, "An Overview on the Effects of Sodium Benzoate as a Preservative in Food Products," *Biotechnol. Heal. Sci.*, vol. 3, no. 3, 2016.

[166] G. O. L. Bruna, A. C. C. Thais, and A. C. C. Lígia, "Food additives and their health effects: A review on preservative sodium benzoate," *African J. Biotechnol.*, vol. 17, no. 10, pp. 306–310, 2018.

[167] C. Boukarim, S. A. Jaoudé, R. Bahnam, R. Barada, and S. Kyriacos, "Preservatives in liquid pharmaceutical preparations," *J. Appl. Res.*, vol. 9, no. 1–2, pp. 14–17, 2009.

[168] "Alzheimer's Disease International. Dementia statistics," *Alzheimer's Disease International website*. [Online]. Available: https://www.alz.co.uk/research/statistics. [Accessed: 11-Nov-2017].

[169] R. B. DeMattos, K. R. Bales, D. J. Cummins, J. C. Dodart, S. M. Paul, and D. M. Holtzman, "Peripheral anti-A beta antibody alters CNS and plasma A beta clearance and decreases brain A beta burden in a mouse model of Alzheimer's disease," *Proc. Natl. Acad. Sci*, vol. 98, pp. 8850–8855, 2001.

[170] N. N. W. A. Banks, B. Terrell, S. A. Farr, S. M. Robinson, "Passage of amyloid beta protein antibody across the blood-brain barrier in a mouse model of Alzheimer's disease," *Peptides*, vol. 23, pp. 2223–2226, 2002.

[171] R. S. G. and L. S. L. D. R. Thakker, M. R. Weatherspoon, J. Harrison, T. E. Keene, D. S. Lane, F. K. William, "Intracerebroventricular amyloid-beta antibodies reduce cerebral amyloid angiopathy and associated micro-hemorrhages in aged Tg2576 mice," *Proc Natl Acad Sci*, vol. 106, pp. 4501–4506, 2009.

[172] M. . N. G. and D. M. D. M. Wilcock, G. DiCarlo, D. Henderson, J. Jackson, K. Clarke, K. E. Ugen, "Intracranially administered anti-Abeta antibodies reduce beta-amyloid deposition by mechanisms both independent of and associated with microglial activation," *J Neurosci*, vol. 23, pp. 3745–3751, 2003.

[173] K. Hynynen *et al.*, "Focal disruption of the blood-brain barrier due to 260-kHz ultrasound bursts: A method for molecular imaging and targeted drug delivery," *J Neurosurg.*, vol. 105, pp. 445–454, 2006.

[174] N. McDannold, N. Vykhodtseva, S. Raymond, F. A. Jolesz, and K. Hynynen, "MRI-guided targeted blood-brain barrier disruption with focused ultrasound: histological findings in rabbits," *Ultrasound Med Biol.*, vol. 31, pp. 1527–1537, 2005.

[175] L. H. Treat, N. McDannold, Y. Zhang, N. Vykhodtseva, and K. Hynynen, "Targeted delivery of doxorubicin to the rat brain at therapeutic levels using MRI-guided focused ultrasound," *Int J Cancer*, vol. 121, pp. 901–907, 2007.

[176] K. H. N. McDannold, N. Vykhodtseva, "Targeted disruption of the blood-brain barrier with focused ultrasound: association with cavitation activity," *Phys Med*

Biol, vol. 21, no. 51, pp. 793–807, 2006.

[177] J. F. Jordão *et al.*, “Antibodies targeted to the brain with image-guided focused ultrasound reduces amyloid-β plaque load in the TgCRND8 mouse model of Alzheimer’s disease,” *PLoS One*, vol. 5, no. 5, pp. 4–11, 2010.

[178] A. Burgess *et al.*, “Alzheimer Disease in a Mouse Model: MR Imaging guided Focused Ultrasound Targeted to the Hippocampus Opens the Blood-Brain Barrier and Improves Pathologic Abnormalities and Behavior,” *RSNA*, vol. 273, 2015.

[179] G. Leinenga and J. Gotz, “Scanning ultrasound removes amyloid- and restores memory in an Alzheimer’s disease mouse model,” *Sci. Transl. Med.*, vol. 7, no. 278, pp. 278ra33-278ra33, 2015.

[180] D. L. Sparks, S. W. Scheff, J. C. Hunsaker, H. Liu, T. Landers, and D. R. Gross, “Induction of Alzheimer-like beta-amyloid immunoreactivity in the brains of rabbits with dietary cholesterol,” *Exp Neurol*, vol. 126, pp. 88–94, 1994.

[181] T. Alecou, M. Giannakou, and C. Damianou, “Amyloid β Plaque Reduction With Antibodies Crossing the Blood-Brain Barrier, Which Was Opened in 3 Sessions of Focused Ultrasound in a Rabbit Model,” *J. Ultrasound Med.*, vol. 36, no. 11, pp. 2257–2270, Nov. 2017.

[182] F. Bard *et al.*, “Peripherally administered antibodies against amyloid beta-peptide enter the central nervous system and reduce pathology in a mouse model of Alzheimer disease,” *Nat Med*, vol. 6, pp. 916–919, 2000.

[183] S. A. Goss, R. L. Johnston, and F. Dunn, “Comprehensive compilation of empirical ultrasonic properties of mammalian tissues,” *J Acoust Soc Am*, vol. 64, pp. 423–457, 1978.

[184] G. Pinton, J. F. Aubry, E. Bossy, M. Muller, M. Pernot, and T. M. Attenuation, “Attenuation, scattering and absorption of ultrasound in the skull bone,” *Med Phys Jan*, vol. 39, no. 1, pp. 299–307, 2012.

[185] D. L. Sparks, “Cholesterol, copper, and accumulation of thioflavine S-reactive Alzheimer’s-like amyloid beta in rabbit brain,” *J Mol. Neurosci.*, vol. 24, pp. 97–104, 2004.

[186] L. Li, D. Cao, D. W. Garber, H. Kim, and K. Fukuchi, “Association of aortic

atherosclerosis with cerebral beta-amyloidosis and learning deficits in a mouse model of Alzheimer's disease, Am," *J. Pathol.*, vol. 163, pp. 2155–2164, 2003.

[187] P. Yan *et al.*, "Characterizing the appearance and growth of amyloid plaques in APP/PS1 mice," *J Neurosci.*, vol. 29, no. 34, pp. 10706–10714, 2009.

[188] J. Prasanthi, E. Schommer, S. Thomasson, A. Thompson, G. Feist, and O. Ghribi, "Regulation of b-amyloid levels in the brain of cholesterol-fed rabbit, a model system for sporadic Alzheimer's disease," *Mech. Ageing Dev.*, vol. 129, pp. 649–655, 2008.

[189] S. Sharma, J. Prasanthi, E. Schommer, G. Feist, and O. Ghribi, "Hypercholesterolemia-induced Aβ accumulation in rabbit brain is associated with alteration in IGF-1 signaling," *Neurobiol. Dis.*, vol. 32, pp. 426–432, 2008.

[190] A. Serrano-Pozo *et al.*, "Stable Size Distribution of Amyloid Plaques Over the Course of Alzheimer Disease," *J Neuropathol Exp Neurol*, vol. 71, pp. 694–701, 2012.

[191] L. M. Refolo *et al.*, "Hypercholesterolemia accelerates the Alzheimer's amyloid pathology in a transgenic mouse model," *Neurobiol Dis*, vol. 7, pp. 321–331, 2000.

[192] K. Fassbender *et al.*, "Simvastatin strongly reduces levels of Alzheimer's disease beta-amyloid peptides Abeta 42 and Abeta 40 in vitro and in vivo," in *Proc. Natl. Acad. Sci. U.S.A*, 2001, pp. 5856–5861.

[193] T.-K. Yang, F.-Y., Lin, Y.-S., Kang, K.-H., & Chao, "Reversible blood-brain barrier disruption by repeated transcranial focused ultrasound allows enhanced extravasation," *J. Control. Release*, vol. 150, no. 1, pp. 111–116, 2011.

[194] M. W. K. Elias, D. Huss, T. Voss, J. Loomba, M. Khaled, E. Zadicario, R. Frysinger, S. Sperling, W. P. Scott, S. Monteith, J. Druzgal, B. Shah, M. Harrison, "A Pilot Study of Focused Ultrasound Thalamotomy for Essential Tremor," *N Engl J Med*, vol. 369, pp. 640–648, 2013.

[195] S. K. Mould D., "The pharmacokinetics and pharmacodynamics of monoclonal antibodies –mechanistic modeling applied to drug development'," *Curr. Opin. Drug Discov. Devel.*, vol. 10, no. 1, pp. 84–96, 2007.

[196] C. Yiallouras, N. Mylonas, and C. Damianou, "MRI-compatible positioning device

for guiding a focused ultrasound system for transrectal treatment of prostate cancer.," *Int. J. Comput. Assist. Radiol. Surg.*, vol. 9, no. 4, pp. 745–53, Jul. 2014.

[197] E. Epaminonda, T. Drakos, C. Kalogirou, M. Theodoulou, C. Yiallouras, and C. Damianou, "MRI guided focused ultrasound robotic system for the treatment of gynaecological tumors," *Int. J. Med. Robot. Comput. Assist. Surg.*, vol. 12, no. 1, pp. 46–52, 2016.

[198] M. Yiannakou, G. Menikou, C. Yiallouras, C. Ioannides, and C. Damianou, "MRI guided focused ultrasound robotic system for animal experiments," *Int. J. Med. Robot. Comput. Assist. Surg.*, vol. 13, no. 4, p. 1804, 2017.

[199] G. Menikou, C. Yiallouras, M. Yiannakou, and C. Damianou, "MRI-guided focused ultrasound robotic system for the treatment of bone cancer," *Int. J. Med. Robot. Comput. Assist. Surg.*, vol. 13, no. 1, p. 1753, 2017.

[200] M. Giannakou, C. Yiallouras, G. Menikou, C. Ioannides, and C. Damianou, "MRI-guided frameless biopsy robotic system with the inclusion of unfocused ultrasound transducer for brain cancer ablation," *Int. J. Med. Robot. Comput. Assist. Surg.*, vol. 15, no. 1, p. 1951, 2019.

[201] N. Mylonas and C. Damianou, "MR compatible positioning device for guiding a focused ultrasound system for the treatment of brain deseases," *Int. J. Med. Robot. Comput. Assist. Surg.*, vol. 10, no. 1, pp. 1–10, 2014.

[202] G. Sagias, C. Yiallouras, K. Ioannides, and C. Damianou, "An MRI-conditional motion phantom for the evaluation of high-intensity focused ultrasound protocols," *Int. J. Med. Robot. Comput. Assist. Surg.*, vol. 12, no. 3, pp. 431–441, 2016.

[203] G. Menikou, M. Yiannakou, C. Yiallouras, C. Ioannides, and C. Damianou, "MRI-compatible breast/rib phantom for evaluating ultrasonic thermal exposures," *Int. J. Med. Robot. Comput. Assist. Surg.*, vol. 14, no. 1, pp. 1–12, 2018.

[204] G. Menikou, M. Yiannakou, C. Yiallouras, C. Ioannides, and C. Damianou, "MRI-compatible bone phantom for evaluating ultrasonic thermal exposures," *Ultrasonics*, vol. 71, pp. 12–19, 2016.

[205] C. Damianou, "The role of phantoms in magnetic resonance imaging-guided focused ultrasound surgery," *Digit. Med.*, vol. 5, no. 2, p. 52, 2019.

[206] C. Damianou, V. Hadjisavvas, N. Mylonas, A. Couppis, and K. Ioannides, “MRI-guided sonothrombolysis of rabbit carotid artery,” *J. Stroke Cerebrovasc. Dis.*, vol. 23, no. 2, pp. 113–121, 2014.

[207] C. Damianou, N. Mylonas, and K. Ioannides, “Sonothrombolysis in combination with thrombolytic drugs in a rabbit model using MRI-guidance,” *Engineering*, vol. 5, no. 10, pp. 352–356, 2013.

[208] C. Damianou, C. Christofi, and N. Mylonas, “Removing atherosclerotic plaque created using high cholesterol diet in rabbit using ultrasound,” *J. Ther. ultrasound*, vol. 3, no. 1, pp. 1–9, 2015.

[209] C. Damianou, K. Ioannides, V. Hadjisavvas, N. Mylonas, A. Couppis, and D. Iosif, “In vitro and in vivo brain ablation created by high-intensity focused ultrasound and monitored by MRI.,” *IEEE Trans. Ultrason. Ferroelectr. Freq. Control*, vol. 56, no. 6, pp. 1189–98, Jun. 2009.